Synthesis and biological activity of molybdenum carbonyl complexes and their peptide conjugates

Dissertation zur Erlangung des naturwissenschaftlichen Doktorgrades
der
Julius-Maximilians-Universität Würzburg

vorgelegt von

Hendrik Pfeiffer
aus Siegen

Würzburg 2012

Eingereicht bei der Fakultät für Chemie und Pharmazie am

16. April 2012

Gutachter der schriftlichen Arbeit

1. Gutachter: Prof. Dr. U. Schatzschneider

2. Gutachter: Prof. Dr. W. Schenk

Prüfer des öffentlichen Promotionskolloquiums

1. Prüfer: Prof. Dr. U. Schatzschneider

2. Prüfer: Prof. Dr. W. Schenk

3. Prüfer: Prof. Dr. A. Krüger

Datum des öffentlichen Promotionskolloquiums

23. Mai 2012

Doktorurkunde ausgehändigt am

“Science is an ocean.
It is as open to the cockboat as the frigate.
One man carries across it a freightage of ingots,
another may fish there for herrings.”

Earl Edward George Bulwer-Lytton

Danksagung

Mein besonderer Dank gilt meinem Doktorvater Herrn Prof. Dr. Ulrich Schatzschneider für die Betreuung und die Möglichkeit zur Durchführung dieser Arbeit mit allen dazugehörigen Freiheiten zur Ausgestaltung des interessanten Themas.
Weiterhin danke ich Herrn Prof. Dr. Wolfdieter A. Schenk für die Bereitschaft das Koreferat meiner Dissertation zu übernehmen.

Herrn Prof. Dr. Nils Metzler-Nolte danke ich für den großzügigen Zugang zu allen Einrichtungen des Lehrstuhls für Anorganische Chemie I der Ruhr-Universität Bochum, an welchem ich die ersten zwei Jahre meiner Promotion verbringen durfte.

Des Weiteren danke ich allen sehr herzlich, die durch ihre Hilfe zum Erfolg dieser Arbeit beigetragen haben:
Johanna Niesel für die Durchführung von Zellkulturexperimenten, Thomas Sowik für die Hilfe bei der Peptidsynthese, Fabian Schönfeld für die Messung und Auswertung der Kristallstruktur sowie meinem ehemaligen Praktikanten Christoph Nagel. Allen Mitarbeitern des Lehrstuhls für Anorganische Chemie I der Ruhr-Universität Bochum und des Arbeitskreises Schatzschneider am Institut für Anorganische Chemie der Julius-Maximilians-Universität Würzburg für die vielfältige Unterstützung und die anregenden Diskussionen. Herrn Jun.-Prof. Dr. Ingo Ott und Herrn Dr. Dr. Aram Prokop für die Zusammenarbeit im Rahmen der DFG Forschergruppe 630.

Darüber hinaus danke ich Caroline Bischof, Eva-Maria Geske, Annika Groß, Johanna Niesel und Thomas Sowik sehr herzlich, die durch ihre Freundschaft und jederzeitige Hilfsbereitschaft die letzten Jahre sehr bereichert haben.

Contents

Abbreviations

AAC	azide-alkyne cycloaddition
ATP	adenosine triphosphate
ATR	attenuated total reflection
bip	biphenyl
Boc	*tert*-butoxycarbonyl
bpy	2,2'-bipyridine
cGMP	cyclic guanylyl monophosphate
CORM	CO-releasing molecule
Cp	cyclopentadienyl
2CT	2-chlorotrityl
CuAAC	copper-catalyzed azide-alkyne cycloaddition
CV	crystal violet
DIFO	difluorinated cyclooctyne
DIPEA	diisopropylethylamine
DMAD	dimethyl acetylenedicarboxylate
DMF	*N,N*-dimethylformamide
DMSO	dimethylsulfoxide
dppe	1,2-bis(diphenylphosphino)ethane
dppn	benzo[*i*]dipyrido[3,2-*a*:2',3'-*c*]phenazine
dppz	dipyrido[3,2-*a*:2',3'-*c*]phenazine
dpq	dipyido[3,2-*d*:2',3'-*f*]quinoxaline
DTPA	diethylene triamine pentaacetic acid
EI	electron ionization
ESI	electro spray ionization
en	ethylendiamine
EPR	electron paramagnetic resonance
ET-CORM	enzymatic-triggerd CO releasing molecule
FAB	fast atom bombardment
FACS	fluorescence-activated cell sorting
FD	field desorption ionization
Fmoc	9-fluorenylmethoxycarbonyl
GTP	guanylyl triphosphate
HBTU	*O*-(tenzotriazol-1-yl)-*N,N,N',N'*-tetramethyluronium hexafluorophosphate
HO	heme oxygenase

HOBt	1-hydroxy-1*H*-benzotriazole
HOMO	highest occupied molecular orbital
HPLC	high-performance liquid chromatography
IBCF	isobutyl chloroformate
Im	imidazole
INT	2-(4-iodophenyl)-3-(4-nitrophenyl)-5-phenyltetrazolium chloride
IR	infrared
LDH	lactate dehydrogenase
LUMO	lowest unoccupied molecular orbital
Mb	myoglobin
MBHA	4-methylbenzhydrylamine
MLCT	metal-to-ligand charge transfer
MS	mass spectrometry
NAD	nicotinamide adenine dinucleotide
NHC	*N*-heterocyclic carbene
NMM	*N*-methylmorpholine
NMR	nuclear magnetic resonance
NOS	NO synthase
ONBD	oxanorbornadiene
OSu	*O*-succinimidyl
Pbf	2,2,5,7,8-pentamethyl-dihydrobenzofuran-5-sulfonyl
PBS	phosphate-buffered saline
phen	1,10-phenanthroline
PS	polystyrene
PTA	1,3,4-triaza-7-phosphatricyclo[3.3.1.1]decane
RP	reversed-phase
RT	room temperature
SERMs	selective oestrogen modulators
sGC	soluble guanylyl cyclase
SPAAC	strain-promoted alkyne-azide cycloaddition
SPECT	single-photon emission computed tomography
SPPS	solid-phase peptide synthesis
TBTU	*O*-(benzotriazol-1-yl)-*N,N,N',N'*-tetramethyluronium tetrafluoroborate
TFA	trifluoroacetic acid
TFAA	trifluoroacetic anhydride
TGF	transforming growth factor

THF	tetrahydrofuran
TIS	triisopropylsilane
TLC	thin-layer chromatography
TMS	tetramethylsilane
tppts	tris(sulphonatophenyl)phosphine
Trt	trityl
TrxR	thioredoxin reductase

1 Introduction

1.1 Medicinal organometallic chemistry

The term "Bioorganometallic chemistry" was first introduced by G. Jaouen in 1993 who defined it as the *"... study of organometallic complexes with bioligands..., and the use of these derived complexes in a variety of applications and basic research studies..."*.[1] This research area touches the fields of organometallic chemistry, medicine, biology and biochemistry. Whereas bioorganometallic chemistry in general also covers naturally occuring organometallic motives in enzymes and proteins such as cobalamines and hydrogenases,[2] medicinal organometallic chemistry focuses on the therapeutical and diagnostic applications of organometallic compounds. In addition to coordination compounds such as cisplatin and its derivatives which have been applied with great success as metal based anti-tumor therapeutics for over 30 years, also organometallic compounds, that contain at least one carbon atom directly bound to a metal or metaloid, have turned out to be promising candidates for use in anti-cancer therapy.[3]

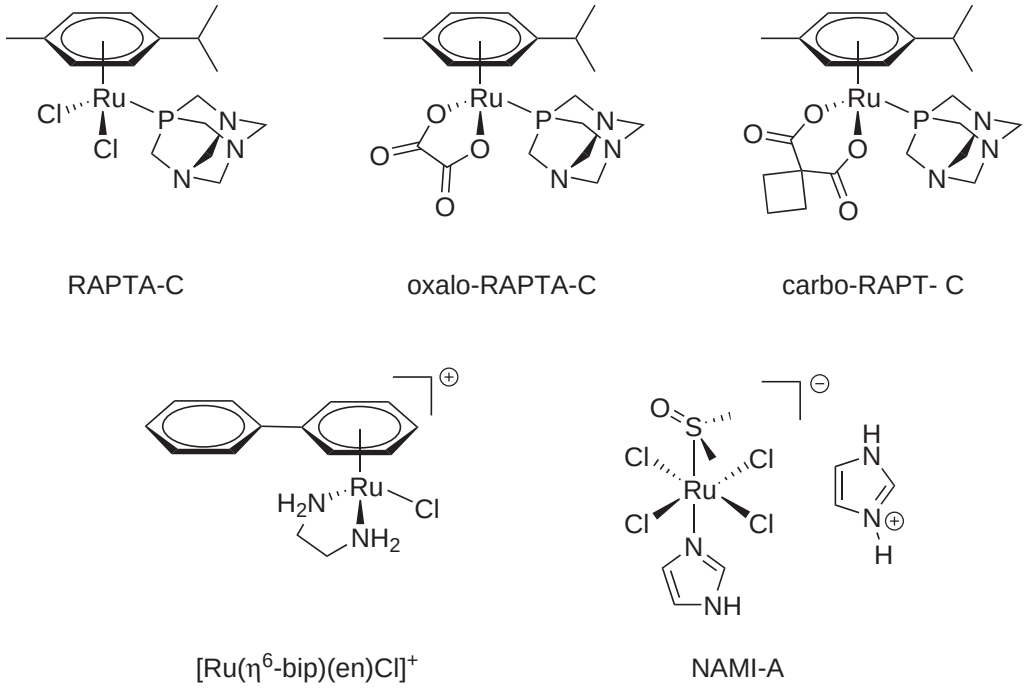

Fig. 1.1: Ruthenium-based organometallic and coordination compounds used as anticancer drugs.

The application of ruthenium arene half-sandwich complexes as potential anti-cancer therapeutics has been investigated in depth by the groups of Dyson and Sadler. "Piano stool" type complexes of the general stucture [(η^6-arene)Ru(en)Cl]$^+$ as shown in Fig. 1.1 were found to exhibit similarities to cisplatin in their activation pathways such as chloride ligand hydrolysis to give an aquo species which then binds to nucleobases of the DNA with a high preference for the N(7) of guanidine. As known for cisplatin, the

hydrolysis does not take place at chloride concentrations present in the blood plasma, but only inside the cell where the chloride concentration is about 25 times lower compared to the blood plasma.[4,5] Moreover, [(η^6-arene)Ru(en)Cl]$^+$ complexes show activity towards cisplatin resistant cell lines, which limits the comparability to cisplatin with regard to the mode of action.[6] Derivatives of ruthenium η^6-arene complexes bearing the RAPTA ligand and two hydrolyzeable chlorides were first thought to act in analogy to [(η^6-arene)Ru(en)Cl]$^+$ and cisplatin type complexes. Therefore, derivatives of the parent compound RAPTA-C were prepared by Dyson *et al.* (oxalo-RAPTA-C, carbo-RAPTA-C, Fig. 1.1) in which the dicarboxylate ligand dissociates in a more controlled way compared to the chloride ligands.[7] In fact, introducing the carboxylate ligand did not lead to an increased *in vitro* cytotoxicity compared to the parent compound RAPTA-C and in addition most RAPTA type complexes were found to be significantly less cytotoxic than cisplatin. Despite thier low cytotoxicity, however, RAPTA-C was highly active against lung metastases in mice suffering from the MCa mammary carcinoma while the effect on the primary tumor was rather low. A similar effect has only been observed for NAMI-A until now which also shows a good antimetastatic activity but low activity on primary tumors (Fig. 1.1).[8] Moreover, NAMI-A was the first ruthenium compound that was investigated on human beings and recently entered phase I/II clinical trials for the treatment of patients suffering from non-small cell lung carcinoma.

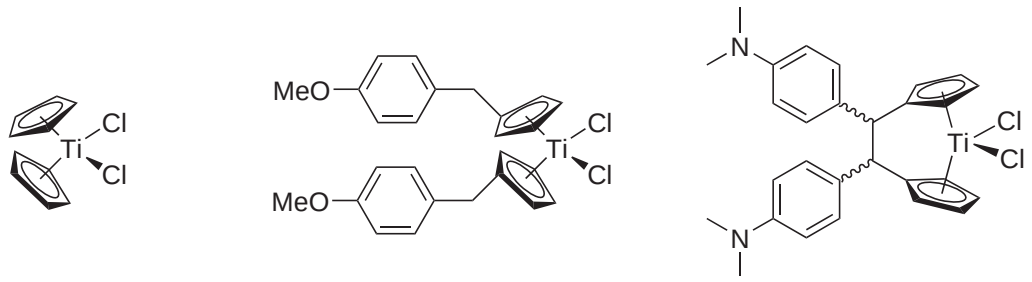

titanocene dichloride titanocene Y titanocene X

Fig. 1.2: Titanocene dichloride and its derivatives titanocene X and Y.

Another class of compounds that follows a structural cisplatin analogy, showing a *cis*-dihalide motif, is represented by the metallocene dichlorides which have been investigated by H. Köpf and M. Tacke (Fig. 1.2). Although metallocene dichlorides of titanium, zirconium, vanadium, niobium, and molybdenum have been investigated in a medicinal context,[9,10] only titanocene dichloride entered clinical trials.[11]. Nevertheless, titanocene dichloride showed some major drawbacks such as low solubility in aqueous medium and hydrolytic instability of the Cp rings, all together making a pharmacological formulation difficult, which finally led to its rejection from clinical trials. Thus, the solubility was increased by introducing amino groups to the organic ligand system and the hydrolytic stability was improved by preparing *ansa*-titanocenes (titanocene X,

Fig. 1.2).[12,13] But despite the efforts that were taken to make titanocene dichloride derivatives more suitable for medicinal application, none of them has re-entered clinical trials so far. Regarding the mode of action, DNA binding of the $[Cp_2Ti]^{2+}$ moiety via the phosphate backbone (titanocene Y, Fig. 1.2), apoptosis induction as well as topoisomerase inhibition have been suggested, but the exact mode of action is still unclear.[14–16]

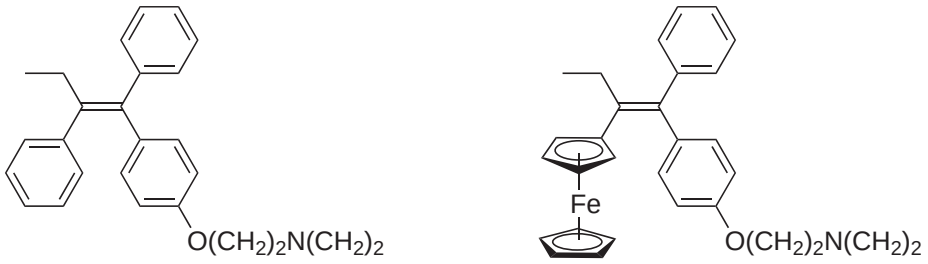

tamoxifen ferrocifen

Fig. 1.3: The selective estrogen modulators (SERMs) tamoxifen and ferrocifen.

Beside anticancer drugs like ruthenium arene or cisplatin derivatives which interact with their expected target mostly via covalent binding, there are also some bioactive organometallic compounds known which exhibit redox-activity or non-covalent receptor binding as their specific mode of action. In this context, ferrocene derivatives of the organic anticancer drug tamoxifen, the so-called ferrocifenes, have been prepared by Jaouen *et al.* (Fig. 1.3).[17–19] Tamoxifen it self belongs to the class of selective estrogen modulators (SERMs) that are used in the treatment of hormon-dependent human breast cancer. Whereas estrogen receptor-expressing breast tumors ER(+) are sensitive towards treatment with SERMs, the estrogen receptor non-expressing breast tumors ER(-) are not. Interestingly, it was found that when one of the phenyl rings in the tamoxifens was exchanged for a ferrocene moiety, the ferrocifen derivatives obtained were also found to be active against the ER(-) type tumors which are not susceptible to treatment with tamoxifens. The common antiproliferative action of tamoxifens and ferrocifens origins from a competitive binding to the estrogen receptor, which leads to a down-regulation of the DNA transcription in the tumor cell. In contrast, the activity of ferrocifens on tumors that do not express the estrogen receptor is proposed to origin from the redox properties of the ferrocene moiety as a second mode of action. In the proposed mechanism, ferrocene acts as a "redox antenna" which promotes oxidation of the metabolite hydroxyferrocifen and finally activates the oxidized intermediate species for the attack by nucleophiles. For a detailed mechanism see: Gasser *et al.*[20]

Another class of compounds where the metal center is not directly involved in the

mode of action but provides its ligand sphere as a shape mimic for an organic moiety, is represented by the ruthenium and iridium organometallic derivatives of the protein kinase inhibitor staurosporine which have been prepared by the group of E. Meggers (Fig. 1.4).[21,22]

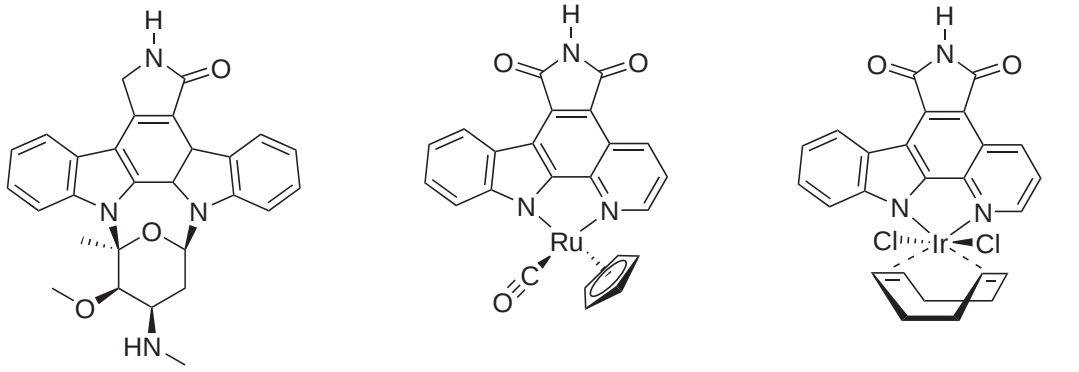

Fig. 1.4: Protein kinase inhibitors staurosporine and its ruthenium and iridium-based analogues.

Kinases are one of the largest enzyme family and therefore play an important role in various aspects of cell physiology such as angiogenesis,[23] making them an important therapeutic target.[24] The introduction of a six-coordinate metal center allows the versatile spatial arrangement of ligands to create various three-dimensional structures, thus providing the opportunity for a fine-tuning of the kinase binding properties. The so prepared ATP-competetive ruthenium-based kinase inhibitors show inhibition values in the nano- to piocomolar range and the interaction with their expected target has been confirmed by co-crystallization of the ruthenium complexes with protein kinases and subsequent characterization by X-ray analysis.

Since auranofin, as one of the first gold coordination compounds, has found wide application in the treatment of rheumatoid arthritis, also organometallic gold compounds have attracted considerable interest as therapeutic agents. Organometallic gold compound that are currently investigated for their potential therapeutic application can be devided in two classes: gold(I) or gold(III) complexes with *N*-heterocyclic carbene ligands (NHC) and cyclometalated gold(III) complexes.[25]

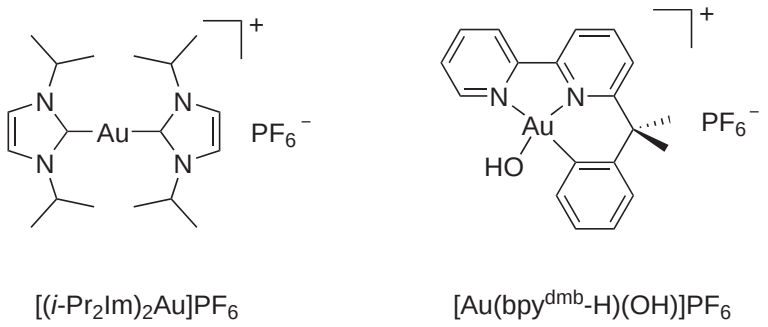

$[(i\text{-}Pr_2Im)_2Au]PF_6$ $[Au(bpy^{dmb}\text{-}H)(OH)]PF_6$

Fig. 1.5: Organometallic gold compounds with cytotoxic activity.

A representative for a NHC complex is $[(i\text{-}Pr_2Im)_2Au]PF_6$ (Fig. 1.5, left) which accumulates in mitochondria of cancer cells, induces apoptosis via caspase-3 and caspase-9 activation and moreover, selectively inhibits mitochondrial thioredoxin reductase (TrxR) which plays a key role in several chronic diseases such as rheumatoid arthritis.[26,27] Furthermore, in a larger series of $[(R_2Im)_2Au]^+$ complexes, the lipophilicity was tuned by introducing various alkyl residues to the NHC ligand to modulate the bioavailability of these complexes. The activation mechanism of gold(I) NHC complexes *in vivo* is supposed to occur via sequential displacement of the NHC ligands by selenocystein and cystein residues of thioredoxin reductase.[26] Since gold(III) complexes are rather unstable under physiological conditions, the preparation of cyclometalated complexes has been used as a strategy to stabilize the high +III oxidation state. Complexes like $[Au(bpy^{dmb}\text{-}H)(OH)]PF_6$ (Fig. 1.5, right) were found to have IC_{50} values in the low micromolar range on HT-29 human colon cancer cells and MCF-7 human breast cancer cells. Morover, their activation mechanism proceedes via hydrolysis of the labile ligand.[25,28] Although many gold(III) complexes show *in vitro* cytotoxcity on human cancer cells, only a few are also found to be active *in vivo*.

Whereas all organometallic compounds mentioned so far, were investigated for their therapeutic application, organometallic complexes of technetium are used for diagnostic purposes. Compounds containing the ^{99m}Tc isotope, which is a γ-emitter, have been established as radiopharmaceuticals for the use in single photon emission computed tomography (SPECT). The clinical application of the ^{99m}Tc isotope for imaging purposes benefits from its moderate half-life time of 6.02 h as well as its continous availability from a generator in hospital at reasonable cost.[29]

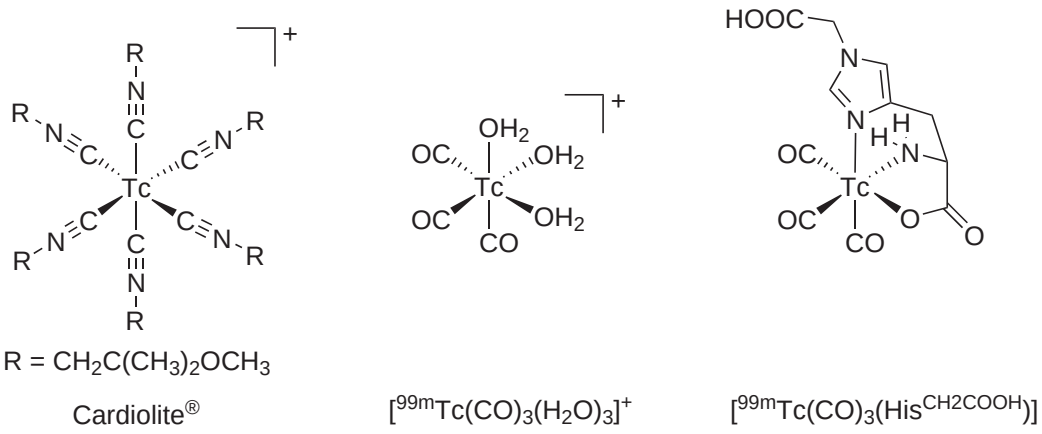

Fig. 1.6: Organometallic $^{99m}Tc^{I}$ complexes for biological applications.

One of the metal-essential first-generation radiopharmaceticals of technetium used in medicinal diagnostics is the isonitrile complex shown in Fig. 1.6 on the left, known under its trade name Cardiolite® which is used for myocardial perfusion imaging. The second generation of technetium radiopharmaceuticals, which can be termed metal-labeled rather than metal-essential, the $Tc(CO)_3$ moiety plays a crucial role. The common precursor of the technetium techentium tricarbonyl moiety is the facially coordinated aquo complex $[^{99m}Tc(CO)_3(H_2O)_3]^+$ (Fig. 1.6, middle) which is air- and water-stable as well as easy to prepare from pertechnetate obtained from a common technetium generator.[30,31] The so obtained technetium aquo complex found wide application in the radiolabeling of biomolecules such as amino acids (Fig. 1.6, right) and peptides[32,33] as well as carbohydrates for *in vivo* imaging purposes.[34]

1.2 Carbon monoxide as a gasotransmitter

Since the toxic physiological effect of carbon monoxide through binding to hemoglobin and thus blocking of the oxygen transport, was first described by J.B. Haldane in the beginning of the twentieth century, CO always has kept its bad reputation in the public as a silent killer. Nevertheless it is endogenously produced in the human body and possesses a crucial physiological role as a molecular messenger. Endogenously produced CO results from the oxidative degradation of hemoglobin through heme oxygenase (HO) which exists in two isoforms, the inducible HO-1 and the constitutively expressed HO-2. The induction of HO-1 is stimulated in tissues by various forms of cellular stress associated with an imbalanced redox state of the cell, thus allowing the generation of high local concentrations of CO to take cytoprotective or homeostatic actions.[35] This corresponds with the observation that patients suffering from a number of diseases such as cystic fibrosis, arthritis or diabetes show elevated levels of HO-1 and moreover exhale significantly more CO than healthy humans. In the degradation process of hemoglobin, heme is converted to biliverdin-IXα by oxidation in the α-*meso* position accompanied by the release of CO and Fe^{2+}. Biliverdin-IX α is then converted to bilirubine-IX α by reduction of the D-pyrrole ring through biliverdin reductase (Fig. 1.7).[36]

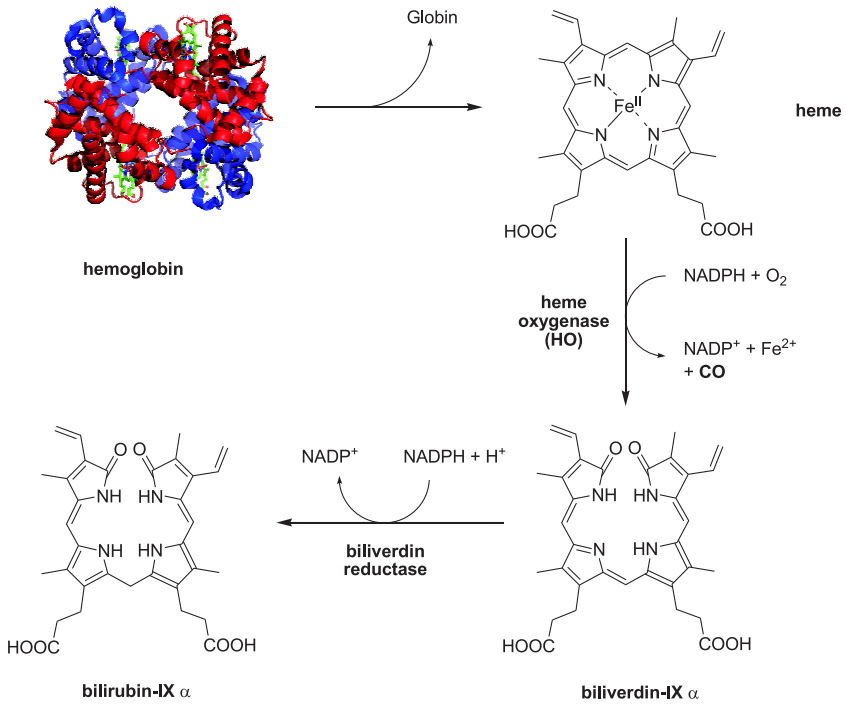

Fig. 1.7: Degradation process of hemoglobin and endogenous production of carbon monoxide by hemeoxygenase (HO).

Since endogenously generated CO has beneficial physiological effects due to a high local concentration on the cellular level, and exogenous CO causes severe toxic systemic effects when applied in high concentration, these two conditions should guide

the development of therapeutic applications for carbon monoxide. The administration of CO gas by inhalation has beneficial effects in the animal model as well as in first clinical trials in the treatment of various proliferative disorders, suppression of transplant rejection, ischemia-reperfusion injury and acute liver failure in mice and rats, thus reflecting the previous defined guideline by proving that also low systemic concentrations of CO represent favourable conditions.[37,38] On the cellular level, heme-containing enzymes and proteins are considered to be the most likely targets for CO, since there is no evidence for an interaction with non-heme containing targets, as it was postulated for the p38 protein kinase.[38] The most-well identified target for CO, in analogy to NO, is the soluble guanylyl cyclase (sGC), which converts guanylyl triphosphate (GTP) to cyclic guanylyl mono-phosphate (cGMP) which amongst others triggers vasodilatory effects (Fig. 1.8).[39]

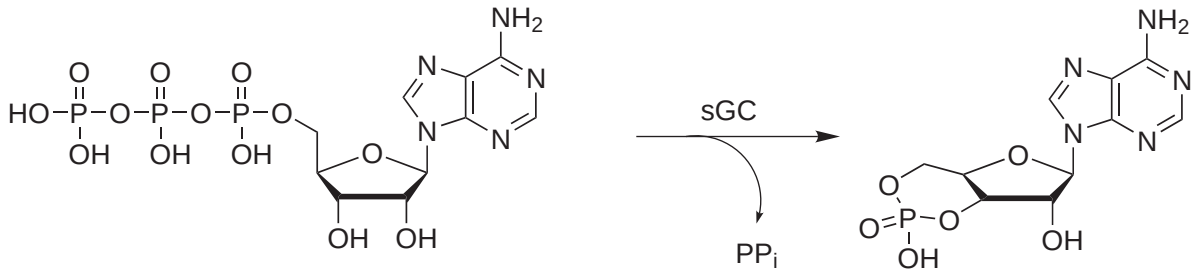

Fig. 1.8: Conversion of guanylyl triphosphate (GTP) to cyclic guanylyl mono-phosphate (cGMP) by soluble guanylyl cyclase (sGC).

Another relationship between the physiological effect of NO and CO is found in the NO synthase pathway. Here, binding of CO to the heme moiety in NO synthase (NOS) increases the production of NO, which in turn increases the level of HO-1 which has several cytoprotective effects as described before. Also, the mitochondrial cytochrome c oxidases were found to be a target of CO where it inhibits the electron transport and triggers the generation of reactive oxygen species which in turn are important cellular messengers in the induction of apoptosis.[35,38] Furthermore, an direkt or indirect triggering of large-conductance calcium-dependent potassium channels (BK_{Ca}) by carbon monoxide was suggested. BK_{Ca} channels are present in almost every kind of tissue and play an important role in the regulation of the vascular tone and the cell membrane potential as well as the release of neurotransmitters.[40] Although the exact molecular mechanisms by which CO influences cellular proceses are not well understood, the assumption of an interaction with metal-proteins as a general mode of action is quite obvious.[35]

1.3 CO releasing molecules (CORMs)

As outlined in Chapter 1.2 for therapeutic applications of carbon monoxide it is desirable to generate elevated local conentrations in the targeted tissue, which corresponds to the naturally occuring process when increased levels of CO are generated by elevated expression of heme oxygenase 1 (HO-1) as a response to cellular stress. To achieve this, there is a need for a carrier system that allows a controlled delivery of defined doses of CO. Beside metal carbonyl complexes, where the CO is bound as a ligand to a metal center, three other classes of compounds have also been found to be suitable carriers that release carbon monoxide under mild physiological conditions: oxalates, dialkylaldehydes and boroncarboxylates. Whereas the first two, oxalates and dialkylaldehydes, were found to release CO much too slowly to be suitable for biological application, one representative of the latter class, disodium boranocarbonate (**CORM-A1**), finds wide application in preclinical testing.[41] Although efforts were made to tune the CO release properties of boroncarboxylates through derivatization of disodium boranocarbonate, these attempts did not lead to significant changes in the CO release profile.[42,43] After the initial exploration of non-metal based CORMs, metal carbonyl complexes have found considerable interest within the last decade and turned out to be the most favourable class of CORMs.[44] One of the first representatives reported is the ruthenium carbonyl dimer $[Ru(CO)_3Cl_2]_2$ (Fig. 1.9, **CORM-2**) which is also commercially available and has been extensively studied *in vitro* and in preclinical animal disease models.[39,45] Whereas **CORM-2** is rather insoluble in aqueous media, *fac*-$[Ru(CO)_3Cl(\kappa^2$-glycinate)] (**CORM-3**) represents the first water-soluble CORM that was studied in depth both *in vitro* and *in vivo* with a special focus on its vasodilatory and anti-inflammatory effects.[46,47]

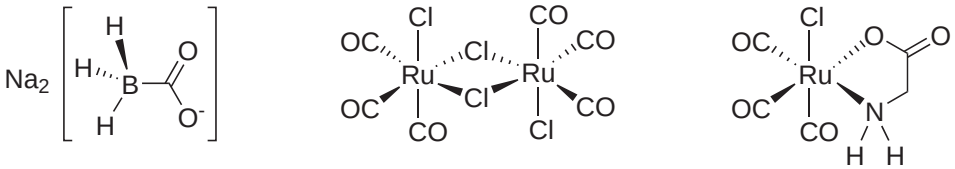

CORM-A1
$t_{1/2}$ = 21 min

CORM-2
$t_{1/2}$ ~ 1 min

CORM-3
$t_{1/2}$ ~ 1 min

Fig. 1.9: First CO releasing molecules (CORMs) and their half-life times of CO release: $Na_2[H_3BCOO]$ (**CORM-A1**), $[Ru(CO)_3Cl_2]_2$ (**CORM-2**) and *fac*-$[Ru(CO)_3Cl(\kappa^2$-glycinate)] (**CORM-**3).

Moreover, the incorporation of **CORM-3** into micells was studied for a targeted delivery[48] as well as its interaction with proteins such as lysozyme and human serum albumin in order to evaluate their role in transportation and activation of **CORM-3** *in vivo*.[49]

Since the first CORMs, based on ruthenium, were reported in 2001, many other classes of metal carbonyl complexes have been explored, mostly covering the groups IV to VIII

of the d-block elements. Among them are complexes of vanadium, chromium, molybdenum and tungsten,[50,51] manganese[52] and rhenium,[53–55] iron[51,56–58] and cobalt[59] as well as iridium.[60] A selection of CORMs based on group VI metals is depicted in Fig. 1.10.

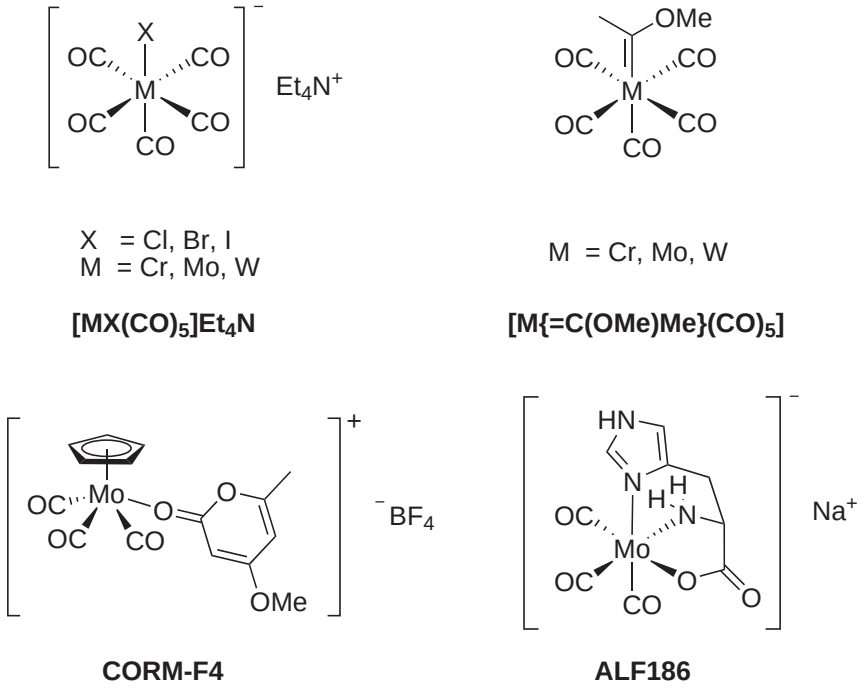

Fig. 1.10: Selected group VI metal-based CORM structures: $[MX(CO)_5]Et_4N$, $[M\{=C(OMe)Me\}(CO)_5]$,[50] CORM-F4[51] and ALF186[61].

A common feature of all CORMs listed above is the ablility to release CO spontaneously upon dissolution in an appropriate solvent, mostly aqueous media. This process occurs via ligand displacement of one or more carbonyl ligands by a solvent molecule either in a dissociative or associative pathway, often followed by oxidation of the metal which leads to further release of CO. As the stability of the M-CO bond is not only determined by the nature and oxidation state of the metal center, but also by the *trans*-effect, the choice of the ancilliary ligands is a crucial point in the conceptual design of a CORM and allows tuning of the CO release profile.[36] Nevertheless, the spontaneous release of CO from a metal carbonyl complex in solution makes a biological application challenging if a targeted delivery is desired. In order to gain control over the temporal and spatial release of CO, a stable metal carbonyl complexes and a certain trigger are needed that will allow accumulation of the CORM in the targeted tissue and activation of CO release only when the target is reached. A strategy that uses enzymatic cleavage of an ester as a trigger has recently been reported.[62] The CO release from an acyloxybutadiene iron tricarbonyl complex is induced by the cleavage of the dienylester through pig liver esterase which gives an instable hydroxybutadiene and finally leads to a loss of the iron tricarbonyl unit (Fig. 1.11). These componds have been termed

enzyme-triggered CORMs (ET-CORMs).

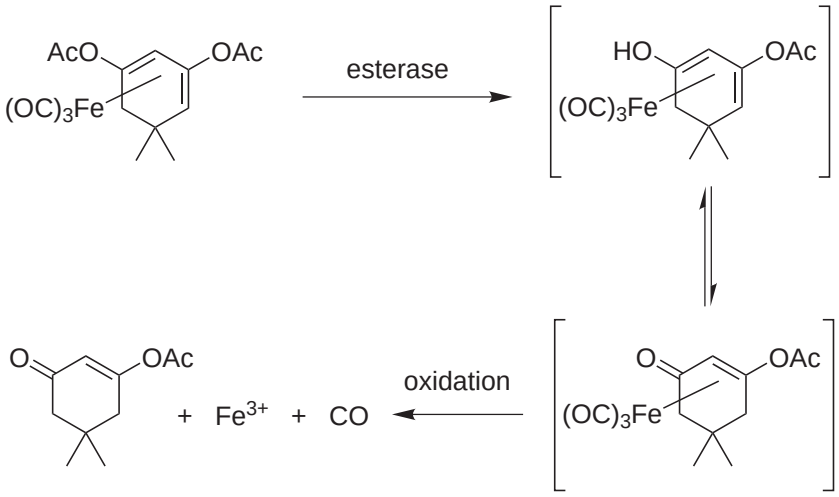

Fig. 1.11: Proposed mechanism for the esterase-triggered CO release from an acyloxybutadiene iron tricarbonyl complex.

Since metal carbonyl complexes are well-known to exhibit a rich photochemistry involving the displacement of carbonyl ligands from an excited state, the idea to establish photoactivation as a trigger for CO release is also promising. The application of such PhotoCORMs has recently been reviewed in detail.[63] After the photoactivated release of CO from dimanganese decacarbonyl ($Mn_2(CO)_{10}$, CORM-1) as one of the first PhotoCORMs and its application in preclinical animal desease models was reported in 2002,[45] the first water-soluble PhotoCORM $[Mn(CO)_3(tpm)]PF_6$ (CORM-L1) (Fig. 1.12, **Mn1**) was described in 2008.[64]

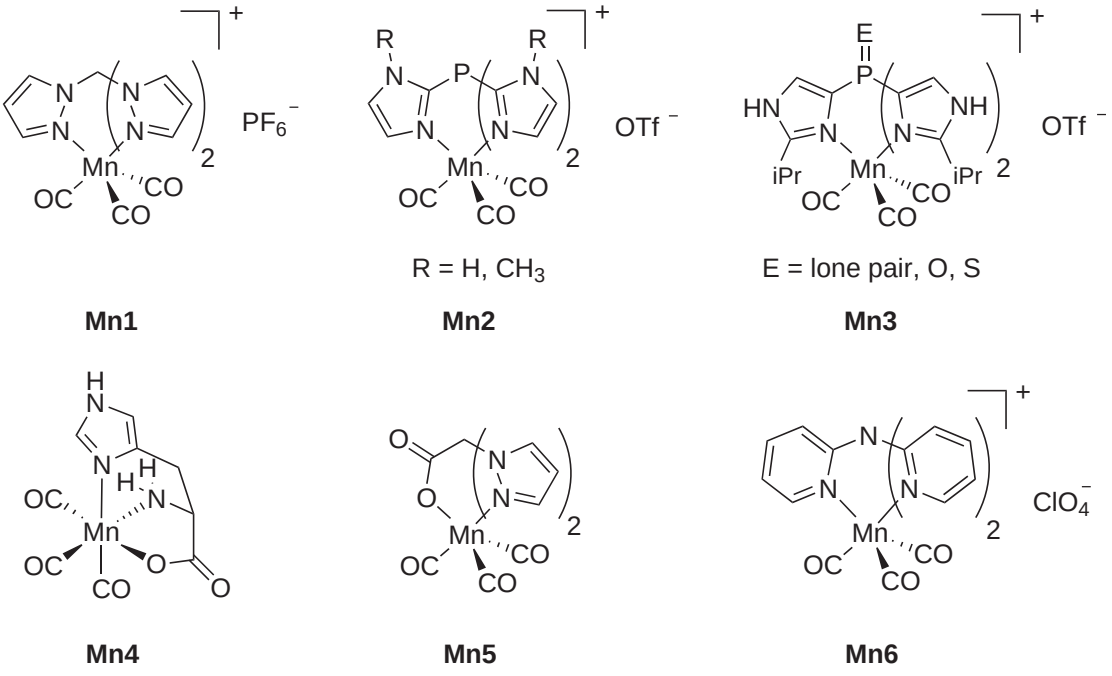

Fig. 1.12: Selected manganese tricarbonyl complexes the have been established as PhotoCORMs.

It was found that CORM-L1 is stable in the dark but releases two equivalents of CO upon irradiation at 365 nm and has a significant light-induced cyotoxicity on HT-29 human colon cancer cells. Moreover, the cellular distribution of the corresponding chloride salt in HT-29 cells was imaged by Raman microspectroscopy using the signal of the carbonyl vibration a an internal probe.[65] In order to develope a strategy for a targeted delivery of PhotoCORMs in biological systems, the $[Mn(CO)_3(tpm)]^+$ complex was linked to a carrier peptide[66] as well as to silica nanoparticles which may allow tumor targeting taking advantage of the enhanced permeability and retention effect.[67] Studies on the photolysis of CORM-L1 by UV/Vis, IR as well as EPR spectroscopy showed that a dinuclear μ-O-Mn_2^{III} species is the final decomposition product.[68] In manganese tricarbonyl complexes with imidazolylphosphane ligands, the substitution pattern of the tridentate ligand was found to influence the CO release properties. Whereas imidazol-2-ylphosphane (**Mn2**) complexes release two equivalents of CO upon irradiation at 365 nm, the corresponding imidazol-4-ylphosphane (**Mn3**) complexes release just one equivalent.[69] The neutral $[Mn(CO)_3$(histidinate)] complex (**Mn4**) releases only one equivalent of CO under irradiation at 365 nm with a half-life time of about 90 min which is rather slow compared to $[Mn(CO)_3(tpm)]PF_6$ (CORM-L1) which has a half-life time of 10 min.[70] A similar behavior was observed for the neutral bispyrazolyl complex (**Mn5**). The polypyridyl complex **Mn6** was also found to relase CO upon irradition with light in the spectral range above 350 nm and moreover causes light-induced vasorelaxation of mouse aorta.[71]

The water-soluble tungsten(0) pentacarbonyl complex $Na_3[W(CO)_5$(tppts)] (with tppts = tris(sulphonatophenyl)phosphine, Fig. 1.13, **W1**) is stable in solution under aerobic conditions in the dark and releases CO upon irradiation at 300 - 370 nm. Studies on the mechanism of CO release in aqueous solution revealed the presence of an intermediate aquo species ($[W(CO)_4H_2O$(tppts)]$^{3-}$) that is oxidized under aerobic conditions, thus leading to further release of CO.[72] The iron cysteamine dicarbonyl complex **Fe1** as well as its derivative **Fe2** represent the first examples of PhotoCORMs that release CO upon irradiation with visible light using a LED lamp with λ_{ex} = 470 nm or an common halogen lamp which is more favorable for biological applications than irradiation at 365 nm as it was used for the CO release from all other PhotoCORMs presented so far. The use of visible light instead of irradiating at 365 nm is supposed to reduce the cell damage caused by UV light. Both complexes release two equivalents of CO and moreover, **Fe1** was tested in the light-induced activation of CO-sensitive ion channels.[73,74] The iron monocarbonyl complex **Fe3** shows very good stability in aqueous solution in the dark but efficiently releases CO when irradiated with UV light and moreover, a photoinduced cytotoxicity against PC-3 prostate cancer cells.[75]

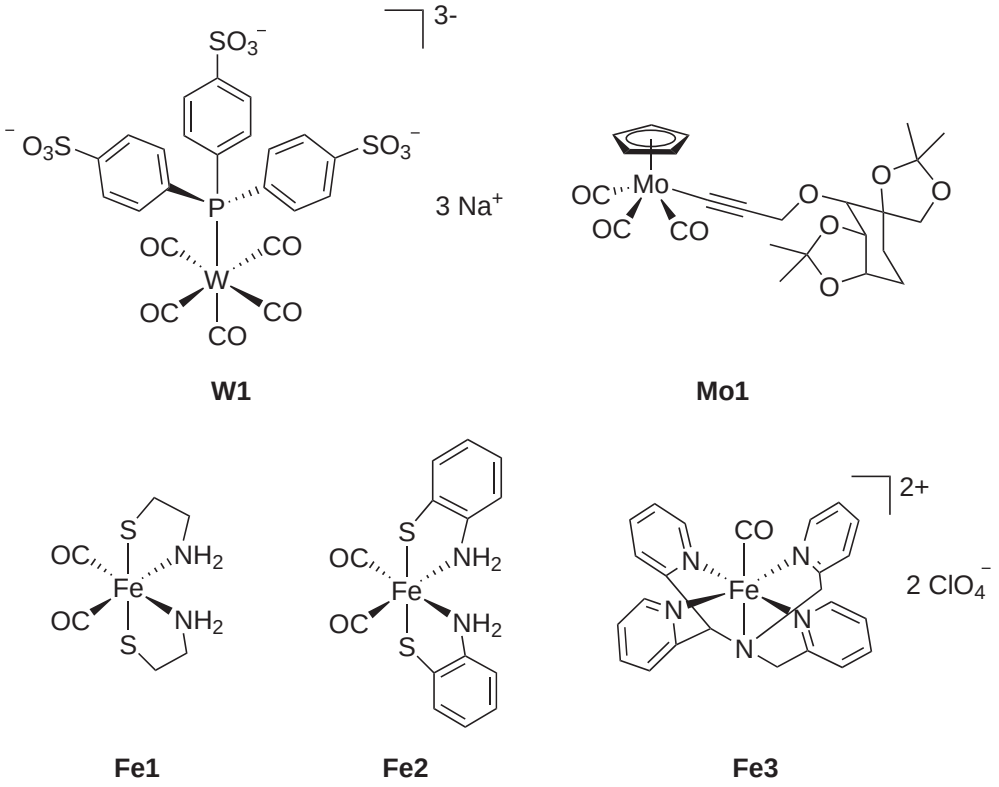

Fig. 1.13: Selected PhotoCORM based on molybdenum, tungsten and iron.

1.4 Photochemistry and photophysics of [M(CO)$_4$(α-diimine)] complexes of group VI transition metals

Since the synthetic approach to [M(CO)$_4$(α-diimine)] complexes with group VI transition metals was investigated in detail for the first time in the early 1960's by Stiddard and Hull,[76,77] a lot of research has been carried out on the rich photophysics and photochemistry of these compounds over the last fifty years. [M(CO)$_4$(α-diimine)] complexes carry four carbonyl ligands which stabilize the low-valent d^6 metal center by their strong σ-donor/π-acceptor properties but also bear electron-accepting α-diimine ligands ranging from polypyridines such as 1,10-phenanthroline oder 2,2'-bipyridine to 1,4-diaza-1,3-butadiene ligands.[78] This gives rise to strong electronic absorption bands in the visible as well as in the near-UV region which are crucial for the access to the photochemical and photopysical properties of those complexes. The absorption band in the visible region is usually located in the range of 450 to 600 nm, depending on the nature and the substitution pattern of the α-diimine ligand, and is assigned to a metal-to-diimine MLCT transition.[79] This is supported by the fact that these absorptions are not present in [M(CO)$_4$(diamine)] complexes with pure σ-donor ligands such as ethylenediamine or *N,N,N'N'*-tetramethylethylenediamine having no electron-accepting properties. At lower energies, a second band is found at around 400 nm which is assigned to a metal-to-CO MLCT transition. Moreover, [M(CO)$_4$(α-diimine)] complexes exhibit a negative solvatochromic behavior, resulting in a hypsochromic shift of the metal-to-diimine MLCT band with increasing solvent polarity.[78]

The photochemical reactivity of these complexes exclusively results in substitution reactions of an axial CO ligand. In general, there are two different mechanisms by which ligand displacement can occur in octahedral or pseudo-octrahedral complexes.[78] The first one is the dissociative photosubstitution shown in Fig. 1.14. In this pathway, dissociation of the metal-CO bond takes place upon excitation, generating a square-pyramidal fragment with one free coordination site. In a later stage of the reaction, this site then becomes occupied by a solvent molecule, which in turn can be replaced by other more nucleophilic ligands such as phosphines or imines. The independence of the photochemical quantum yield from the chemical nature, sterical demand and concentration of the entering ligand indicates that the dissociation is the rate-determining step in this reaction which follows a zero-order rate law.[80]

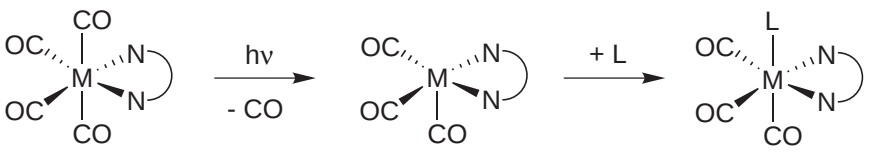

Fig. 1.14: Dissociative photosubstitution mechanism of the axial CO ligand in [M(CO)$_4$(α-diimine)] complexes.

The second mechanism is the associative photosubstitution shown in Fig. 1.15. Here, the ligand L enters the coordination sphere of the excited state complex whereupon the carbonyl ligand dissociates simultaneously via a seven-coordinate intermediate. In contrast to the dissociative mechanism, the photochemical quantum yield strongly depends on the concentration as well as the chemical nature of the entering ligand, as indicated by a first order, second order, or pseudo-first order rate law (in the presens of an excess of ligand L).

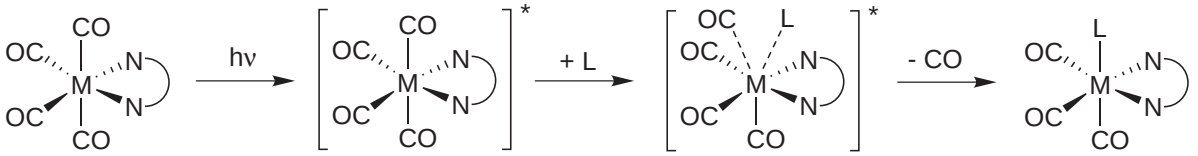

Fig. 1.15: Associative photosubstitution mechanism of the axial CO ligand in [M(CO)$_4$(α-diimine)] complexes.

Within the group VI metals, several trends in the photochemical reactivity are observed. The photochemical quantum yield for CO substitution decreases in the order Cr » Mo > W. Also, the mechanism of substitution varies within the triad. Whereas molybdenum and tungsten diimine complexes follow parallel dissociative and associative pathways, the contribution of an associative mechanism is negligible or even absent for chromium.[78,80,81] For molybdenum and tungsten, the contribution of the associative and dissociative pathways also depends on the irradiation wavelength used. In general, near-UV irradiation predominantly leads to a dissociative substitution involving metal-to-CO MLCT excited states while visible irradiation results in an associative substitution involving metal-to-imine MLCT excited states. Moreover, the observed overall quantum yield for the CO photosubstitution decreases dramatically when changing from near-UV to visible irradiation.[78,81]

1.5 Click reactions in bioconjugation strategies

The term "click" reaction was first used by Sharpless in 2001[82] to classify a variety of reactions that match criteria such as high efficiency, chemo- and stereoselectivity, modularity as well as fast reaction kinetics.[83] A subclass of click reactions that tolerate functional groups present in bio(macro)molecules has been termed "bioorthogonal".[84] These have a wide scope in the labeling of biomolecules with markers such as dyes[85] or metal complexes[66] as well as in linking together large peptides or proteins.[86]

1.5.1 α-Effect amines in bioconjugation reactions

Since aldehydes and ketones can easily be incorporated into biomolecules such as peptides, the use of imine-based chemistry in bioconjugation reactions has found wide application due to its high chemoselectivity. A major drawback of the reversible reaction of primary amines with carbonyl compounds is the fact that under acidic conditions, the equilibrium favours the free carbonyl, causing an inherently low efficiency.[87] A solution to this issue is the use of amines which have an electronegative atom containing one or more lone pairs adjacent to the nucleophilic nitrogen atom and thus possess a higher nucleophilicity than other amines. The enhanced nucleophilicity of such amines leads to the formation thermodynamically stabilized imines that are favoured by the equilibrium shown in Fig. 1.16. The enhanced nucleophilicity triggered by adjacent heteroatoms was first reported in 1960[88] for a series of diverse nucleophiles and later named the "α-effect" by Edwards and Pearson.[89] Detailed investigations, especially on the reactivity of α-effect amines, were carried out by Jencks and Carriuolo a few years later.[90]

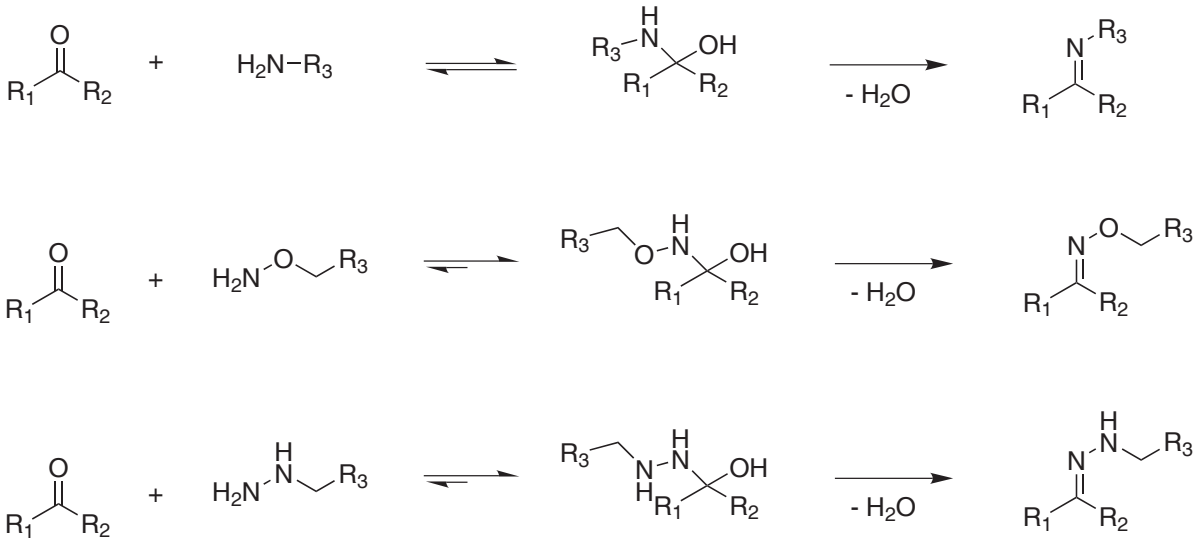

Fig. 1.16: Reactions of carbonyls with amines and α-effect amines towards imines, oximes and hydrazones.

Bioconjugation strategies take advantage of the formation of hydrolytically stable Schiff bases. Examples usually involve α-effect amines such as aminooxy or hydrazide groups that react with either aromatic aldehydes or glyoxylates in oxime and hydrazone ligations, respectively.[87] These reactions proceed in aqueous solution with a pH optimum of 5-6 and are therefore highly useful for labeling of biomacromolecules. However, they are limited to *in vitro* applications since the pH optimum cannot be achieved in most tissues *in vivo*.[86] The equilibrium constants are typically in the range of 10^4 - 10^6 l·mol^{-1} for hydrazone ligations and > 10^8 l·mol^{-1} for oxime ligations. This is important when reactions are carried out with reactants at low micromolar concentration. In the case of small equilibrium constants, the system re-equilibrates at low concentrations accompanied by partial dissociation of the product, leading to incomplete reactions.[91] An advanced method to enhance the reaction rates of α-effect amine ligations without applying one reactant in large excess is the use of aniline as a nucleophilic catalyst. In this strategy, the carbonyl component reacts with aniline in a pre-equilibrium to give a protonated aniline Schiff base that efficiently reacts with the α-effect amine in a transimination reaction. Dirksen *et al.* showed that imine ligation reactions in aqueous solution could be accelerated up to 400-fold at pH 4.5 and still up to 40-fold at unfavourable pH values (pH 7) by nucleophilic catalysis as shown in Fig. 1.17.[87]

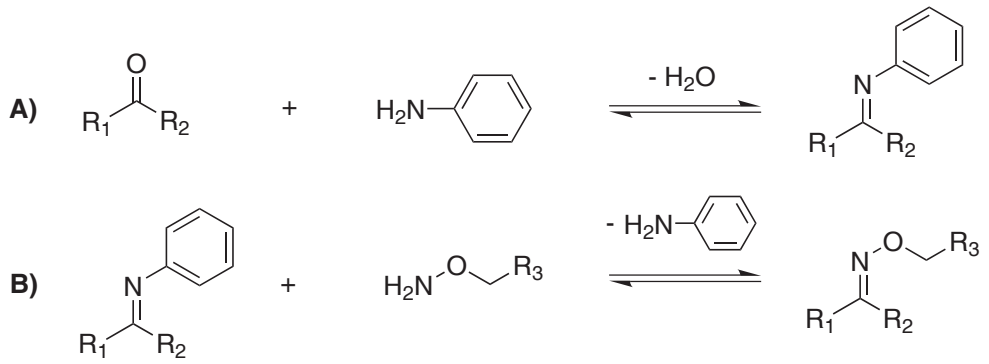

Fig. 1.17: Aniline-catalyzed oxime ligation. A) imine formation, and B) transimination.

1.5.2 Azide-alkyne click reactions

Among the click reactions, the most widely used is probably the copper(I)-catalyzed 1,3-dipolar cycloaddition of azides and terminal alkynes (CuAAC) which gives 1,2,3-triazoles. Compared to the thermal 1,3-dipolar Huisgen cycloaddition,[92] which shows no regioselectivity and gives a 1:1 mixture of 1,4- and 1,5-substituted triazols,[93] the copper-catalyzed version selectively gives the 1,4-substituted isomer only (Fig. 1.18).[94]

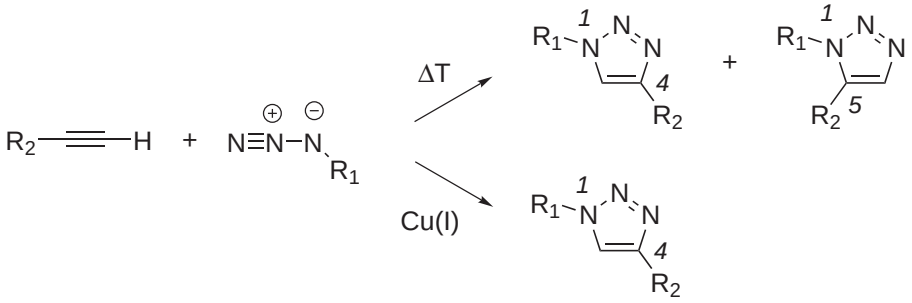

Fig. 1.18: Thermal 1,3-dipolar cycloadditions (top) and copper(I)-catalyzed (bottom) of azides and alkynes.

The stepwise mechanism of the catalyzed variant is assumed to start with the formation of a Cu(I) acetylide complex via side-on coordination of the alkyne followed by deprotonation and change to a terminal binding mode.[95] The next step involves a copper-azide coordination followed by formation of an allene-metallacycle to give the 1,2,3-triazole with C(5)-coordinated copper and subsequent reductive elimination of the copper species (Fig. 1.19).

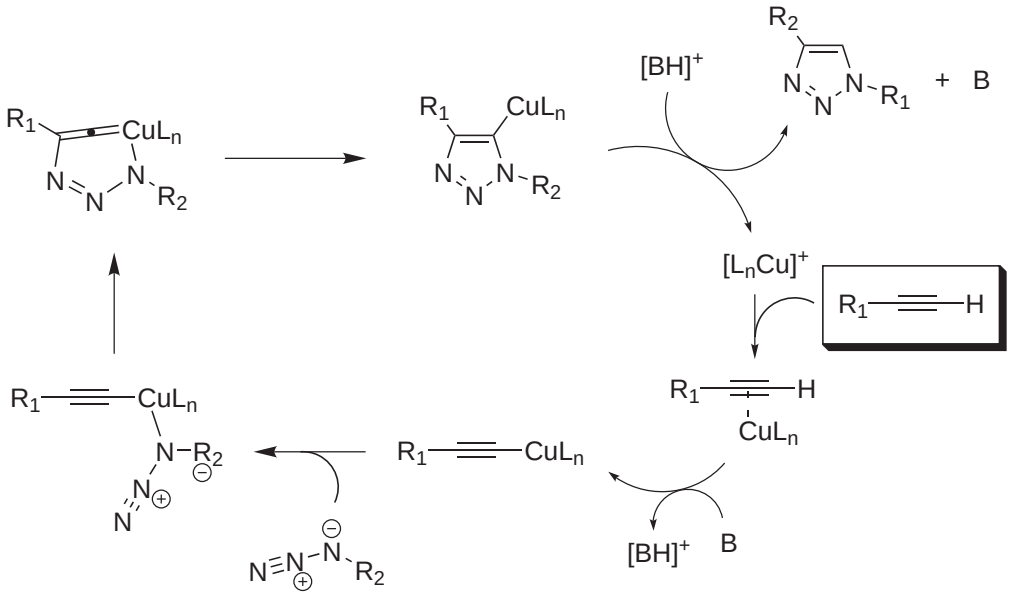

Fig. 1.19: Proposed mechanism of the copper-catalyzed alkyne-azide cycloaddition.

Suitable copper(I) catalysts can either be generated from copper(II) salts by reduction using sodium ascorbate or direct use of copper(I) salts. A minor side reaction is the oxidative dimerization of the alkyne in a Glasser-type reaction.[96] Nevertheless, all reaction conditions are fully compatible with the Fmoc and Boc coupling strategy used in solid phase peptide synthesis (SPPS).[97,98]
Since exogenous metals like copper can potentially have toxic effects in biological systems, the interest in copper-free 1,3-dipolar cycloaddition has significantly increased in the past few years.[99] Therefore, alternative ways have been developed that allow one to perform click reactions under mild conditions without using any metal catalyst. Most approches involve modifications on the alkyne component and include either strain-promoted or electron-deficient systems, or a combination of both. The first-generation systems for strain-promoted azide-alkyne cycloadditions (SPAAC) were mainly based on cyclooctynes without electon-withdrawing groups. The deviation from the ideal sp-hybridization bond angle of 180° leads to an increased reactivity towards organic azides. Assuming that the lowest unoccupied molecular orbital (LUMO) of the alkyne and the highest occupied molecular orbital (HOMO) of the azide participate in the cycloaddition reaction, one or two fluorine atoms were introduced in the second- and third-generation cyclooctynes to lower the LUMO of the alkyne by reducing the electron density. Reaction rates of third-generation difluorinated cyclooctynes (DIFOs) were more than one order of magnitude higher compared to the non-fluorinated cyclooctynes. Reaction rates could also be enhanced by increasing the strain energy in functionalized dibenzocyclooctynes (Fig. 1.20).[83,84]

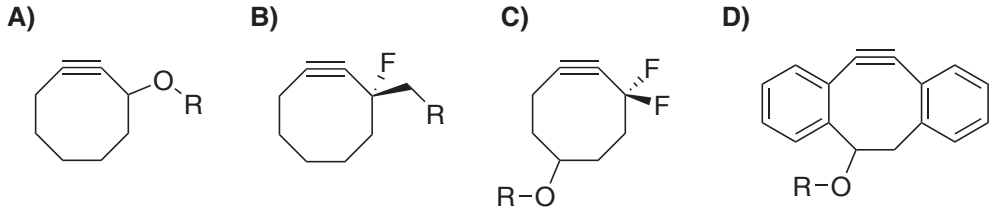

Fig. 1.20: Different generations of cyclooctynes used in strain promoted alkyne azide cycloadditions (SPAAC): non-fluorinated (A), monofluorinated (B), difluorinated (C), and dibenzocyclooctynes (D).

Other systems, also involving ring-strain as well as electron-deficiency, are represented by activated oxanorbornadienes. These compounds react with azides in a tandem [3+2] cycloaddition-retro-Diels-Alder (crDA) reaction to give 1,2,3-triazoles. In the case of asymmetrically substituted oxanorbornadienes ($R_1 \neq R_2$), two regioisomers are obtained (Fig. 1.21).[100]

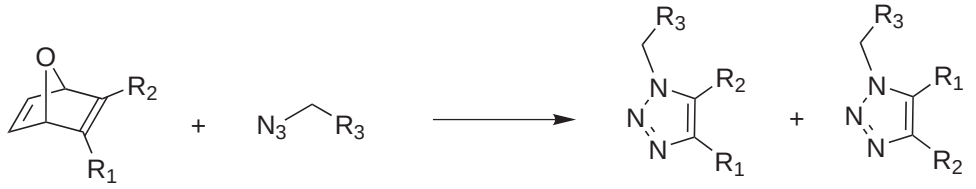

Fig. 1.21: Cycloaddition reaction of activated oxanorbornadienes with azides to give substituted 1,2,3-triazoles.

It was found that the cycloaddition of azide and oxanorbornadiene preferential proceeds via a pathway involving the most electron-deficient substituted double bond to give a triazoline intermediate and finally, after elemination of furan, two regioisomeric 1,4,5-trisubstituted triazoles (Fig. 1.22, path A). As a side reaction, the cycloaddition can also occur at the unsubstituted double bond. In this case a monosubstituted 1,2,3-triazole and a 3,4-substituted furan derivative are obtained as side products also via a triazoline intermediate (Fig. 1.22, path B). The latter case occurs especially when the substituents R_1 od R_2 are changed from ester to amide groups, but only to minor extent. Another way to avoid this side reaction is the use of oxanorbornadienes with methyl group in the 2- and 5- or 3-position.[100–102] Click reactions using trifluoromethyl-substituted oxanorbornadienes have already found application in bioconjugation reactions for linking radiolabels such as ^{111}In-DTPA complexes to carrier peptides.[101]

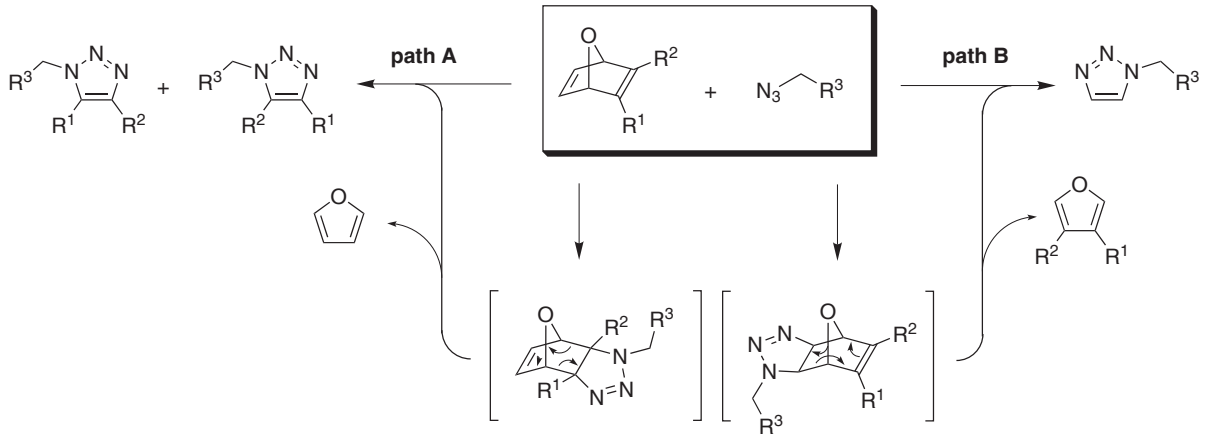

Fig. 1.22: Reaction pathways for the formation of triazole compounds from azides and oxanorbonrnadienes via triazoline intermediates.

2 Motivation

Molybdenum carbonyl compounds are known to exhibit promising biological properties. For example, $Mo(CO)_3$ and $Mo(CO)_5$ complexes were found to act as CO releasing molecules (CORMs) for the cellular delivery of this small-molecule messenger and a series of neutral $Mo(allyl)(CO)_2$ complexes was shown to have cytotoxic activity against a human colon cancer cell line. In contrast, the biological activity of $Mo(CO)_4$ and cationic $Mo(allyl)(CO)_2$ complexes has not been investigated in this context so far.

Since molybdenum tetracarbonyl complexes show a well developed photochemistry, photoactivation is expected to be a good trigger for a possible biological activity, including their CO release properties and moreover, may allow its temporal and spatial control. In particular, photoactivation using visible instead of UV light is more suitable for biological applications since visible light is known not to cause any cell damage. The metal-to-ligand charge transfer transition (MLCT) in molybdenum tetracarbonyl complexes with bidentate N-N ligands appears at around 450 nm and thus allows triggering of the biological activity using visible light. Since $Mo(CO)_4$(N-N) complexes are neutral and thus have a low bioavailability, they must be functionalized, for example by conjugation to carrier peptides to facilitate solubility in physiological medium and uptake by cellular target structures. Mild bioorthogonal coupling methods that do not interfere with the reactivity of functional groups present in peptides and proteins and moreover avoid the use of transition metal catalysts, which can cause toxic effects in biological systems, represent suitable conjugation strategies. Thus, the first part of the present work will focus on the synthesis of molybdenum tetracarbonyl complexes with aldehyde-functionalized bidentate polypyridyl N-N ligands, which then will then be use to attach the complexes to peptides using a mild bioconjugation procedure like the oxime ligation reaction, which uses an aminooxy functionality on the peptide. Then, photochemical studies based on UV/Vis and IR spectroscopy will be used for visible light triggering of the CO release of these complexes and peptide conjugates.
In a second section, the modulation of the biological activity of $[Mo(allyl)(CO)_2(N\text{-}N)X]^{+/0}$ complexes (with X = Hal or py) by variation of the bidentate polypyridyl N-N ligand will be studied on human cancer cells using biochemical methods such as cytotoxicity and apoptosis induction assays. Here it is expected that the biological activity is correlated with the size of the bidentate polypyridyl N-N ligand.
Finally, a particularly promising strategy to prepare bioconjugates of the abovementioned compounds is the replacement of the halide by a coordinated azide ligand, which might then be reacted with electron-deficient alkynes to form metal-coordinated triazoles as a catalyst-free alternative to the copper-catalyzed azide-alkyne (CuAAC) click reaction, thus avoiding the use of copper which has potential adverse effects in

biological systems, such as cytotoxicity on cell cultures. Moreover, after preparation of azid containing neutral molybdenum allyl dicarbonyl complexes, peptide conjugates of these complexes will be synthesized by employing electron-deficent alkynes as linkers in a catalyst-free azide-alkyne click reaction.
Thus, the general aim of this work is to synthesize novel molybdenum tetracarbonyl and molybdenum allyl dicarbonyl complexes and study the modulation of their biological activity by variation of the coligands and conjugation to carrier peptides. For the latter reactions, catalyst-free bioorthogonal coupling methods such as the oxime ligation and copper-free azide-alkyne click reactions will be evaluated to open the way to specific cellular uptake and delivery.

3 Results and discussion

3.1 Molybdenum tetracarbonyl complexes as CORMs

3.1.1 Synthesis of [Mo(CO)$_4$(N-N)] complexes and their peptide conjugates

As [Mo(CO)$_4$(α-diimine)] complexes with aromatic bidentate N-N donor ligands exhibit an well-developed photochemistry and are known to have MLCT absorptions in the visible range, they represent promising candidates as photoCORMs. Since the first synthesis of [Mo(CO)$_4$(phen)] was reported in 1935 by Hieber *et al.*,[103] such complexes traditionally have been synthesized by heating molybdenum hexacarbonyl and a N-N-chelating ligand in an appropriate solvent to reflux under an inert atmosphere.[76,77,104,105] Since these reactions usually take an extended time under normal conditions and yields are rather low, a microwave-assisted synthesis protocol was explored as an alternative in the present work.[106–108] To test conditions using an inexpensive ligand, molybenum hexacarbonyl was reacted in a model procedure with 1,10-phenanthroline in a toluene/diglyme mixture in a CEM microwave reactor under aerobic conditions in a sealed vial. [Mo(CO)$_4$(phen)] (**3**) was obtained in greater than 60% yield after just 5 min of irradiation at 180 °C. Since a considerable amount of insoluble byproducts formed due to thermal decomposition of molybdenum hexacarbonyl at temperatures above 156 °C, the reaction conditions were further optimized. Thus, in the synthesis of [Mo(CO)$_4$(bpy)] (**4**), the temperature was reduced to 130 °C and the reaction time was extended to 15 min to give the desired product in greater than 80% yield. The same conditions were employed in the synthesis of [Mo(CO)$_4$(bpy^{CH_3,CHO})] (**5**) which was isolated in 62% yield and pure form after column chromatography on silica using dichloromethane as the eluent. The functionalized bidentate aromatic ligand 4'-methyl-2,2'-bipyridine-4-carboxaldehyde (**2**) to be used for bioconjugation is easily accessible in two steps. First, 4-picoline was dimerized using Raney nickel to give 4,4'-dimethyl-2,2'-bipyridine (**1**). Then, one of the methyl groups was selectively oxidized with 1.1 equivalents of selenium dioxide to give the monoaldehyde (Fig. 3.1), which in turn is a suitable coupling partner for use in the oxime or hydrazone ligation reactions.[91,109]

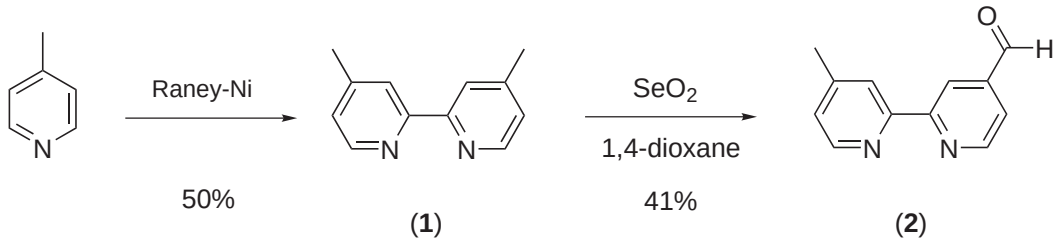

Fig. 3.1: Two-step synthesis of 4'-methyl-2,2'-bipyridine-4-carboxaldehyde (**2**).

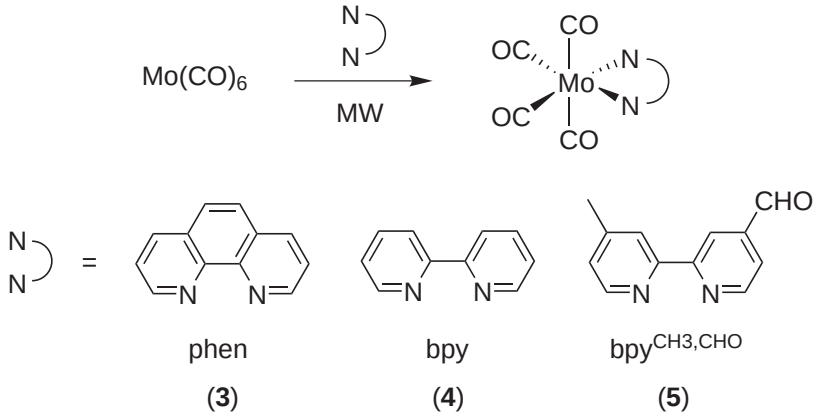

Fig. 3.2: Microwave-assisted synthesis of [Mo(CO)$_4$(α-diimine)] complexes: (**3**) toluene/diglyme, 180℃, 5 min, 62%; (**4**) THF, 130℃, 15 min, 88%; (**5**) THF, 130℃, 15 min, 62%.

The IR spectrum of the aldehyde-functionalized complex (**5**) shows three strong vibrational bands for the CO ligands at 2011, 1868 and 1804 cm^{-1}, confirming the expected C_s symmetry. The vibrational band at 2011 cm^{-1} can be assigned to the axial carbonyl ligands due to the strong *trans*-effect by the π-acceptor ability of the ligands opposite to each other, whereas the bands at 1868 and 1804 cm^{-1} are due to the symmetric and antisymmetric vibrations of the equatorial carbonyl ligands, respectively.[110] A fourth band for a second antisymmetric vibration of the equatorial CO ligands is only visible as a shoulder at 1880 cm^{-1}. The C=O vibrational band of the aldehyde group is found at 1709 cm^{-1} (Fig. 3.3).

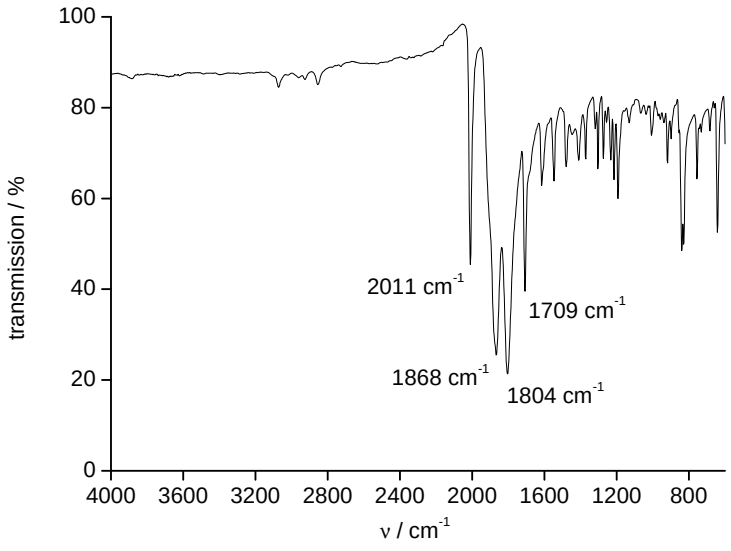

Fig. 3.3: ATR-IR spectrum of [Mo(CO)$_4$(bpy^{CH_3,CHO})] (**5**).

The ^{1}H-NMR spectrum of [Mo(CO)$_4$(bpy^{CH_3,CHO})] (**5**) shows eight signals in addition to that of the DMSO solvent (Fig. 3.4). The integrals are consistent with the expected number of ten protons. Two singlets, one for the methyl group at 2.54 ppm and another one for the aldehyde proton at 10.16 ppm in addition to six different signals between

7.5 and 9.5 ppm for six aromatic protons, reflect the reduced symmetry of the complex. The signals for the H-6 and H-6' protons are found as doublets at 9.24 and 8.83 ppm with a coupling constant of 5.5 Hz, which is also found for the H-5 and H-5' protons at 7.97 and 7.53 ppm. The H-5/H-5' protons appear as a doublet of doublets, including a ^4J long-range coupling of 1.6 Hz towards the H-3 and H-3' protons, which are located at 9.02 and 8.71 ppm.

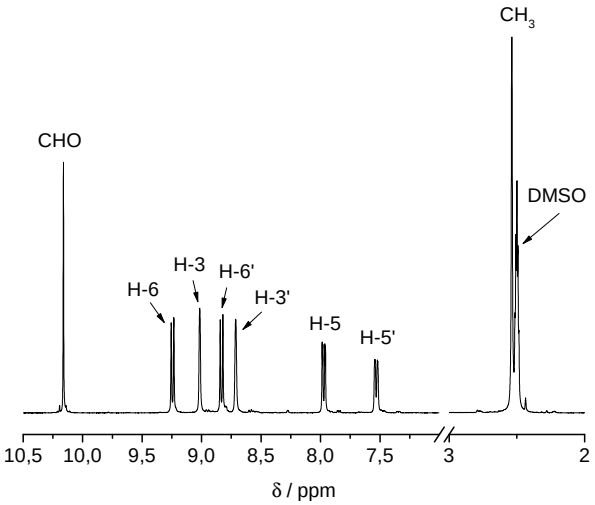

Fig. 3.4: 250 MHz ^{1}H-NMR spectrum of [Mo(CO)$_4$(bpy^{CH_3,CHO})] (**5**) in DMSO-d$_6$.

The ^{13}C-NMR of the complex also shows the expected ten signals for the aromatic carbon atoms in the range of 120 to 160 ppm as well as one signal for the methyl group at 20.74 ppm and one for the aldehyde carbon atom at 191.45 ppm (Fig. 3.5). Moreover, three signals for the four carbonyl ligands are observed. The most lowfield shifted signal at 204.88 ppm is assigned to the two equivalent axial carbonyl ligands, which strongly deshield each other. The other two signals at 222.60 and 221.73 ppm are assigned to the equatorial carbonyl ligands. This also reveals a C_s symmetry of the complex, which is consistent with the results obtained from IR and ^{1}H-NMR spectroscopy. The FD mass spectrum shows one peak for the molecular ion at m/z = 405.2.

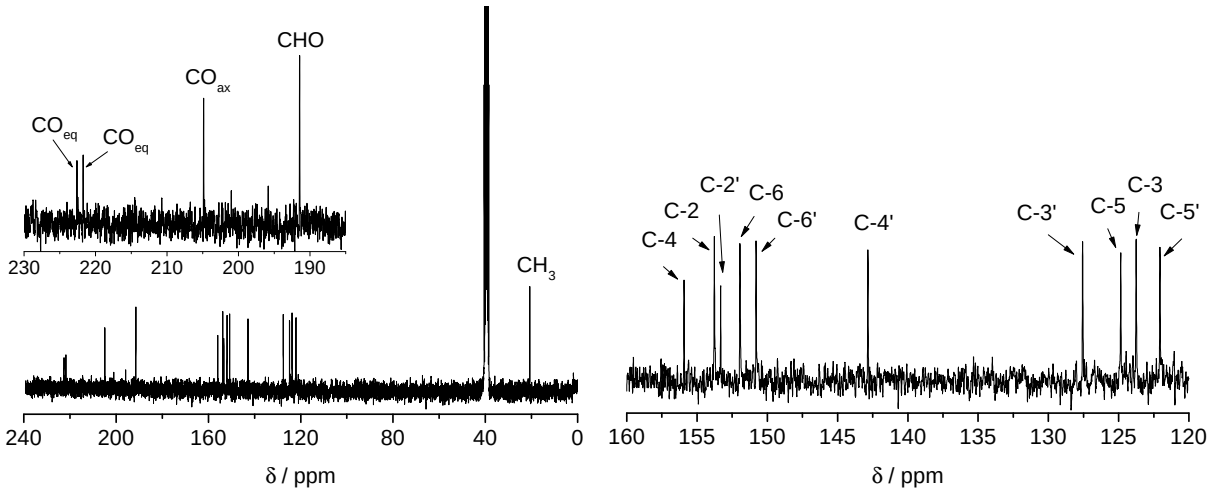

Fig. 3.5: 62.5 MHz ^{13}C-NMR spectrum of $[Mo(CO)_4(bpy^{CH_3,CHO})]$ (**5**) in DMSO-d_6.

To link this complex to peptides using the bioorthogonal oxime ligation reaction described in Chapter 1.5.1, aminooxy acetic acid (**8**) was synthesized by acid hydrolysis of the dimethylketoxime (**7**) to give **8** as the hemi-hydrochloride.[111–113] The amino group was subsequently protected as the 9-fluorenyl-methoxycarbonyl (Fmoc) group using a standard procedure, which then allows use of the aminooxy acetic acid in solid-phase peptide synthesis (SPPS, Fig. 3.6).[114] The overall yield of Fmoc-Aoa-OH (**9**) was about 30% over three steps starting from acetone oxime (**6**). Analytical data of Fmoc-Aoa-OH as well as aminooxy acetic acid and the corresponding ketoxime were in full accordance with the expected values.

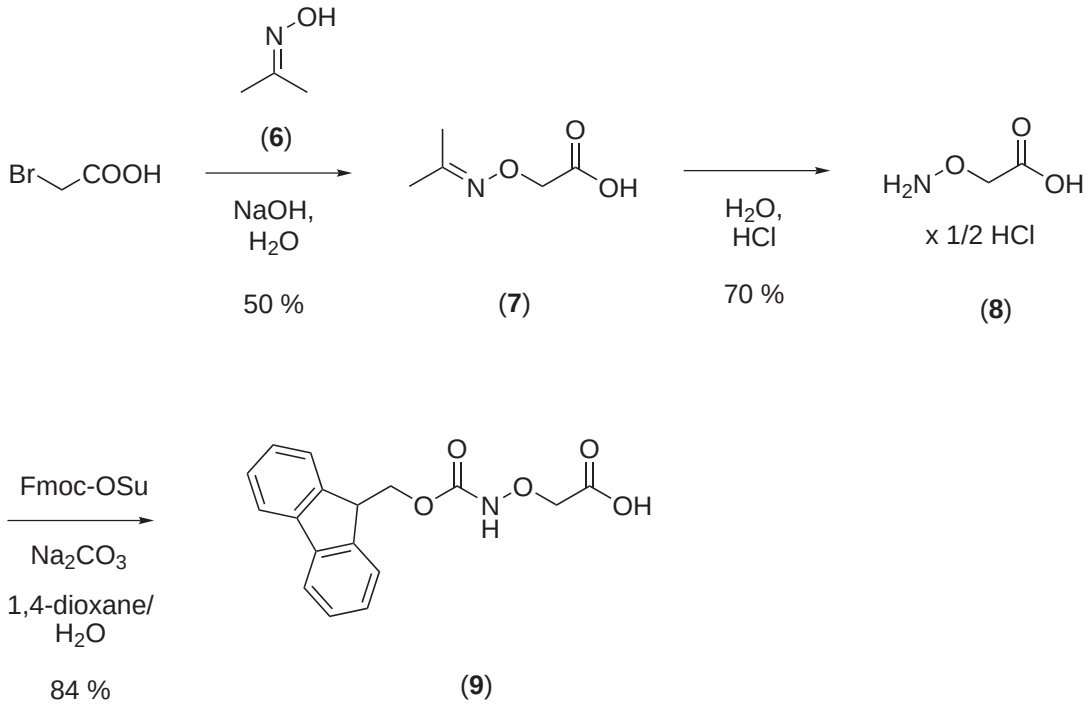

Fig. 3.6: Synthesis of *N*-(9-fluorenylmethoxycarbonyl)aminooxy acetic acid (**9**).

To optimize the oxime ligation reaction, a model peptide consisting of three amino acids (H-Gly-Leu-Arg-OH) with aminooxy acetic acid attached to the *N*-terminus was synthesized on a preloaded Fmoc-Arg(Pbf)-Wang resin using an automated CEM Liberty peptide synthesizer under the conditions described below. In a first approach, $[Mo(CO)_4(bpy^{CH_3,CHO})]$ (**5**) was reacted with the functionalized peptide (**10a**) following the on-resin labelling strategy shown in Fig. 3.7. Thus, the resin with the attached peptide was shaken together with a solution of the complex in *N,N*-dimethylformamide for 2 h. After removal of the reaction mixture and extensive washing with dimethylformamide, a dark-red resin was obtained (Fig. 3.8).

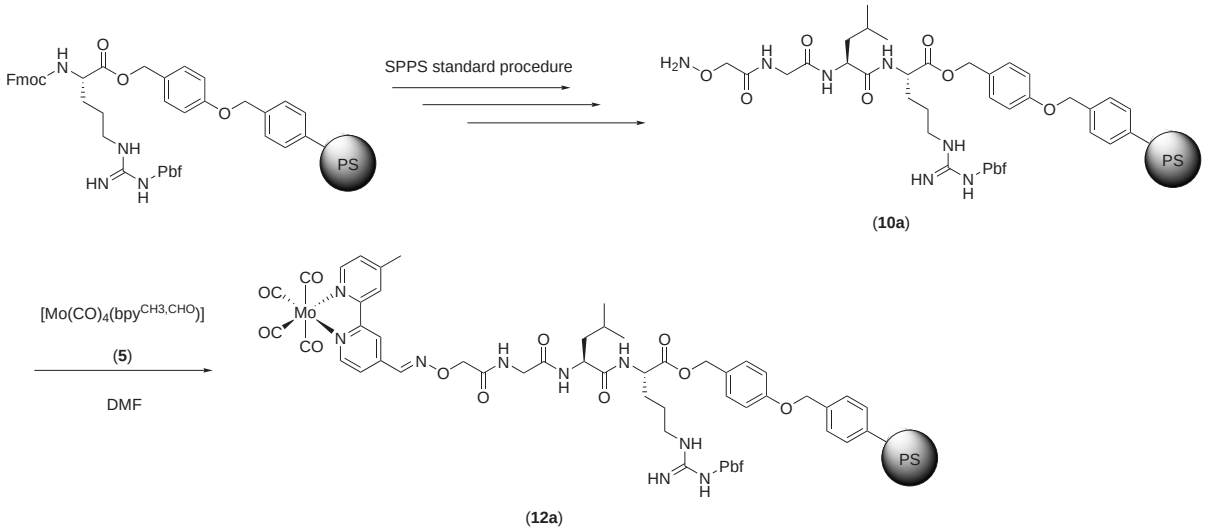

Fig. 3.7: On-resin labeling strategy in the synthesis of a $[Mo(CO)_4(bpy^{CH_3,CHO})]$ peptide conjugate.

The ATR-IR spectrum of the resin showed the characteristic pattern of the molybdenum tetracarbonyl unit with vibrational bands at 2010, 1901 and 1863 cm^{-1} as observed for the complex (**5**) itself, demonstrating a successful coupling (Fig. 3.9). Unfortunately, the molybdenum tetracarbonyl unit was not stable towards concentrated trifluoroacetic acid (TFA) required in the following cleavage step from the resin, as indicated by the formation of dark-brown products which were insoluble in any polar solvents, such as acetonitrile-water mixtures.

Fig. 3.8: Dark-red resin obtained after coupling of $[Mo(CO)_4(bpy^{CH_3,CHO})]$ (**5**).

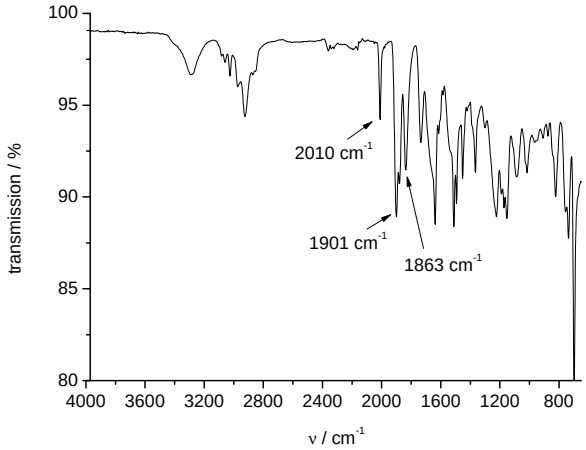

Fig. 3.9: ATR-IR spectrum of the dark-red resin obtained after coupling of $[Mo(CO)_4(bpy^{CH_3,CHO})]$ (**5**).

Therefore, in an alternative approach, a post-labelling strategy was employed, involving coupling of complex **5** and peptide **10** in solution (Fig. 3.10). The peptide was cleaved from the resin under standard conditions using a mixture of TFA, TIS and water and after work-up, RP-HPLC analysis as well als ESI mass spectrometry revealed a purity of greater than 95%. Thus, there was no need for further HPLC purification.

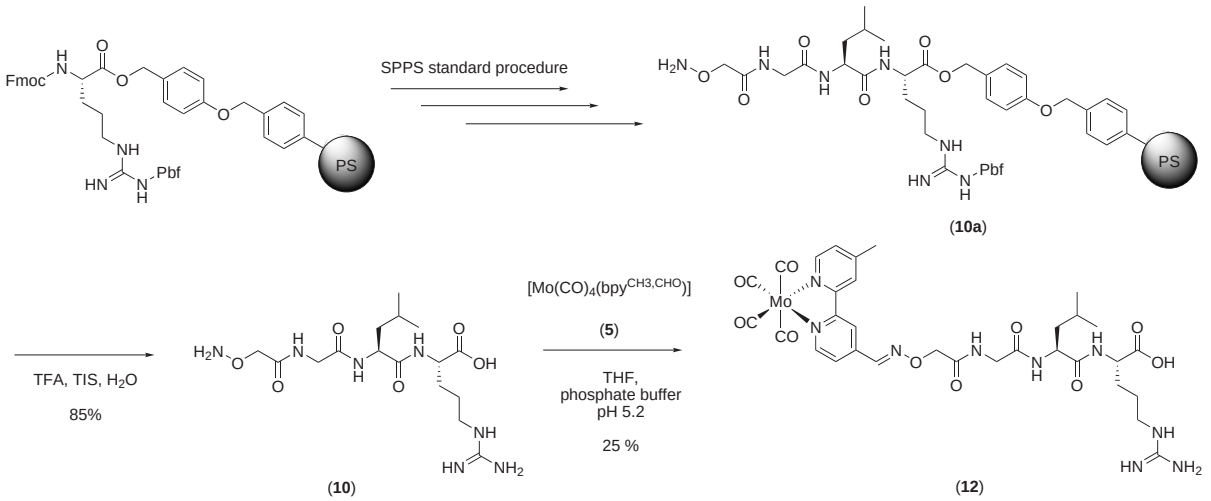

Fig. 3.10: Synthesis of $[Mo(CO)_4(bpy^{CH_3,C=N\text{-}Aoa\text{-}Gly\text{-}Leu\text{-}Arg\text{-}OH})]$ (**12**) via oxime ligation.

The Aoa-Gly-Leu-Arg-OH model peptide (**10**) was used to test various conditions in the oxime ligation with $[Mo(CO)_4(bpy^{CH_3,CHO})]$ (**5**) as summarized in Tab. 3.1.

Table 3.1: Reaction conditions tested in the oxime ligation of peptide (**10**) and $[Mo(CO)_4(bpy^{CH_3,CHO})]$ (**5**).

buffer (100 mM)	pH	organic solvent	buffer/THF ratio	result
anilinium acetate	4.4	THF	1:9	++
sodium phosphate	5.2	THF	1:9	-
sodium phosphate	5.2	THF	1:1	+++
sodium acetate	4.5	THF	1:9	-
sodium acetate	4.5	THF	1:1	+

Although *N,N*-dimethylformamide is widely used in SPPS, it is rather unfavourable when reactions are carried out in solution since it is very difficult to remove during the work-up procedure. Anyhow, the ligation worked best when carried out in a 1:1 mixture of tetrahyfrofuran and phosphate buffer at pH 5.2. Mixtures containing just 10% THF did not provide sufficient solubility for the complex, while the use of sodium and anilinium acetate buffer showed drawbacks in the workup procedure. The conversion could easily be monitored by TLC using silica as the solid phase and dichloromethane as the eluent. After desalting of the reaction mixture by solid-phase extraction and subsequent purification by preparative HPLC, the peptide conjugate **12** was obtained in moderate yield (25%) but high purity (97%) as seen in Fig. 3.11. Reactions carried out in anilinium or sodium acetate buffer also worked quite well but showed major drawbacks in the work-up procedure because the reaction mixtures could not be desalted properly by solid-phase extraction. This might be due to the fact that aniline as well as acetic acid react as ion-pairing reagents, making a separation from the peptide conjugate on a reversed phase column difficult.

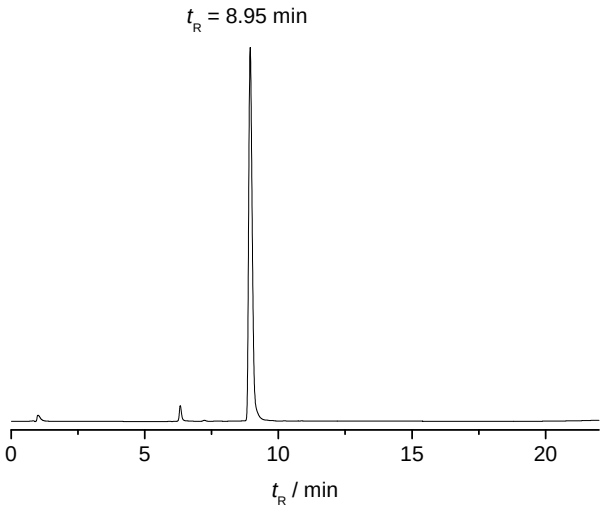

Fig. 3.11: Analytical HPLC chromatogram (254 nm) of the peptide conjugate **12**.

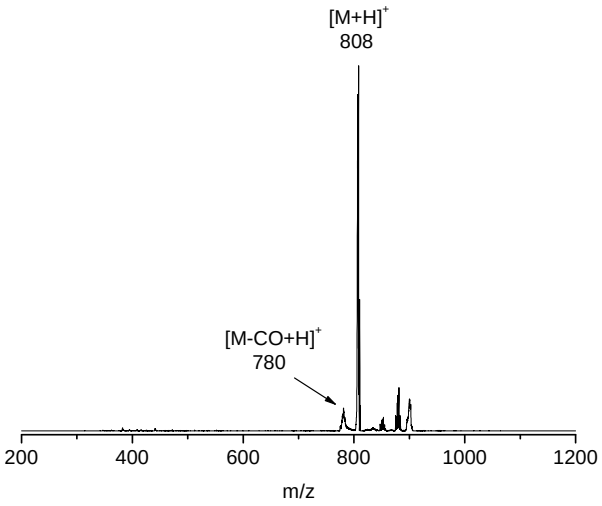

Fig. 3.12: ESI+ mass spectrum of the peptide conjugate **12** dissolved in methanol.

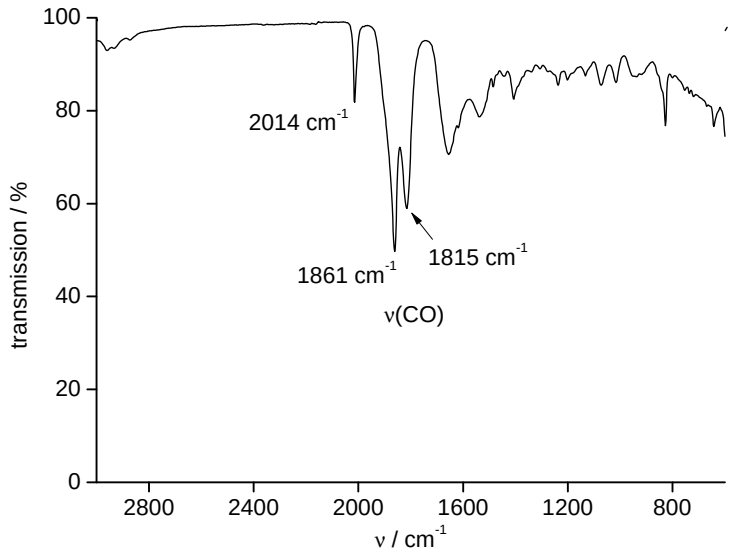

Fig. 3.13: ATR-IR spectrum of the peptide conjugate **12**.

The ESI+ mass spectrum of **12** shows the main peak at m/z = 808 and only one fragmentation peak at m/z = 780, resulting from loss of one carbon monoxide ligand (Fig. 3.12). Three CO vibrational bands in the IR spectrum of the conjugate at 2014, 1861 and 1815 cm^{-1} demonstrate that the composition and symmetry at the molybdenum center is preserved in the product (Fig. 3.13).

After successful synthesis of the model peptide conjugate **12**, the same conditions were applied in the ligation of $[Mo(CO)_4(bpy^{CH_3,CHO})]$ (**5**) to a larger, bioactive peptide. The transforming growth factor beta 1 (TGF-β_1) plays an important role in cell proliferation and differentiation and is often overexpressed in various types of tumor cells, allowing the escape from immune surveillance. Therefore, deactivation of this protein through TGF-β_1 binding peptides is of considerable interest in strategies for tumour

targeting and treatment. In order to promote a possible application of CO releasing molecules in cancer therapy, the amino acid sequence H-Leu-Pro-Leu-Gly-Gln-Ser-His-OH, which has a high affinity towards TGF-β_1, was synthesized using manual solid-phase peptide synthesis and *N*-terminally functionalized with aminooxy acetic acid (Fig. 3.14, Aoa).[115] Subsequent oxime ligation of [Mo(CO)$_4$(bpy^{CH_3,CHO})] (**5**) to the peptide **11** to gave the conjugate **13** in moderate yield (30%) but high purity (> 90%) after purification by preparative HPLC.

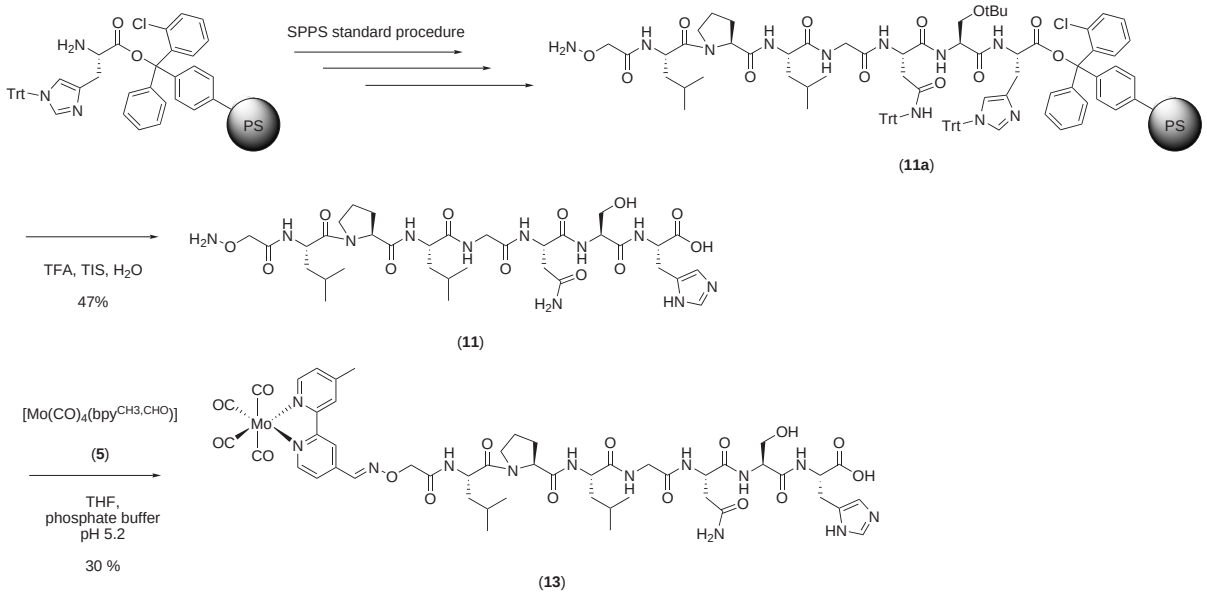

Fig. 3.14: Synthesis of [Mo(CO)$_4$(bpy$^{CH_3,C=N\text{-}Aoa\text{-}TGF\text{-}\beta_1\text{-}OH}$)] (**13**) via oxime ligation.

As observed for the model peptide conjugate, the lipophilicity of **13** is significantly higher than the peptide itself, resulting in a shift of retention time in the analytical HPLC from 14.59 to 30.26 min. Beside the HPLC trace recorded at 254 nm, the UV/Vis absorption was also monitored at 468 nm to identify molybdenum tetracarbonyl species by their MLCT absorption. If was found that only the peak at t_R = 30.26 min shows an absorption at 468 nm and thus was assigned to the conjugate (Fig. 3.15). The IR spectrum of the conjugate **13** shows three carbonyl vibrational bands at 2015, 1861, and 1812 cm^{-1}, again demonstrating the conservation of C_s symmetry in the intact [Mo(CO)$_4$] unit (Fig. 3.16). The ESI$^-$ mass spectrum shows the main peak at m/z = 1198.4 and only one fragmentation peak at m/z = 988.5, resulting from loss of the whole molybdenum tetracarbonyl unit (Fig. 3.17).

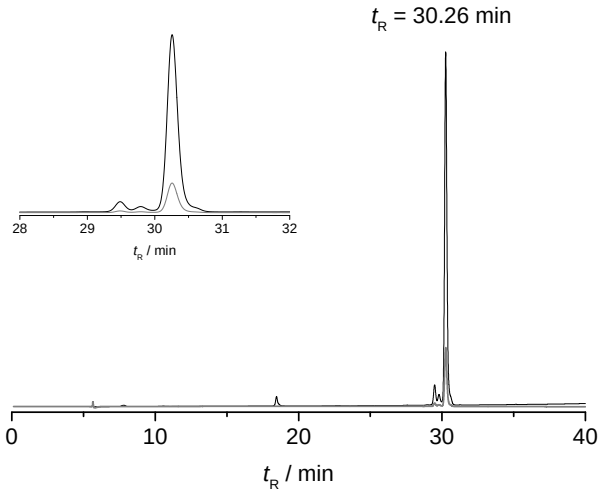

Fig. 3.15: Analytical HPLC chromatogram (black - 254 nm, grey - 468 nm) of the peptide conjugate **13**.

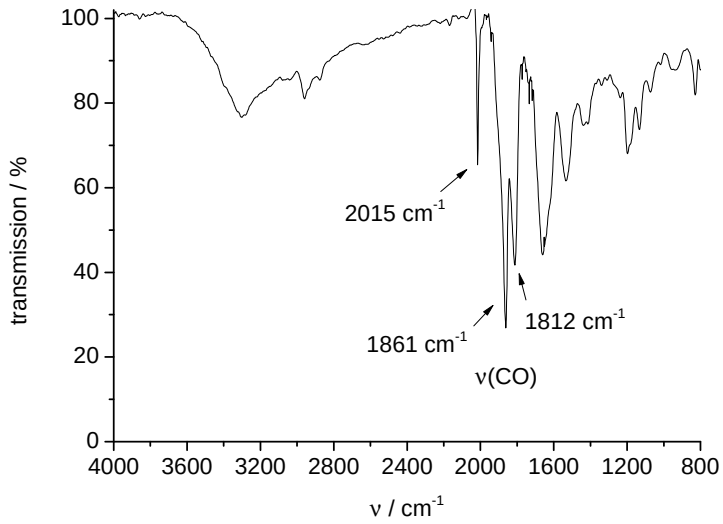

Fig. 3.16: ATR-IR spectrum of the peptide conjugate **13**.

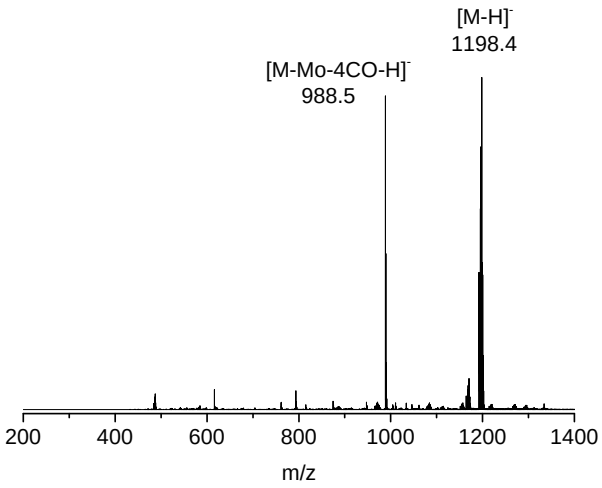

Fig. 3.17: ESI$^-$ mass spectrum of the peptide conjugate **13** dissolved in methanol.

3.1.2 CO release studies

The CO release from **5** and **12** was studied in the dark and at different excitation wavelengths using the myoglobin assay. In this assay, a solution of the carbonyl compound dissolved in dimethylsulfoxide is incubated with reduced horse skeletal muscle myoglobin (MbFe(II)) under an inert atmosphere and the conversion to MbFe(II)CO upon irradiation is monitored by UV/Vis spectroscopy. The amount of CO released is quantified from the absorption of the MbFe(II)CO in the Q-band region at 540 nm as described in Chapter 5.1.2. Although, complex **5** is rather unpolar, it was soluble under the conditions of the myoglobin assay in the concentration applied (10 μM) and no precipitation was observed over the course of the experiment. Results from these experiments are summarized in Tab. 3.2. All experiments were carried out at least as triplicate.

Table 3.2: CO release properties of complex (**5**) and conjugate (**12**) in the dark and at different irradiation wavelengths.

	dark		**365 nm**		**468 nm**	
	$t_{1/2}$ / min	**eq.CO**	**$t_{1/2}$ / min**	**eq.CO**	**$t_{1/2}$ / min**	**eq.CO**
(**5**)	92±20	2.5±0.7	54±13	3.0±1.0	44±7	2.4±0.4
(**12**)	123±38	1.6±0.1	n.d.	n.d.	40±14	1.0±0.4

[0]n.d. - not determined

The complex as well as the peptide conjugate are not stable in solution in the dark and the half-lifes for both compounds are in the same range of about 100 min. However, the number of CO equivalents released are 1.0 units lower for the conjugate compared to the complex. This effect was already observed for $[Mn(CO)_3(tpm)]^+$ complexes and their corresponding peptide conjugates. It might be due to the unkown hydratation state of the peptide conjugate as reported before, thus making the preparation of stock solutions with well-defined concentration difficult.[66] Irradiation at 365 and 468 nm both lead to release of the same number of CO equivalents and the final molar amount of carbon monoxide liberated is the same as observed in the dark reaction. However, the half-lifes decrease significantly to 50% of the value observed in the absence of light. Thus, although the compounds are not pure PhotoCORMs due to some CO release in the dark, it is significantly accelerated by photoactivation, independent of the excitation wavelength used. Typical UV/Vis spectral changes in the Q band region of a solution of reduced horse skeletal myoglobin upon CO release from complex **5** under irradiation at 468 nm are shown in Fig. 3.18 and Fig. 3.19. The corresponding time-dependent formation of MbCO is depicted in Fig. 3.20.

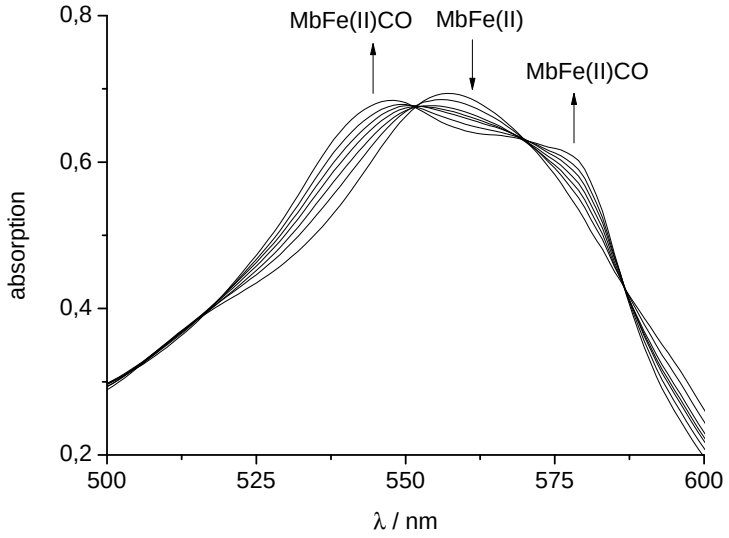

Fig. 3.18: UV/Vis spectral changes in the Q band region of a solution of reduced horse skeletal myoglobin (50 μM) and $[Mo(CO)_4(bpy^{CH_3,CHO})]$ (**5**) (10 μM) in 0.1 M phosphate buffer upon irradiation a 468 nm (t = 0 to 240 min).

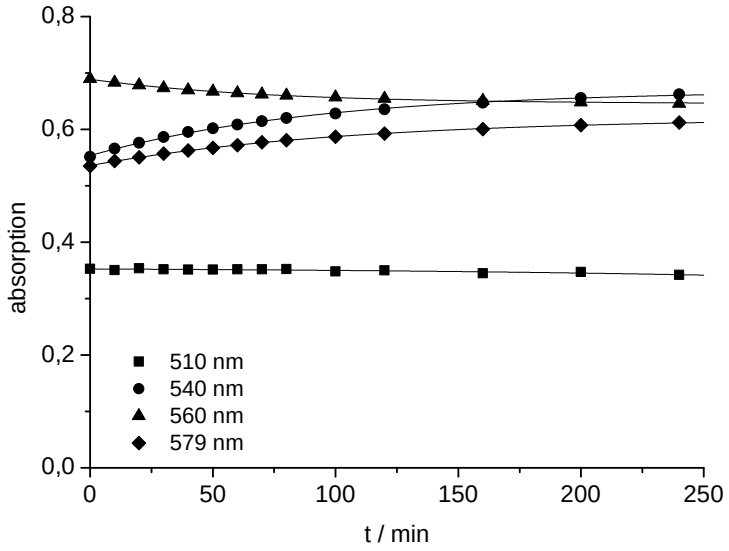

Fig. 3.19: Changes in absorption in the Q band region of a solution of reduced horse skeletal myoglobin (50 μM) and $[Mo(CO)_4(bpy^{CH_3,CHO})]$ (**5**) (10 μM) upon irradiation a 468 nm, monitored at 510, 540, 560, and 579 nm.

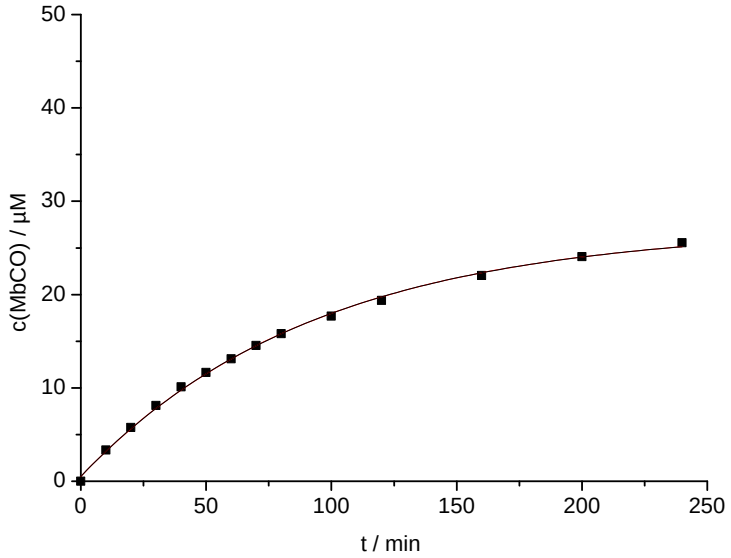

Fig. 3.20: Time-dependent formation of MbCO in mixtures of [Mo(CO)$_4$(bpy^{CH_3,CHO})] (**5**) (10 μM) with reduced horse skeletal myoglobin (50 μM) was followed by monitoring changes in the absorption at 540 nm upon irradiation at 468 nm.

Since the CO release behavior of the complex is independent of the irradiation wavelength and irradiation at 365 nm is rather unfavourable for biological applications due to the cell damage that is caused by UV light, CO release properties of the conjugate were only determined at 468 nm. Moreover, the preservation of the CO release properties in the conjugate is accompanied by an increased solubility in aqueous solutions and other polar solvents such as dimethylsulfoxid, making the conjugate suitable for further investigations on the mechanism of CO release.

3.1.3 Buffer stability tests

To test the stability of the conjugate in physiological buffer and to identify possible decomposition products that might form after CO release, **12** was incubated in buffered acetonitrile solution and the decomposition under aerobic conditions was monitored by analytical RP-HPLC and ESI mass spectrometry. The color of the solution faded with time, already visually indicating decomposition of the metal carbonyl moiety. The ESI mass spectrum shows peaks for two major species. One is assigned to the peptide with the bipyridine ligand still attached but lacking the molybdenum tetracarbonyl moiety (Fig. 3.21), ([M-Mo-4CO+H]$^+$ and [M-Mo-4CO+2H]$^{2+}$), and the other one that is due to loss of one CO ligand (m/z = 780) as already shown in Fig. 3.12 but much more prominent in this case.

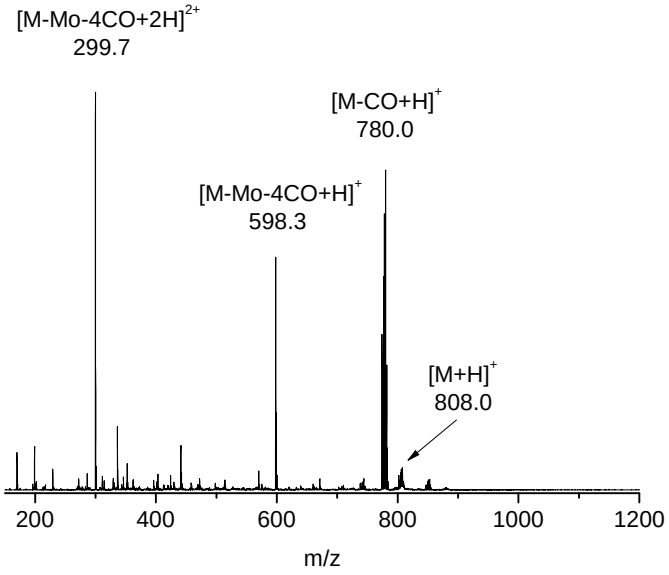

Fig. 3.21: ESI$^+$ mass spectrum of **12** after 2 h in buffered acetonitrile.

Monitoring of the decomposition by HPLC alone reveals the formation of just one follow-up product (Fig. 3.22, peak A). The integral of the conjugate (peak B) shows a linear decrease to 50% of the initial value after 7 h (Fig. 3.23). Both species were identified by their UV/Vis spectra recorded using the HPLC diode array detector as well as HPLC-MS as described below. In the UV/Vis, the parent conjugate (peak B) exhibits a weak MLCT band at 468 nm which is not present in the decomposition product (peak A). Thus, peak A was identified as the peptide with the bipyridine ligand attached but lacking the [Mo(CO)$_4$] unit.

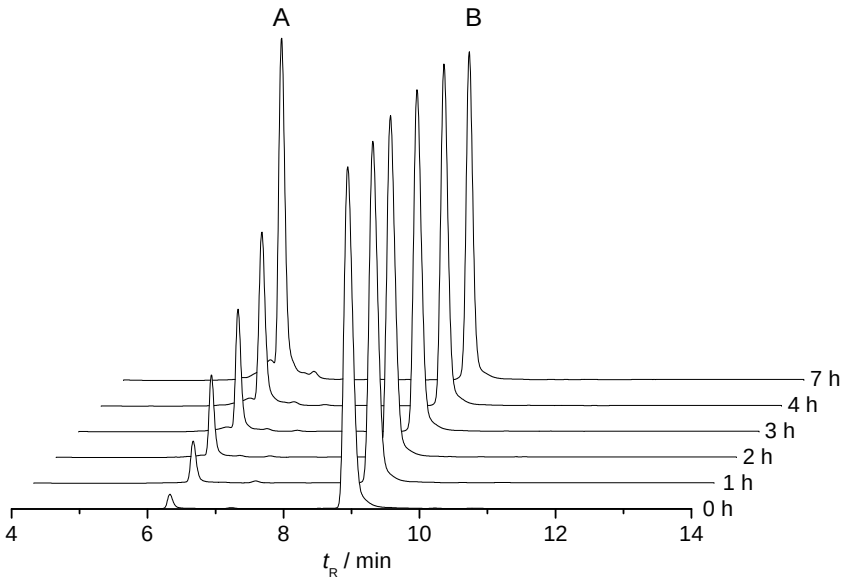

Fig. 3.22: Decomposition of conjugate **12** in buffered acetonitrile monitored by RP-HPLC (254 nm) over the course of 7 h. Intensities of all traces are normalized to peak B, the undecomposed conjugate. A is the decomposition product.

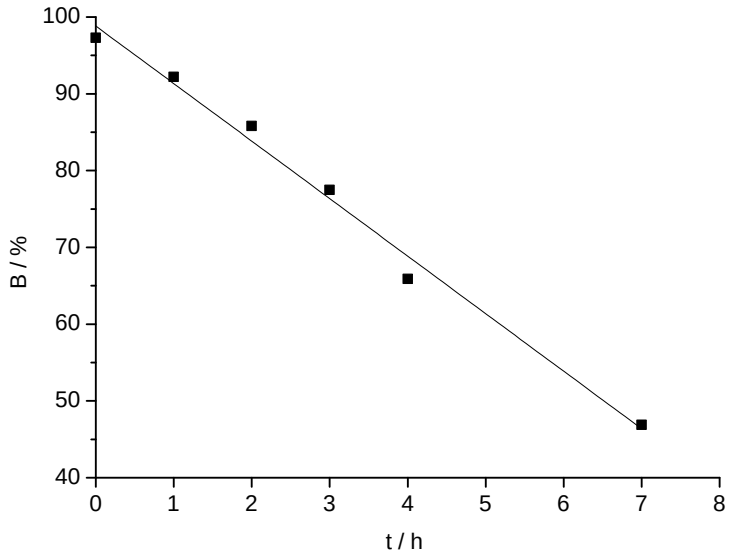

Fig. 3.23: Time-dependent change of the integral of peak B, assigned to the parent conjugate (**12**), upon decomposition in buffered acetonitrile monitored by RP-HPLC (254 nm) over the course of 7 h.

Since the results obtained by ESI-MS reveal two decomposition products while only one decomposition product was detected by analytical HPLC, the species resulting from the loss of one CO ligand is assumed to be an unstable intermediate which can only be detected on the time scale of the mass spectrometric experiment and then further decomposes to give the conjugate just bearing the bipyridine ligand without the molybdenum tetracarbonyl unit.

3.1.4 Photochemical studies

Since the initial loss of one CO ligand from the coordination sphere of conjugate **12** finally triggers the release of the whole $Mo(CO)_4$ unit, as demonstrated by HPLC analysis and mass spectrometry, combined with the observation that solutions of the conjugate decolorize over time, give rise to the assumption that oxidation of the metal center is promoted by displacement of one carbonyl ligand and therefore posseses a crucial role in the mechanism of CO release. In order to gain insight in the actual mechanism, photolysis studies on conjugate **12** were carried out in dimethylsulfoxide under aerobic conditions, or in CO- and argon-saturated solution including the corresponding dark control experiments. Spectral changes were monitored by UV/Vis spectroscopy. Dimethylsulfoxide was chosen as the solvent because it provides optimal solubility for the conjugate and can also react as a nucleophile in a ligand substitution reaction. Results of these experiment obtained by UV/Vis spectroscopy are summarized in Tab. 3.3 and Tab. 3.4.

Table 3.3: Dark stability of conjugate **12** in DMSO monitored by UV/Vis spectroscopy using the absorptions at 387 and 468 nm.

	k / s^{-1}		**$t_{1/2}$ / h**	
	λ_{max} 387 nm	**λ_{max} 468 nm**	**λ_{max} 387 nm**	**λ_{max} 468 nm**
aerobic	$-(4.74\pm0.20)\cdot10^{-5}$	$-(4.72\pm0.51)\cdot10^{-5}$	4.1 ± 0.2	4.0 ± 0.4
Ar saturated	$-(4.32\pm0.39)\cdot10^{-5}$	$-(5.62\pm0.25)\cdot10^{-5}$	4.5 ± 0.4	3.4 ± 0.2
CO saturated[1]	$-(1.33\pm0.05)\cdot10^{-6}$	$-(2.05\pm0.62)\cdot10^{-6}$	48 ± 2	44 ± 9

[1]linear decay (zero order rate law)

Table 3.4: Photolysis studies on conjugate **12** in DMSO with irradiation at 468 nm monitored by UV/Vis spectroscopy using the absorptions at 387 and 468 nm.

	k / s^{-1}		**$t_{1/2}$ / min**	
	λ_{max} 387 nm	**λ_{max} 468 nm**	**λ_{max} 387 nm**	**λ_{max} 468 nm**
aerobic	$-(1.51\pm0.05)\cdot10^{-4}$	$-(1.63\pm0.03)\cdot10^{-4}$	81 ± 3	75 ± 1
Ar saturated	$-(1.06\pm0.13)\cdot10^{-4}$	$-(1.45\pm0.08)\cdot10^{-4}$	110 ± 13	80 ± 4
CO saturated[1]	$-(4.76\pm0.12)\cdot10^{-6}$	$-(6.77\pm0.14)\cdot10^{-6}$	600 ± 15	660 ± 14

[1]linear decay (zero order rate law)

Under aerobic conditions and in the dark, a first-order exponential decay of both MLCT bands at 387 and 486 nm with half-life times of about 4 h was observed. When the

dark experiment was carried out in argon-saturated solution, the half-life time of the band at 387 nm did not change compared to the experiment under aerobic conditions, whereas the one of the band at 468 nm decreased from 4 to 3.4 h. Moreover, an increase in absorbtion in the range of 550 to 700 nm was observed. In CO-saturated solution, the decrease of the MLCT bands changed from exponential to linear behavior with a half-life time of 48 h for the 387 nm band and 44 h for the 468 nm band. When solutions of (**12**) were irradiated at 468 nm under aerobic conditions, half-life times of about 80 min for both MLCT bands were observed. Again, saturation with argon had only a marginal effect on the half-life times, which were found to be 110 min (387 nm) and 80 min (468 nm). Nevertheless, the increase of absorption in the range of 550 to 700 nm was much stronger compared to the corresponding dark experiment. Moreover, it was accompanied by an isosbestic point at 520 nm and a bathochromic shift of 32 nm from 468 to 500 nm. When the photolysis was carried out in CO-saturated solution, half-life times for the linear decrease were 600 (387 nm) and 660 min (468 nm), respectively. Assuming that the mechanism of CO-substitution in the ground state of $[Mo(CO)_4(N\text{-}N)]$ complexes has associative character, as is known for a substitution occuring from a MLCT exited state,[78] the increasing absorption in the range of 550 to 700 nm as well as the bathochromic shift indicate the formation of a new species, which probably contains a coordinated DMSO molecule. The replacement of an axial CO by any labile ligand in turn destabilizes the electron-rich low-valent d^6 metal center and promotes its oxidation. This is supposed to be the reason why the formation of a new species can only be observed under anaerobic conditions. Since the increase of absorption between 550 and 700 nm in the dark experiments is lower than during irradiation,the ligand substitution is more efficient upon photoexcitation. The marginal linear decrease of absorption that was observed in the dark as well as with light activation when experiments were performed in CO-saturated solution and not accompanied by an increase in absorption in the range of 550 to 700 nm as it was found to occur under anaerobic conditions is indicative of a competition between free CO and DMSO solvent in a ligand exchange reaction and therefore, no DMSO-containing intermediate species is formed that can be oxidized on the time scale of the substitution reaction.

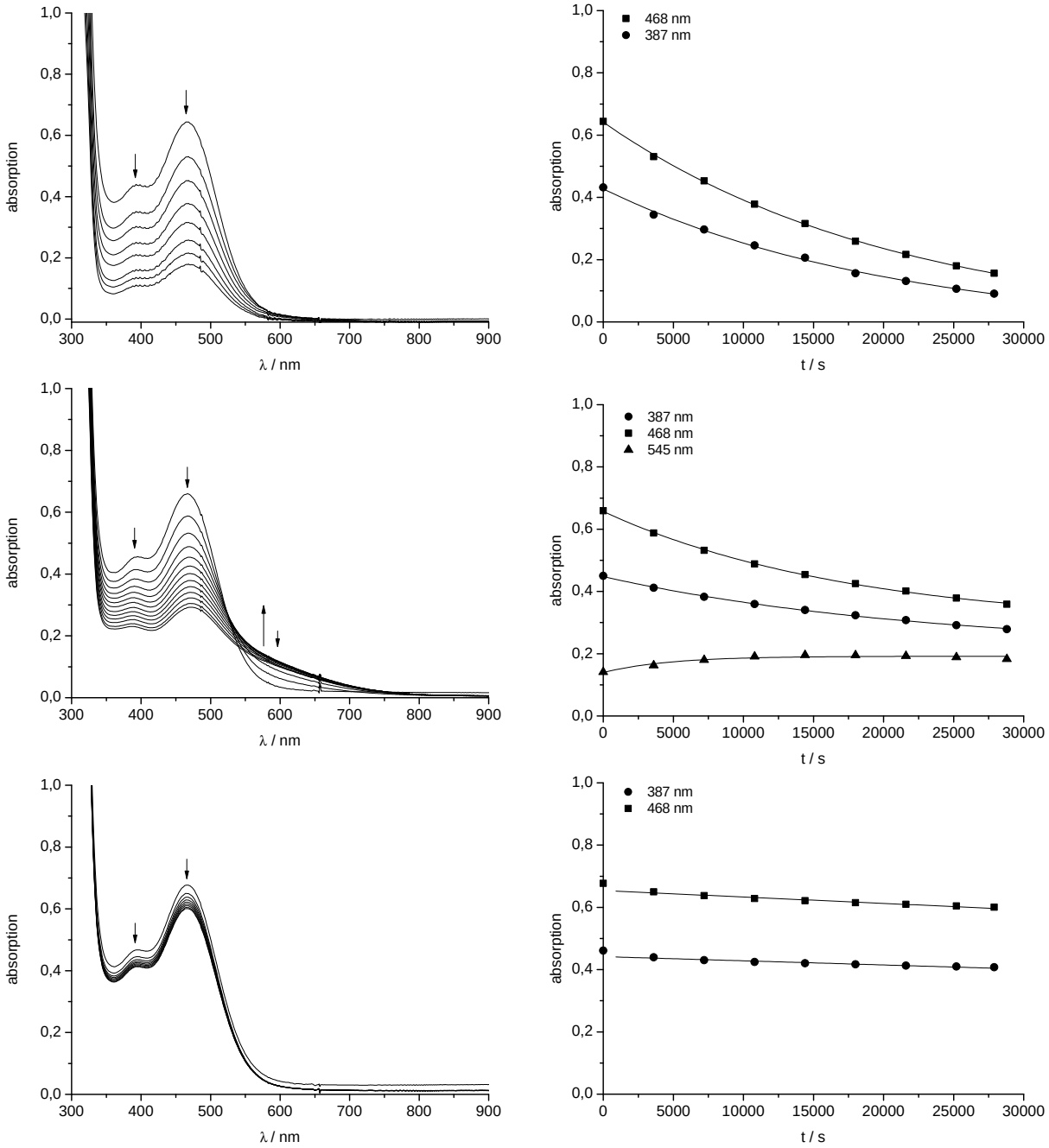

Fig. 3.24: Spectral changes of **12** in dimethylsulfoxide upon incubation in the dark, monitored by UV/Vis spectroscopy (left) and the decrease of the MLCT bands over time (right) under aerobic conditions (top), argon-saturated solution (middle) and CO gas (bottom).

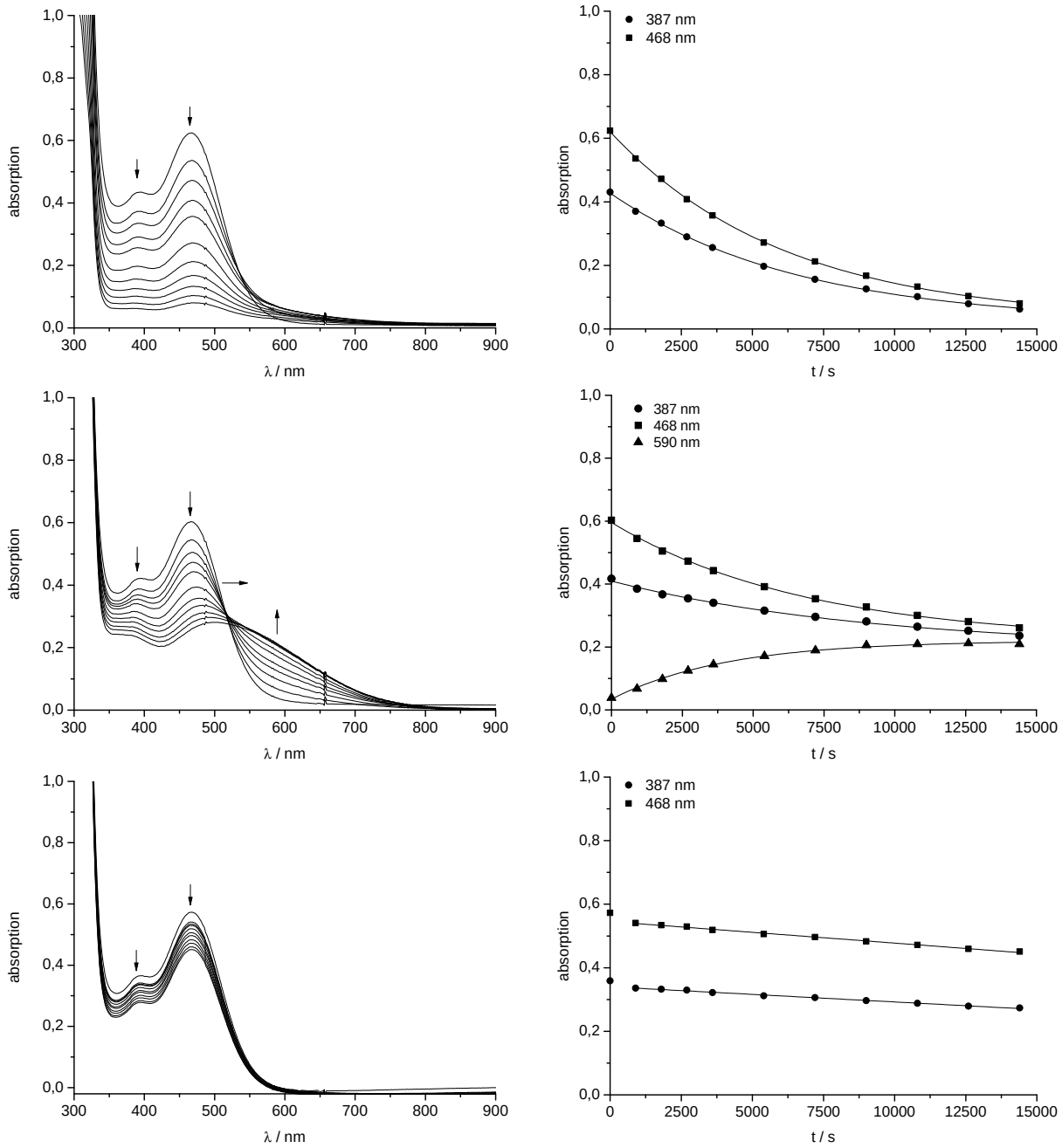

Fig. 3.25: Spectral changes upon photolysis of **12** at 468 nm in dimethylsulfoxid, monitored by UV/Vis spectroscopy (left) and the decrease of the MLCT bands over time (right) under aerobic conditions (top), argon (middle) and in CO-saturated solution (bottom).

In addition to UV/Vis spectroscopy, the stability of conjugate **12** in the dark as well as upon photolysis at 468 nm in was monitored by IR spectroscopy in solution. Since the IR flow-cell used was not gas-tight, studies under argon or CO atmosphere could no be carried out. The concentration of **12** in the IR experiments had to be chosen about 25 times higher (3 mM) as in the UV/Vis experiments (125 μM) to achieve a sufficient signal intensity greater than 0.1 for the vibrational band with the lowest intensity at 2010 cm^{-1}. Results of these experiments are summarized in Tab. 3.5. The IR spectrum of

the conjugate (**12**) shows four well-resolved vibrational bands for the carbonyl ligands at 2010, 1898, 1873, and 1828 cm^{-1}, which is in contrast to the solid state spectrum, where only three bands at 2015, 1861, and 1815 cm^{-1} are observed (Fig. 3.13). Upon incubation in the dark, all carbonyl vibrational bands decrease exponentially over time (Fig. 3.26 and Fig. 3.27) with rate constants of about $-2 \cdot 10^{-4}$ s^{-1} and half-life times of 50 to 60 min. When irradiated at 468 nm, the decrease of the vibrational bands at 1898, 1873, and 1828 cm^{-1} was 2.5-fold faster and rate constants of about $-5 \cdot 10^{-4}$ s^{-1} were observed, whereas the half-life times were reduced to 20 min. In contrast, the decrease of the vibrational band at 2010 cm^{-1} was accelerated by one order of magnitude ($-1 \cdot 10^{-3}$ s^{-1}) with a half-life time of 9 min. Moreover, a new band was found to grow in with irradiation time at 1770 cm^{-1} (Fig. 3.28).

Table 3.5: Photolysis studies on conjugate **12** in DMSO with irradiation at 468 nm as well as its dark stability under aerobic conditions, monitored by IR spectroscopy.

	dark		**468 nm**	
ν**(CO)**	**k / s^{-1}**	**$t_{1/2}$ / min**	**k / s^{-1}**	**$t_{1/2}$ / min**
2010 cm^{-1}	$-(1.70 \pm 0.14) \cdot 10^{-4}$	68 ± 6	$-(1.24 \pm 0.02) \cdot 10^{-3}$	9 ± 1
1898 cm^{-1}	$-(1.89 \pm 0.30) \cdot 10^{-4}$	62 ± 10	$-(4.92 \pm 0.01) \cdot 10^{-4}$	23 ± 1
1873 cm^{-1}	$-(2.28 \pm 0.32) \cdot 10^{-4}$	51 ± 7	$-(5.26 \pm 0.20) \cdot 10^{-4}$	22 ± 1
1828 cm^{-1}	$-(2.34 \pm 0.32) \cdot 10^{-4}$	50 ± 7	$-(5.56 \pm 0.23) \cdot 10^{-4}$	21 ± 1

Since the vibrational band at 2010 cm^{-1}, which is assigned to the axial carbonyl ligands as mentioned earlier, decreases 10-fold faster upon irradiation compared to the dark experiment, a preferential displacement of one of these ligands seems to occur upon photoexcitation at 468 nm. Combined with the observation of a new carbonyl vibrational band at 1770 cm^{-1}, this indicates the formation of a new metal carbonyl species. The position of the new band in the spectrum is comparable to those observed in facially coordinated molybdenum tricarbonyl complexes bearing pure σ-donor ligands, such as $[Mo(CO)_3([9]aneN_3)]$ with $[9]aneN_3$ = 1,4,7-triazacyclononane.[116] The vibrational bands at 1898, 1873, and 1828 cm^{-1} were found to decrease 2.5-fold faster upon irradiation compared to the dark experiment. The same trend was also observed when spectral changes of **12** in dimethylsulfoxide under aerobic conditions were monitored by UV/Vis spectroscopy. Herein, irradiation at 468 nm also led to a 2.5-fold faster decrease in absorption compared to the dark experiment.

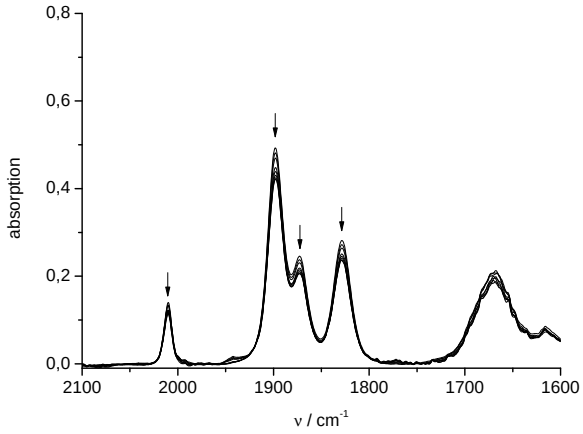

Fig. 3.26: Spectral change of **12** under aerobic conditions in DMSO in the dark, monitored by IR spectroscopy.

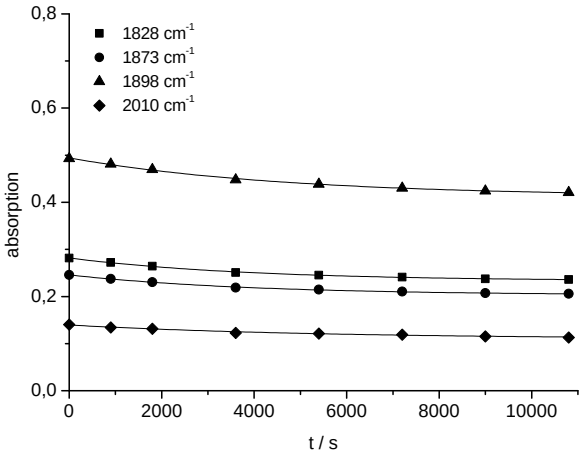

Fig. 3.27: Spectral change of **12** under aerobic conditions in DMSO in the dark. Decay of absorption over time.

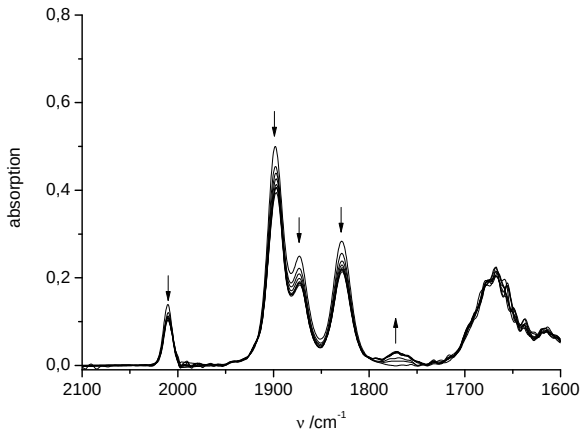

Fig. 3.28: Photolysis of **12** at 468 nm under aerobic conditions in DMSO, monitored by IR spectroscopy.

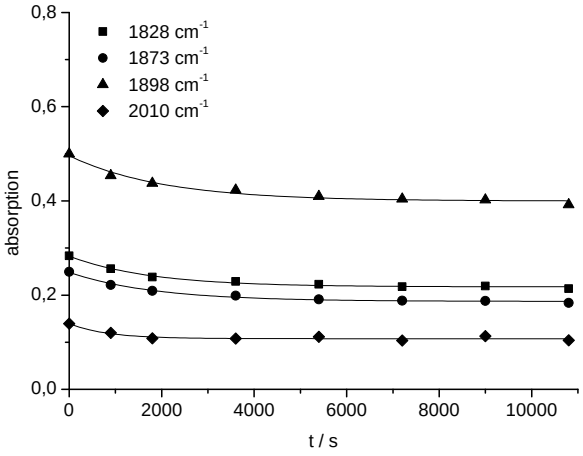

Fig. 3.29: Photolysis of **12** at 468 nm under aerobic conditions in DMSO. Decay of absorption over time.

Proposed mechanism of CO release

In summary, the results obtained from HPLC analysis, mass spectrometric measurements and UV/Vis as well as IR spectroscopic studies, indicate that the mechanism of CO release from conjugate **12** in the dark does not differ from the one observed upon photoexcitation at 468 nm, but is accelerated 2.5 to 3.5-fold in the latter case depending on whether the photolysis was monitored by IR or UV/Vis spectroscopy. A potential mechanism for the light-triggerd CO release from $[Mo(CO)_4(bpy^{R^1,R^2})]$ compound shown is in Fig. 3.30. In a first step, a photoexcited state of the molybdenum tetracarbonyl complex is formed upon irradiation of the MLCT transition at 468 nm. In the excited state, DMSO enters the coordination sphere of the complex, while one of the axial CO ligands dissociates simultaneously from the metal center follwing an associative substitution mechanism resulting in a *fac*-coordinated molybdenum tricarbonyl species. Since the ligand substitution could be suppressed when experiments were carries out in CO saturated solution, the tricarbonyl species is assumed to be

in an equilibrium with the tetracarbonyl species. Substitution of one of the axial CO ligands by a DMSO molecule is supposed to destabilize the low-valent molybdenum(0) center which then is oxidized, leading to a loss of the metal from the bipyridine ligand accompanied by further release of CO.

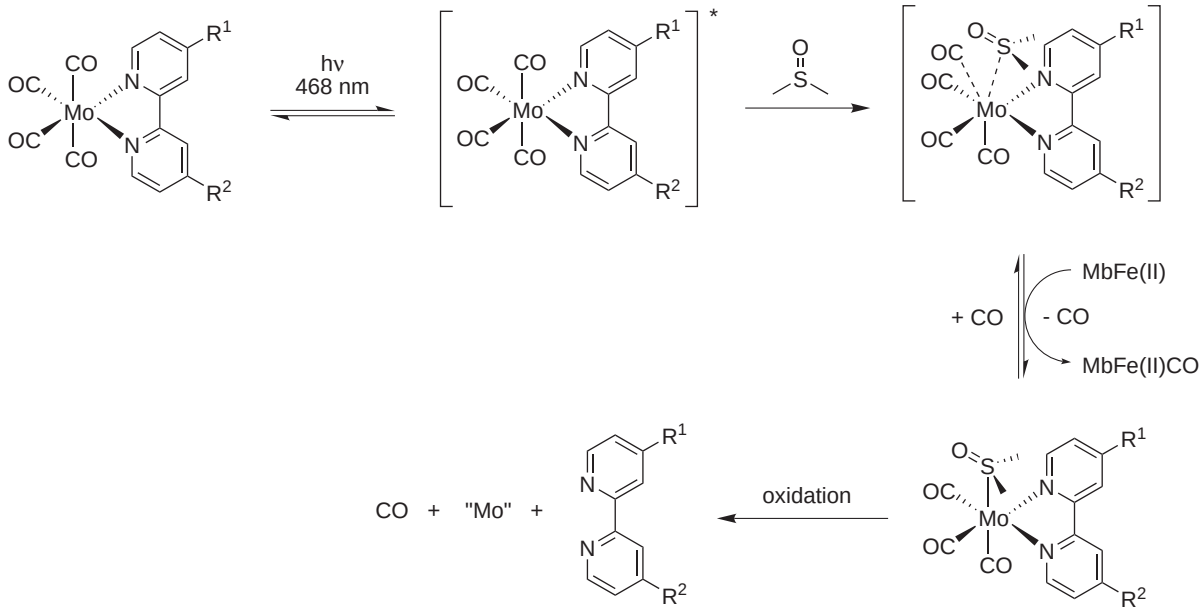

Fig. 3.30: Postulated mechanism for the light-triggered CO release from $[Mo(CO)_4(bpy^{R^1,R^2})]$ compounds with irradiation at 468 nm, as investigated by UV/Vis and IR spectroscopy as well as HLPC analysis and ESI mass spectrometry. DMSO was chosen as representative for any coordinating solvent molecule.

3.2 Biological activity of molybdenum allyl dicarbonyl complexes

3.2.1 Synthesis of [Mo(η^3-allyl)$(CO)_2$(N-N)(py)]PF_6 complexes

One of the first synthetic approaches towards [Mo(η^3-allyl)$(CO)_2$(N-N)(N)]X complexes was reported by Hull and Stiddard employing the three-step synthesis shown in Fig. 3.31, A.[117] In this procedure, molybdenum hexacarbonyl is first reacted with a bidendate nitrogen donor ligand followed by oxidative addition of an allyl halide to give the corresponding neutral [Mo(η^3-allyl)X$(CO)_2$(N-N)] complexes with X = halide. Finally, the halide is exchanged for pyridine to give [Mo(η^3-allyl)$(CO)_2$(N-N)(py)]X with X = BF_4^- or BPh_4^-. Another route reported by tom Dieck and Friedel is based on the synthesis of [Mo(η^3-allyl)X$(CO)_2(NCCH_3)_2$] complexes containing labile acetonitrile ligands which can easily be replaced by other ligands (Fig. 3.31, B).[118] Due to the rapid and highly efficient displacement reaction, the latter route is especially convenient in the preparation of complexes bearing *mer*- or *fac*-coordinating tridentate ligands or when difficult-to-prepare bidentate ligands are used.[119,120]

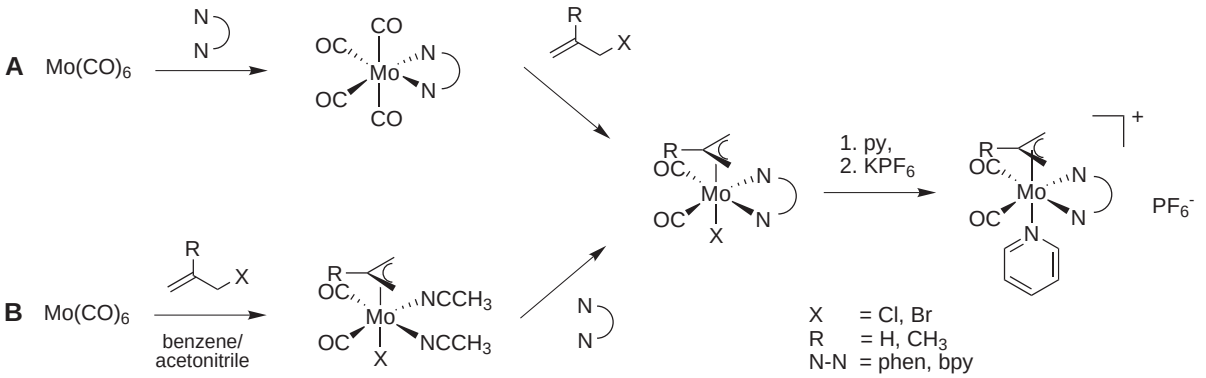

Fig. 3.31: Synthetic routes towards [Mo(η^3-allyl)$(CO)_2$(N-N)(py)]X complexes according to Stiddard and Hull (**A**) and tom Dieck and Friedel (**B**).

In contrast to the methodes reported in the literature, a new two-step route was followed in the present work, starting with a one-pot synthesis of [Mo(η^3-allyl)Cl$(CO)_2$(N-N)] complexes (Fig. 3.32). The bidentate N-N ligands were used to modulate the biorelevant porperties of the complexes such as lipophilicity/hydrophilicity. 2,2'-bipyridine (bpy) and 1,10-phenanthroline (phen) were obtained from commercial sources, while the synthesis of dipyido[3,2-*d*:2',3'-*f*]quinoxaline (dpq), dipyrido[3,2-*a*:2',3'-*c*]phenazine (dppz), and benzo[*i*]dipyrido[3,2-*a*:2',3'-*c*]phenazine (dppn) was performed according to literature procedures (Fig. 3.33).[121] The one-pot synthesis worked best when carried out in boiling tetrahydrofuran using an 1.1-fold excess of molybdenum hexacarbonyl and a 10-fold excess of allyl chloride over the N-N ligand, which could easily be removed in the work-up procedure by either sublimation of $Mo(CO)_6$ or extended washing with *n*-hexane.

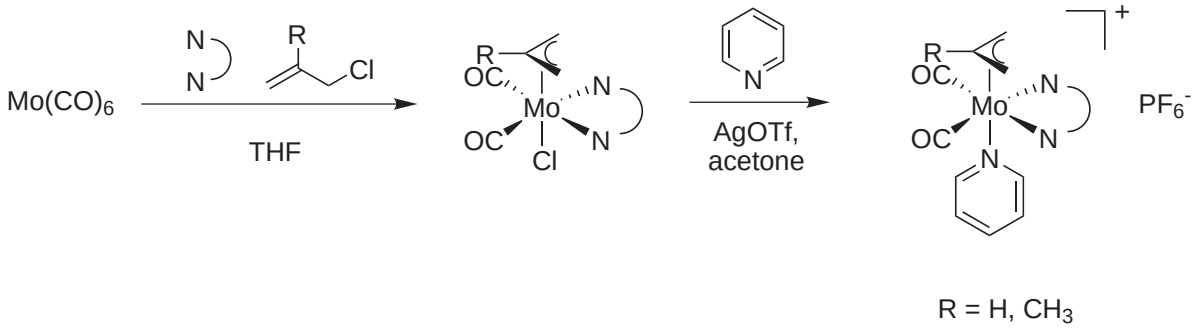

Fig. 3.32: New two-step synthetic route to [Mo(η^3-allyl)$(CO)_2$(N-N)(py)]PF_6 complexes.

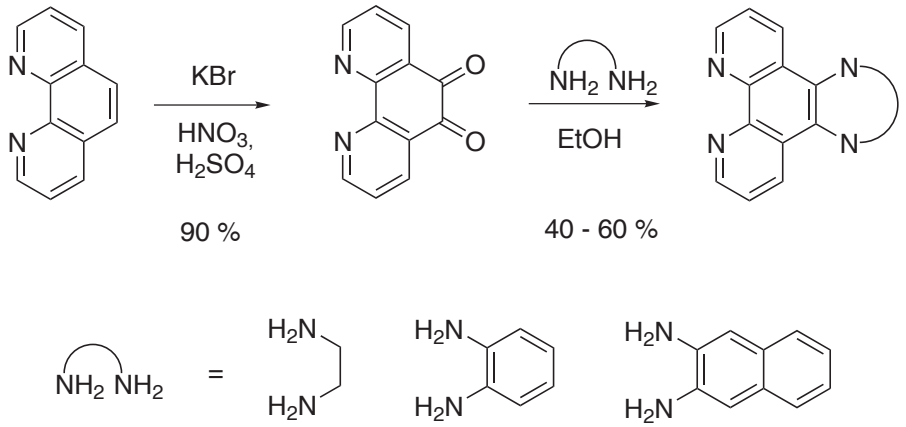

Fig. 3.33: Synthesis of bidentate polypyridyl ligands dpq, dppz, and dppn.

The desired complexes were obtained in yields of 49 to 88% and pure form according to microanalysis and were therefore used without further purification. Additionally, all compounds were characterized by ^{1}H- and ^{13}C-NMR spectroscopy as well as IR spectroscopy, except for [Mo(η^3-allyl)Cl$(CO)_2$(dppz)] and [Mo(η^3-allyl)Cl$(CO)_2$(dppn)] with the most extended aromatic π system, where characterization by NMR spectroscopy was not possible due to insufficient solubility in the deuterated solvents available.
In a second step, the chloride ligand was precipitated as silver chloride by the addition of silver triflate to give an intermediate species coordinated by acetone, which was the solvent used in this synthesis. This labile ligand was then replaced by pyridine and the complex finally isolated as the hexafluorophosphate salt. The isolated yields ranged from 43 to 85%. All complexes were characterized by ^{1}H- and ^{13}C-NMR, IR spectroscopy, ESI mass spectrometry, and microanalysis. All data are in good agreement with the expected values. The NMR spectroscopic characterization of [Mo(η^3-allyl)$(CO)_2$(N-N)(py)]PF_6 with N-N = dpq, dppz, and dppn was again limited to ^{1}H-NMR due to insufficient solubility in common deuterated solvents, although it was somewhat better compared to the neutral chlorido complexes but still not good enough to obtain ^{13}C-NMR data.

The IR spectra of all complexes from the [Mo(η^3-allyl)Cl(CO)$_2$(N-N)] as well as the [Mo(η^3-allyl)(CO)$_2$(N-N)(py)]PF_6 series exhibit two CO vibrational bands, one for the symmetric vibration (A') at 1930$\pm$4 cm^{-1} and another one for the antiymmetric vibration (A") at 1861$\pm$31 cm^{-1}, as expected for *cis*-dicarbonyl ligands in a complex with C_s symmetry. In the series of allyl complexes [Mo(η^3-allyl)Cl(CO)$_2$(N-N)], the IR band of the antisymmetric CO vibration (A") experiences a shift of more than 30 cm^{-1} from 1831 cm^{-1} to 1865 cm^{-1} with increasing size of the polypyridyl ligand due to its increased π-acceptor properies. The effect of the bidentate ligand on the symmetric CO vibration (A') is somewhat smaller, resulting in a shift of 10 cm^{-1} from 1925 cm^{-1} to 1935 cm^{-1} upon going from bpy to dppn. In addition to the *trans*-effect, changes at the axial allyl ligand also influence the position of the CO vibrations. Whereas only a marginal shift towards higher wavenumbers is observed in the symmetric vibrational band for the methallyl series compared to the allyl series, the antisymmetric vibrational band is shifted from 1831 to 1850 cm^{-1} in the bpy complexes and from 1842 to 1852 cm^{-1} in the phen complexes when going from allyl to methallyl (Tab. 3.6).

Table 3.6: CO vibrational bands in [Mo(η^3-allyl)(CO)$_2$(N-N)Cl] complexes.

compound	**N-N ligand**	**allyl-R**	ν**(CO) / cm^{-1}**	
			A'	**A"**
14	bpy	CH_3	1925	1850
16	phen	CH_3	1927	1852
15	bpy	H	1925	1831
17	phen	H	1930	1842
18	dpq	H	1932	1840
19	dppz	H	1935	1859
20	dppn	H	1935	1865

The symmetric and antisymmetric CO vibrational bands of all compounds in the [Mo(η^3-allyl)(CO)$_2$(N-N)(py)]PF_6 series exhibit a small shift towards higher wavenumbers compared to the corresponding chlorido complexes but no trend within the series itself can be indentified (Tab. 3.7).

Table 3.7: CO vibrational bands in [Mo(η^3-allyl)$(CO)_2$(N-N)(py)]PF_6 complexes.

compound	N-N ligand	allyl-R	ν(CO) / cm^{-1}	
			A'	A"
21	bpy	CH_3	1944	1860
23	phen	CH_3	1938	1870
22	bpy	H	1944	1841
24	phen	H	1938	1869
25	dpq	H	1948	1861
26	dppz	H	1948	1860
27	dppn	H	1948	1869

The ^{1}H NMR spectra of all [Mo(η^3-allyl)$(CO)_2$(N-N)(L)] complexes show two sets of three signals for an AM_2X_2 spin system that is consistent with a symmetrical η^3-coordination of the allyl ligand and two sets of signals for the bidentate polypyridyl and pyridine ligand which indicates the presence of two isomers in solution. The allyl ligand undergoes rapid conformational changes on the NMR time scale leading to an *endo/exo* isomerisation as described in the literature for various kinds of molybdenum allyl dicarbonyl complexes.[122–124] The binding mode with the *syn-* and *anti*-protons of the allyl ligand in an ecliptical position relative to the carbonyl ligands is referred to as the *endo*-isomer while the other one is the *exo*-isomer (Fig. 3.34). The isomerisation process occurs via rotation of the η^3-allyl ligand around the metal-allyl axis with a rotational barrier of about 16 kJ/mol.[123] Unexpectedly, the *endo/exo* isomerism was not observed in the [Mo(η^3-methallyl)$(CO)_2$(N-N)] complexes and the the *exo*-isomer was found to be the only isomer present in solution. This might be due to an increased rotational barrier because of the sterical more demanding methallyl group. For all other complexes, the *endo/exo*-isomer ratio was determined by ^{1}H NMR spectroscopy to be 80:20.

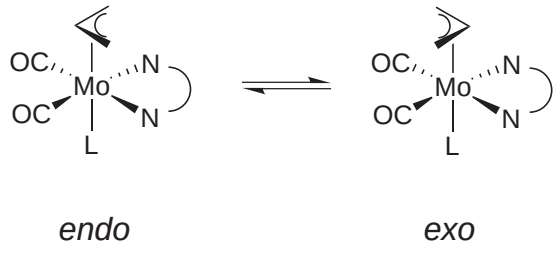

Fig. 3.34: *Endo/exo*-isomerisation in [Mo(η^3-allyl)$(CO)_2$(N-N)]-compexes.

3.2.2 Determination of log*P* values

The *n*-octanol/water partition coefficient log*P* is an important pharmacological model parameter to measure the lipophilicity of a substance. With the aid of this dimensionless parameter, one can estimate the distribution behavior of a molecule in organs and tissues. Along with plasma protein binding and acid/base properties, lipophilicity is one of the main intrinsic factors that influence the bioavailability of a pharmacological substance. According to Lipinski's "rule-of-five", which describes the drug-likeness of a compound by assessment of its physical properties such as molecular weight, lipophilicity, and the number of hydrogen donor and acceptor groups, the log*P* value should be below 5 for a drug-like compound.[125–127] Compounds having log*P* values > 0 are lipophilic, whereas those with log*P* values < 0 are hydrophilic.
In the present work, the log*P* values of the [Mo(η^3-allyl)$(CO)_2$(N-N)(py)]PF_6 complexes and the corresponding N-N ligands were determined using the "shake-flask" method according to the procedure reported by Kunz *et al.*[69] The partition coefficient of cisplatin served as a reference (Tab. 3.8).

Table 3.8: *n*-octanol/water partiton coefficients log$P_{7.4}$ of [Mo(η^3-allyl)$(CO)_2$(N-N)(py)]PF_6 complexes, the corresponding N-N ligands and cisplatin.

compound	N-N ligand	allyl-R	log$P_{7.4}$
22	bpy	H	-0.40±0.01
21	bpy	CH_3	-0.20±0.06
24	phen	H	-0.08±0.01
23	phen	CH_3	0.13±0.01
25	dpq	H	0.47±0.01
26	dppz	H	1.86±0.14
27	dppn	H	1.72±0.07
bpy	-	-	1.73±0.02
phen	-	-	1.53±0.05
dpq	-	-	0.93±0.21
dppz	-	-	n.d.
dppn	-	-	n.d.
cis-Pt$(NH_3)_2Cl_2$	-	-	-1.18±0.04

Among the series of compounds tested, cisplatin was the most hydrophilic one, a fact that might be due to partial hydrolysis of the chloride ligands, which is a well-known activation mechanism for cisplatin and related platinum(II) complexes. In contrast, the molybdenum complexes investigated have no labile ligands that might dissociate on the time scale of the experiment. Therefore, ligand exchange effects contributing to the partition behavior can be neglected. In general, the log$P_{7.4}$ values were found to increase from -0.40 to 1.72 with the size of the N-N ligand as well as with changes in the substitution pattern at the *meso*-position of the allyl ligand. It was found that

for bpy and phen complexes a methyallyl ligand increases the lipophilicity significantly by 0.20 units compared to the corresponding allyl complexes, but not to the same extent as the change in N-N ligand from the bipyridine to phenanthroline does. From the sub-series of allyl and methallyl complexes with bipyridine and phenanthroline ligands, the hydrophobic substituent constant π(X) was calculated for the methyl group. This parameter specifies the additive contribution of a substituent to the log*P* value in a homologous series of compounds in comparison to an unsubstituted reference system.[128]

$$\pi(CH_3) = \log P_{7.4}(\text{methallyl}) - \log P_{7.4}(\text{allyl})$$

In the sub-series mentioned above, $\pi(CH_3)$ was found to be (0.20$\pm$0.01). This value can be used to estimate the change in lipophilicity in a series of [Mo(η^3-allyl-R)$(CO)_2$(N-N)(py)] complexes upon introducing a methyl group to the allyl ligand.
The largest difference in log*P* values of about 1.4 was observed between the dpq and dppz complex. The lipophilicity of the dpq complex (**25**) as well as the dpq ligand alone is significantly reduced compared to the phen complex (**24**) and the phen ligand. This may be due to the presence of two additional nitrogen atoms in the dpq ligand that allow formation of hydrogen bonds in aqueous solution. This hydrophilic effect seems to be fully compensated when additional aromatic moieties are introduced to the polypyridyl ligands as indicated by a strong increase of lipophilicity for the dppz (1.86$\pm$0.14) and the dppn complex (1.72$\pm$0.07). The partition coefficients for the dppz and dppn ligand could not be determined because concentrations in the aqueous phase were below the detection limit of the UV/Vis spectrometer.

3.2.3 Biological activity on human cancer cells

Cytotoxicity studies on HT-29 and MCF-7 cancer cells

To evaluate the *in vitro* cytotoxicity of the [Mo(η^3-allyl)$(CO)_2$(N-N)(py)]PF_6 complexes listed in Tab. 3.9 on adherent HT-29 human colon carcinoma cells and MCF-7 human breast cancer cells, their IC_{50} values were determined by using the crystal violet assay which quantifies the cell biomass of live cells.

Table 3.9: IC_{50} values (in μM) of [Mo(η^3-allyl)$(CO)_2$(N-N)(py)]PF_6 complexes and cisplatin on HT-29 and MCF-7 cancer cells.

compound	N-N ligand	allyl-R	HT-29	MCF-7
21	bpy	CH_3	75±16	52±2.0
22	bpy	H	27±1.0	32±1.0
23	phen	CH_3	6.7±0.3	2.1±0.2
24	phen	H	2.2±0.4	2.5±0.3
25	dpq	H	5.5±0.2	n.d.
26	dppz	H	1.9±0.3	n.d.
27	dppn	H	1.8±0.8	n.d.
cis-Pt$(NH_3)_2Cl_2$	-	-	7.0±2.0	2.0±0.3[129]

The cytotoxic activity of the tested complexes on HT-29 cells initially increases with the size of the polypyridyl ligand from bpy to dpq but then remains constant for the largest dppz and dppz ligands. Whereas both the allyl and methallyl bpy compounds exhibit a rather moderate activity of 27 and 75 μM respectively, the corresponding phen complexes are already more active, both showing IC_{50} values of 2 to 7 μM. Then activities remain at the same level for the dpq, dppz, and dppn complexes. Furthermore, the methallyl complexes of phen and bpy exhibit a slightly higher activity than the corresponding allyl compounds. The activity of the bpy and phen complexes on MCF-7 cells reflects the trend observed in HT-29 cells. Again, the activity increases by one order of magnitude upon going from bpy to phen, and the bpy methyallyl complex has a 1.5-fold higher IC_{50} value compared to the allyl complex. Since an increased size of the polypyridyl ligand unexpectedly did not result in an increased activity in HT-29 cells, the cytotoxic activity of the dpq, dppz and dppn complexes on MCF-7 cells was not determined. In conclusion, the tested complexes do not show any selective cytotoxic activity towards HT-29 versus MCF-7 cells. IC_{50} values on HT-29 cancer cells for the dpq and dppz complexes are comparable to values reported for ruthenium arene polypyridyl complexes [Ru(η^6-C_6Me_6)Cl(N-N)]OTf,[129] in contrast to the value reported for the dppn complex, which was about one order of magnitude lower then the corresponding ruthenium arene dppn complex. IC_{50} values for the phen, dpq, dppz, and dppn complexes are in the range reported for cisplatin.[129] Moreover, values for each [Mo(η^3-allyl)$(CO)_2$(N-N)(py)]PF_6 complex on both cell lines are lower than the corre-

sponding ones from a homologous series of $[Ru(bpy)_2(N\text{-}N)]Cl_2$ complexes.[121] Assuming that the cytotoxicity of this class of compounds is mainly determined by the increasing size and lipophilicity of the polypyridyl ligand, a constant increase of IC_{50} values should be expected upon going from bpy to dppn, as reported for a homologous series of *fac/mer*-$[RhCl_3(DMSO)(N\text{-}N)]$ complexes.[128] Since the cytotoxicity of Mo(η^3-allyl)$(CO)_2(N\text{-}N)(py)]PF_6$ complexes is only partially influenced by the size of the N-N ligand, their mode of action might not result only from their lipophilicity.

Cytotoxicity studies on NALM-6 leukemia cells

Compounds **22**, **24**, and **21** as well as the ligands bpy and phen were also chosen for further cytoxicity studies on non-adherent NALM-6 leukemia cells in order to evaluate a possible difference in activity on adherent versus non-adherent cancer cells. Cytotoxicity was measured by quantification of lactate dehydrogenase (LDH), which is rapidly released from the cytoplasm into the cell culture supernatant upon disintegration of the cell membrane, indicating necrosis as the main mode of action.[130] After 1 h of incubation, compounds **22** and **21** as well as bpy and phen showed no immediate cytotoxic effect on NALM-6 cells as demonstrated by almost 100% cell viability for concentrations of up to 100 μM (Fig. 3.35 - Fig. 3.37). This contrasts with **24**, where significant necrosis with less than 20% cell viability was detected at a concentration of 100 μM and an IC_{50} value of 63 μM was calculated (Fig. 3.38).

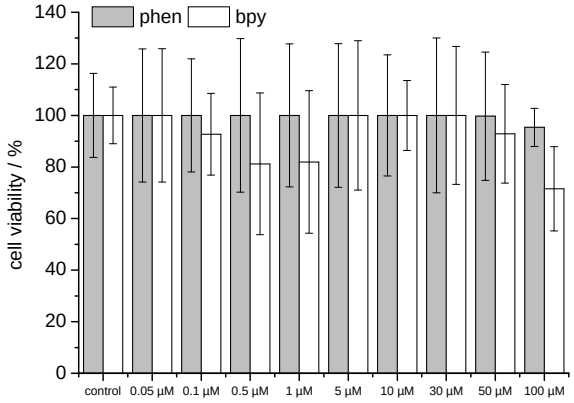

Fig. 3.35: Cell viability of NALM-6 cells determined by the release of LDH after an incubation period of 1 h for the ligands bpy and phen.

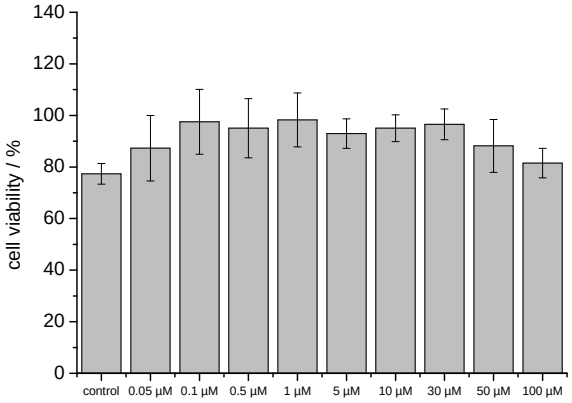

Fig. 3.36: Cell viability of NALM-6 cells determined by the release of LDH after an incubation period of 1 h for $[Mo(\eta^3\text{-allyl})(CO)_2(bpy)(py)]PF_6$ (**22**).

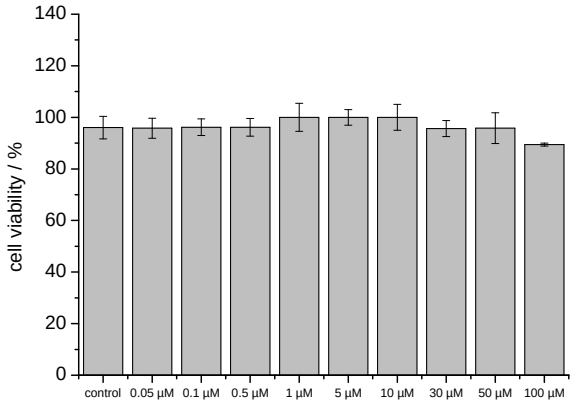

Fig. 3.37: Cell viability of NALM-6 cells determined by the release of LDH after an incubation period of 1 h for [Mo(η^3-methallyl)$(CO)_2$(bpy)(py)]PF_6 (**21**).

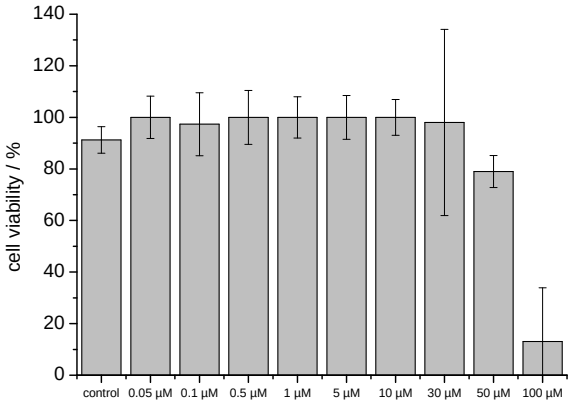

Fig. 3.38: Cell viability of NALM-6 cells determined by the release of LDH after an incubation period of 1 h for [Mo(η^3-allyl)$(CO)_2$(phen)(py)]PF_6 (**24**).

Inhibition of cell proliferation of NALM-6 leukemia cells

The inhibition of cell proliferation of NALM-6 leukemia cells by complexes **22**, **24**, **21** as well as ligands bpy and phen was evaluated *in vitro*. The viability and cell count were determined with a CASY Cell Counter and Analyzer System after an incubation time of 24 h.

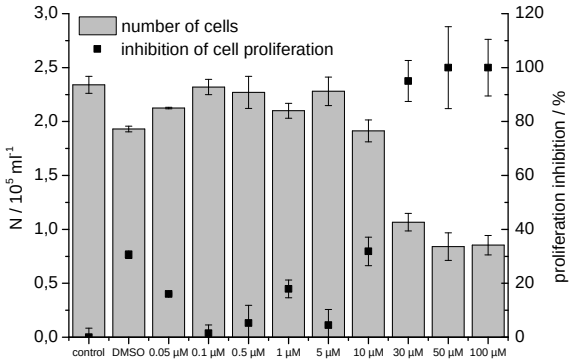

Fig. 3.39: Inhibition of cell proliferation in NALM-6 cells by the bpy ligand.

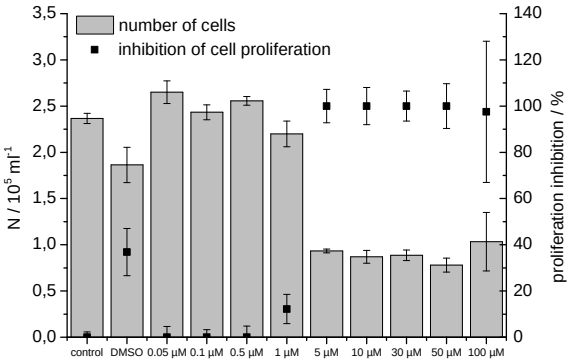

Fig. 3.40: Inhibition of cell proliferation in NALM-6 cells by the phen ligand.

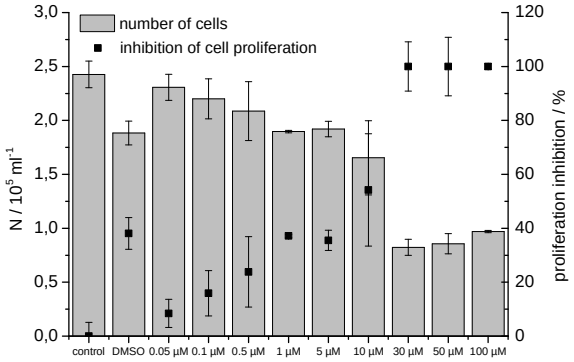

Fig. 3.41: Inhibition of cell proliferation in NALM-6 cells by [Mo(η^3-allyl)$(CO)_2$(bpy)(py)]PF_6 (**22**).

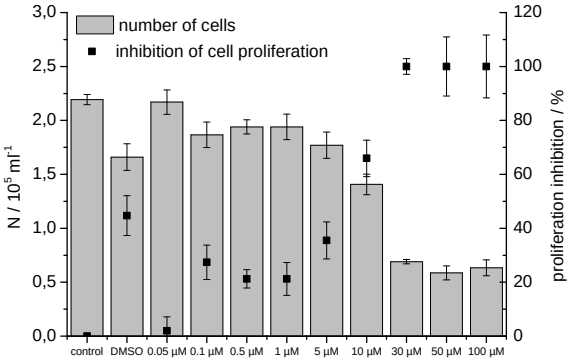

Fig. 3.42: Inhibition of cell proliferation in NALM-6 cells by [Mo(η^3-methallyl)$(CO)_2$(bpy)(py)]PF_6 (**21**).

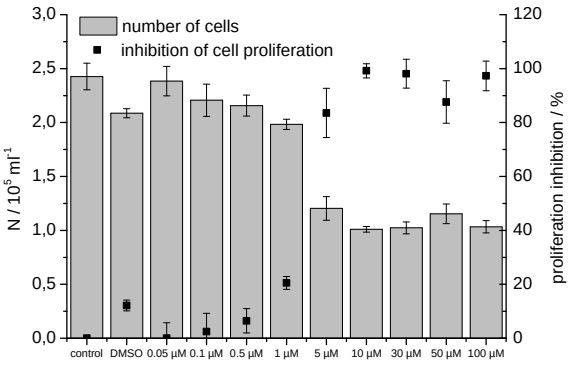

Fig. 3.43: Inhibition of cell proliferation in NALM-6 cells by [Mo(η^3-allyl)$(CO)_2$(phen)(py)]PF_6 (**24**).

For the bipyridine complexes **22** and **21** as well as the bpy ligand, a significant inhibition of cell proliferation of about 30% was observed for a concentration as low as 10 μM. This effect increased to 100% inhibition for concentrations of 30 μM and above. The phen complex **24** (Fig. 3.43) and phen (Fig. 3.40) itself exhibit a similar behavior with no difference in proliferation inhibition (Tab. 3.10). Thus, there is essentially no difference in activity between the complex and the free ligand. However, an increased size of the polypyridyl ligand going from bpy to phen correlates with a slightly increased activity.

Table 3.10: IC_{50} values (in μM) of [Mo(η^3-allyl)$(CO)_2$(N-N)(py)]PF_6 complexes and the ligands bpy and phen on NALM-6 leukemia cells.

compound	N-N ligand	allyl-R	NALM-6
22	bpy	H	10
21	bpy	CH_3	13
24	phen	H	1.8
bpy	-	-	8.9
phen	-	-	2.3

Apoptosis induction studies on NALM-6 leukemia cells

To gain further insight into the mechanism of cell death induced by the [Mo(η^3-allyl)-$(CO)_2$(N-N)(py)]PF_6 complexes, apoptosis induction was studied by measuring the amount of DNA fragmentation in NALM-6 cells upon incubation with selected compounds. The early release of intracellular proteins like lactate dehydrogenase (LDH) due to a loss of cell membrane integrity is a clear indicatior of necrotic cell death. On the other hand, apoptosis, as a controlled and regulated way of cell death, is characterized by irreversible fragmentation of the genomic DNA, called hypoloidy. Therefore, the degree of DNA fragmentation in NALM-6 cells was measured after 72 h of incubation with complexes **22**, **24**, **21** as well as the ligands phen and bpy.

For the latter two, a significant induction of apoptosis with > 90% of apoptotic cells in NALM-6 cells was observed for concentrations of 30 μM and above (Fig. 3.44). The

phen ligand exhibits a higher activity than bpy and does not induce apoptosis below 5 μM while no apoptosis below 30 μM is induced by the bpy ligand. A similar behavior was observed for the bpy complexes (Fig. 3.45 and Fig. 3.46) and the phen complex (Fig. 3.47), which showed no difference in activity compared to the ligands. This is in good agreement with the results obtained from the proliferation inhibition studies where 100% inhibition was observed in the same concentration range for both complexes and ligands, demonstrating that triggering of apoptosis is the primary mode of action of these compounds in NALM-6 cells. For the phen complex, a lower level of apoptosis with about 60% of apoptotic cells is observed at 100 μM concentration which differs from the observation made for all other compounds tested. This is in good agreement with results obtained from the LDH release measurements where significant necrosis occured in the presence of **24** at a concentration of 100 μM. Obviously, at high concentration, necrosis is the main mode of action at an early stage of cell death (1 h), thus lowering the overall degree of apoptosis that was measured after 72 h of incubation time. For all other tested compounds, only induction of apoptosis and no necrotic effect was observed at high concentration.

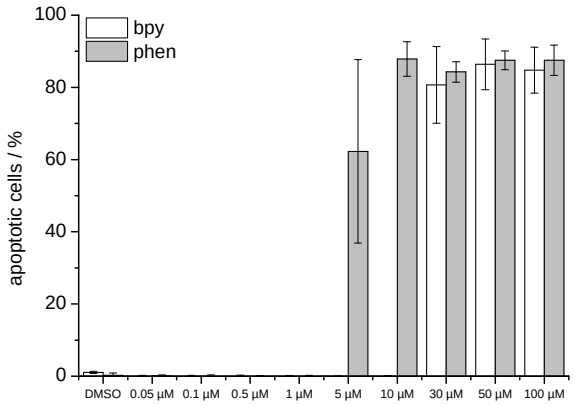

Fig. 3.44: Apoptosis induction in NALM-6 cells by the ligands bpy and phen after 72 h.

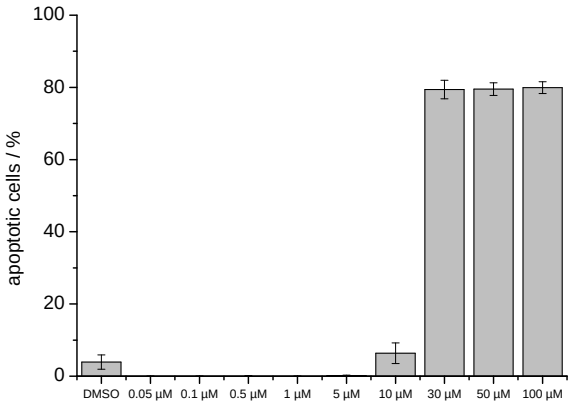

Fig. 3.45: Apoptosis induction in NALM-6 cells by [Mo(η^3-allyl)(CO)$_2$(bpy)(py)]PF$_6$ (**22**) after 72 h.

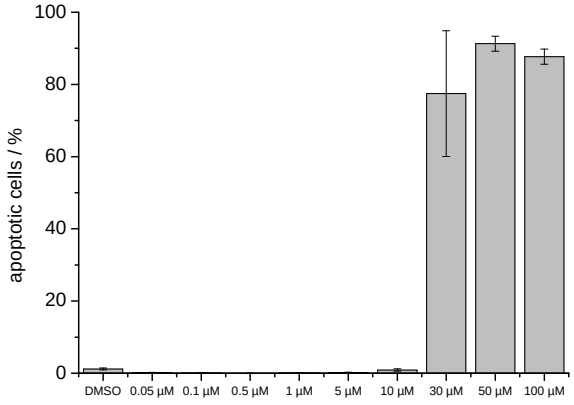

Fig. 3.46: Apoptosis induction in NALM-6 cells by [Mo(η^3-methallyl)(CO)$_2$(bpy)(py)]PF$_6$ (**21**) after 72 h.

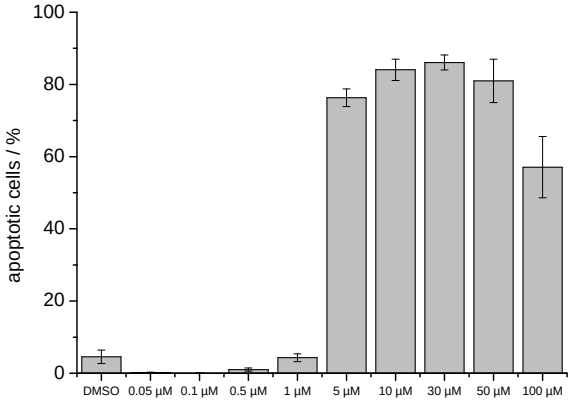

Fig. 3.47: Apoptosis induction in NALM-6 cells by [Mo(η^3-allyl)(CO)$_2$(phen)(py)]PF$_6$ (**24**) after 72 h.

Cytotoxicity studies on MCF-7 (-) cells

The protease caspase-3 plays a crucial role in the activation of apoptotic pathways. It is essential for certain proceses associated with typical signs of apoptosis, such as DNA fragmentation and formation of apoptotic bodies.[131] To study a possible dependence of caspase-3 expression on the cell proliferation, the activity of **22** and bpy was determined in MCF-7 (+/-) cells as described before. Normally, caspase-3 is not expressed in MCF-7 cells, here referred to as MCF-7 (-), but they can be reconstitued to obtain caspase-3 expressing cells (MCF-7 (+)).[132,133]

To assess the degree of necrosis that contributes to the cytotoxic activity of **22** and bpy on adherent MCF-7 (-) breast cancer cells, the LDH release assay was also carried out with these compounds. It was found that neither **22** nor bpy cause any necrosis in MCF-7 (-) cells at concentrations of up to 75 μM after 1 h of incubation (Fig. 3.48).

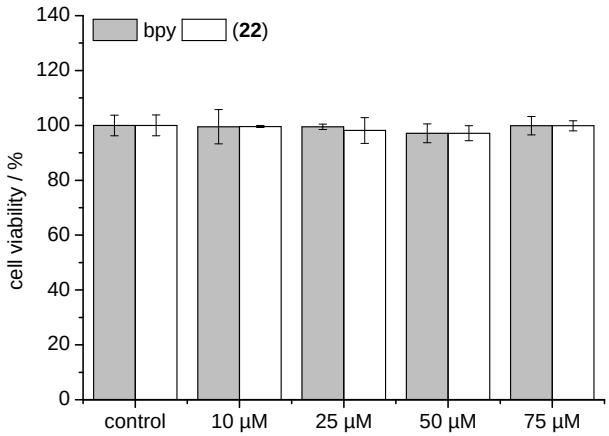

Fig. 3.48: Cell viability of MCF-7 (-) cells after an incubation period of 1 h with [Mo(η^3-allyl)$(CO)_2$(bpy)(py)]PF_6 (**22**) or bpy.

Inhibition of cell proliferation in MCF-7 (+/-) cells

The results of the cell proliferation inhibition studies are depicted in Fig. 3.49 and Fig. 3.50. There are significant differences in the activity of **22** and bpy on MCF-7 (+/-) cells. While the complex shows 100% inhibition of cell proliferation even at the lowest applied concentration of 10 μM, the bpy ligand is only active at concentrations of 50 μM and above. Moreover, bpy has a slightly higher activity on MCF-7 (-) cells (IC_{50} = 19 μM) than on MCF-7 (+) cells (IC_{50} = 32 μM), an effect which was not observed for **22**. Since inhibition values were 100% over the whole concentration range tested, no IC_{50} values could be determined for the latter complex.

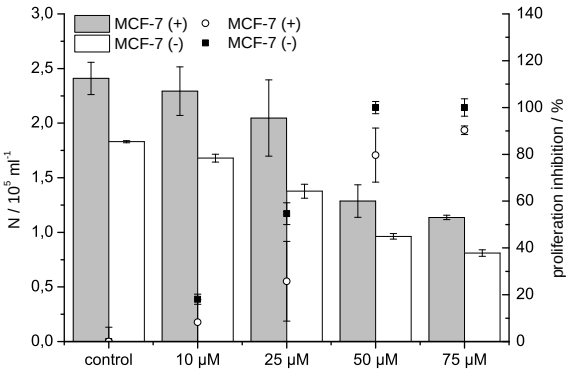

Fig. 3.49: Inhibition of cell proliferation in MCF-7 (+/-) cells by the bpy ligand.

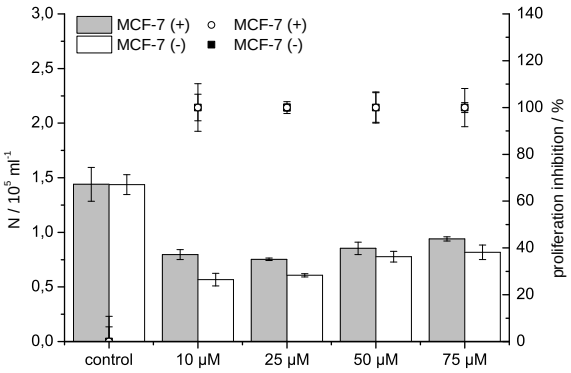

Fig. 3.50: Inhibition of cell proliferation in MCF-7 (+/-) cells by [Mo(η^3-allyl)$(CO)_2$(bpy)(py)]PF_6 (**22**).

Apoptosis induction studies on MCF-7 (+/-) cells

In the apoptosis studies on MCF-7 (+/-) cells, the activities of the complex **22** and the bpy ligand itself were found to differ significantly. The bpy ligand induces only about 20% apoptosis at 75 μM and shows no sign of apoptosis below 50 μM. On the other hand, the complex exhibits over 80% apoptosis at the maximum concentration of 75 μM and still induces 20% apoptosis even at the lowest concentration tested of 10 μM. This behavior was found in both MCF-7 (+) as well as MCF-7 (-) cells, revealing an apoptosis pathway that is independent of caspase-3 expression.

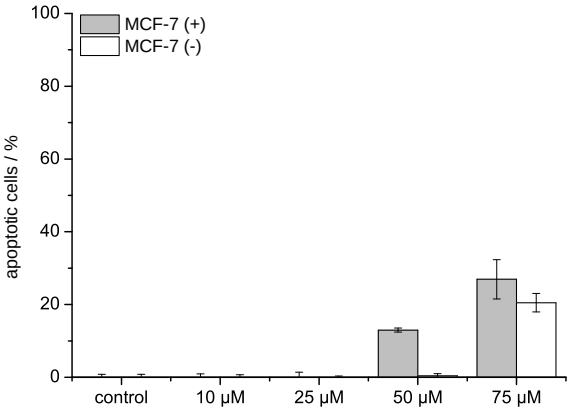

Fig. 3.51: Apoptosis induction in MCF-7 (+/-) cells by the bpy ligand after 72 h.

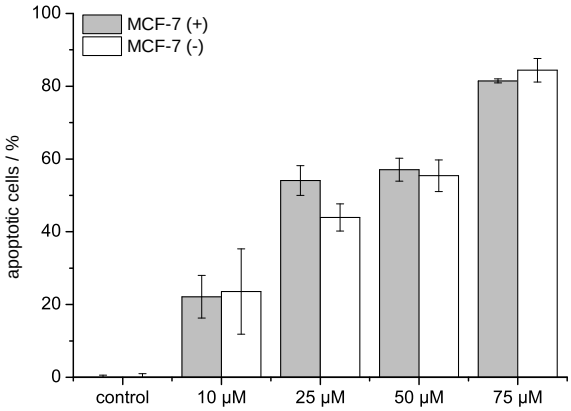

Fig. 3.52: Apoptosis induction in MCF-7 (+/-) cells by [Mo(η^3-allyl)$(CO)_2$(bpy)(py)]PF_6 (**22**) after 72 h.

Discussion

A series of seven [Mo(η^3-allyl-R)$(CO)_2$(N-N)(py)]PF_6 complexes with N-N = bpy, phen, dpq, dppz, dppn and R = H, CH_3 was synthesized following a new two-step approach starting with a on-pot synthesis of [Mo(η^3-allyl-R)Cl$(CO)_2$(N-N)] complexes. All compounds were obtained in good to moderate yield and analytical data were in full accordance with the expected values. Octanol/water-partition coefficients of all complexes were determined by applying the shake-flask methode. Log$P_{7.4}$ values were found to increase from -0.40 to 1.72 with the size of the N-N ligand as well as going from allyl to methallyl complexes. Compounds **22**, **24**, and **21** show Log$P_{7.4}$ values below 0 and thus are considered to be more hydrophilic while **23**, **25**, **26**, and **27** are more soluble in the *n*-octanol phase and thus are more lipophilic

The IC_{50} values of [Mo(η^3-allyl)$(CO)_2$(N-N)(py)]PF_6 complexes determined on adherent HT-29 and MCF-7 cancer cells decrease with the size of the bidentate ligand which is in good correlation with an increase of lipophilicity along the series. The activity of the phen, dpq, dppz and dppn complexes is comparable to that reported for cisplatin and ruthenium arene polypyridyl complexes, well studied for their anticancer activity.[121,129] IC_{50} values for the bpy and phen complexes on MCF-7 cells are comparable to values reported for neutral [Mo(η^3-allyl)X$(CO)_2$(N-N)] complexes with X = OTf, Cl, Br.[134] No difference in activity on HT-29 cells compared to MCF-7 cells was observed for all compounds tested. Whereas many studies on polypyridyl comlexes are traditionally focused on DNA interaction, a modification of cell membrane function and cell adhesion properties has also been discussed as possible mode of action[121] and brings the influence of lipophilicity into play. However, cytotoxicity testings do not give any insight into the exact mode of action, which therefore should be the matter of further investigations.

To assess a difference between adherent and non-adherent cells, the activity of complexes **22**, **24**, and **21** as well as the corresponding bidentate ligands towards non-adherent NALM-6 leukemia cells was also tested. These complexes were selected because they combine a moderate lipophilicity, which is favoured for solubility reasons, with a high cytotoxic activity, as shown for HT-29 and MCF-7 cells. The complexes and the free ligands show only minor differences in proliferation inhibition as well as apoptosis induction. For both, an increased ligand size/lipophilicity is correlated with an increased activity on both, HT-29 and MCF-7 cells. No necrotic effects were detected for all compounds tested at all concentrations that were applied, except for **24** at a maximum concentration of 100 μM. Therefore, apoptosis induction is considered to be the main mode of action for theses compounds towards NALM-6 cells.

Complex **22** and bpy were selected to test their activity towards caspase-3 espressing MCF-7 (+) and non-expressing MCF-7 (-) human breast cancer cells. Both compounds showed no necrotic effects at all. The complex **22** exhibits a significantly higher activity

in apoptosis induction as well as proliferation inhibition compared to the ligand itself, which contrasts with the results obtained from the studies on NALM-6 cells, where no difference in activity between complex and ligand was observed. Moreover, apoptosis induced by **22** was found to be at the same level in MCF-7 (+) and MCF-7 (-) cells, revealing a mode of action independent from expression of caspase-3. This is in contrast to the fact that expression of caspase-3 is normally to be thought crucial for the induction of DNA fragmentation as a hallmark of apoptosis. Although caspase-3 is not expressed in MCF-7 (-) cells, extensive DNA fragmentation by **22** was detected. Therefore, further biological studies will be needed to elucidate the pathway of apoptosis induction by this compound.

3.3 Click reactions with azide-containing molybdenum allyl dicarbonyl complexes

The application of the copper-catalyzed 1,3-dipolar cycloaddition (CuAAC) is well-established for organic azides and alkynes in bioconjugation reactions. In addition, the corresponding catalyst-free reactions have also attracted considerable interest the during the past few year as described in Chapter 1.5, since metalions originating from the catalyst can have severe toxic effecs in biological systems. Nevertheless, examples of copper-free methods for the conjugation of metal complexes to bioactive molecules are rare. In 2008 and 2010 Berkel *et al.* reported on the use of strained oxanorbonadienes as linkers in the conjugation of an ^{111}In-DTPA complex to a peptide for radio-labelling purposes.[101,102] However, as most alkyne-azide cycloadditions reported before, these examples also just involve azides incorporated in the organic ligand. 1,3-Dipolar cycloadditions of metal azide complexes and organic alkynes have not been reported in the literature for bioconjugation reactions. Thus, the reaction of an azide-containing molybdenum allyl dicarbonyl complex with electron-deficient alkynes for the conjugation to peptides was studied in the present work. Initially, the azido complex [Mo(η^3-allyl)(N_3)$(CO)_2$(bpy)] (**30**) was prepared in two steps, starting with molybdenum hexacarbonyl (1 eq.) which was reacted with 2,2'-bipyridine (0.9 eq.) and a large excess of allyl chloride (10 eq.) in a one pot-synthesis as described before (Chapter 3.2.1) to give [Mo(η^3-allyl)Cl$(CO)_2$(bpy)] (**15**) in good yield (74%). In a second step, the chloride ligand was removed by precipitation as silver chloride using silver triflate in degassed acetonitrile to give an intermediate solvato species. This labile ligand then was exchanged for azide by addition of solid sodium azide to give [Mo(η^3-allyl)(N_3)$(CO)_2$(bpy)] (**30**) in a moderate yield of 56%.

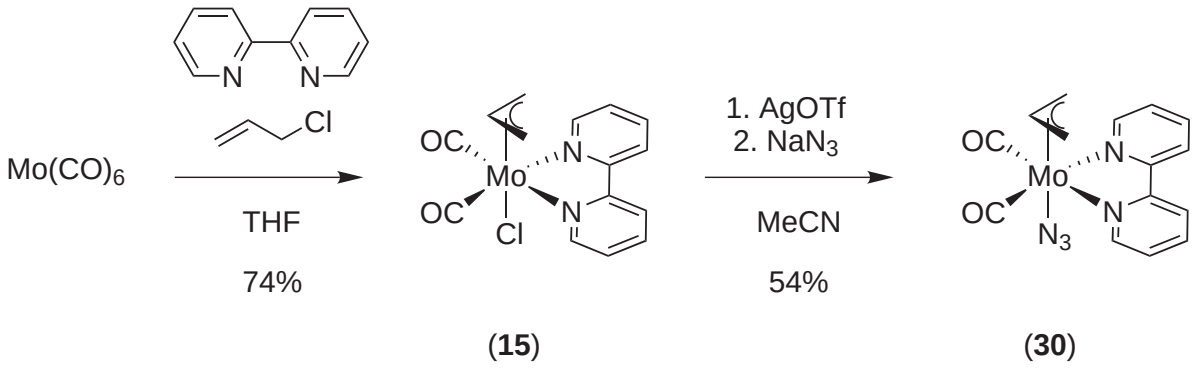

Fig. 3.53: Synthesis of [Mo(η^3-allyl)(N_3)$(CO)_2$(bpy)] (**30**).

The ATR-IR spectrum of **15** shows two carbonyl vibrational bands at 1925 and 1831 cm^{-1} (Fig. 3.54) while the corresponding bands for the azide complex **30** are found at 1928 and 1836 cm^{-1}. Moreover in the latter, the azide vibrational band is found at 2036 cm^{-1} (Fig. 3.55). The *endo/exo*-isomer ratio determined by ^{1}H-NMR spectroscopy was 75:25 for the chlorido complex and 84:16 for the azido complex. All other analytical data obtained for **15** and **30** are in full accordance with the expected values.

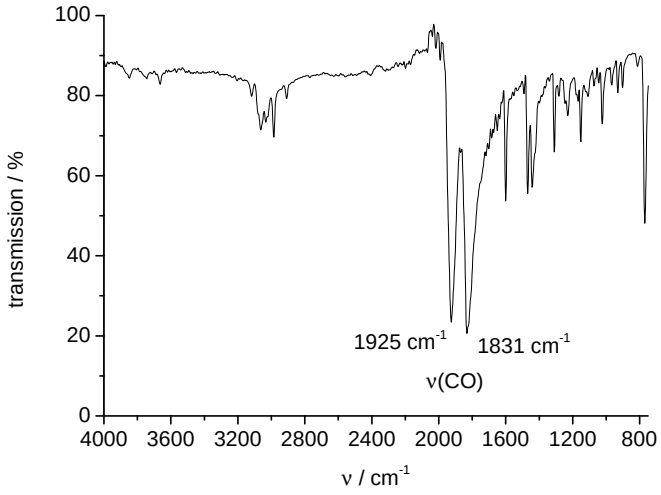

Fig. 3.54: ATR-IR spectrum of Mo(η^3-allyl)Cl$(CO)_2$(bpy) (**15**).

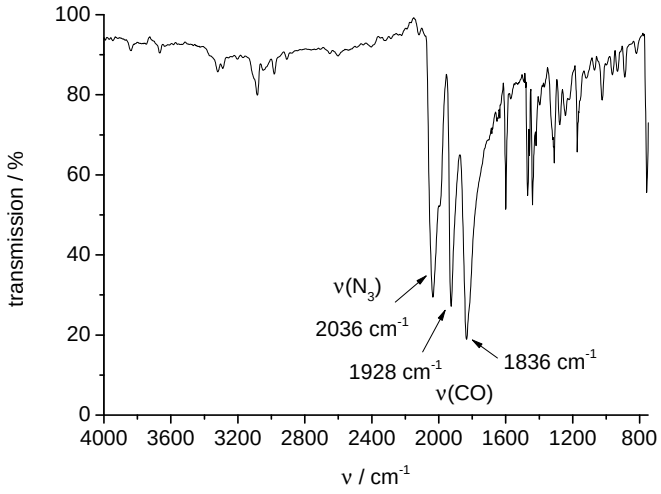

Fig. 3.55: ATR-IR spectrum of Mo(η^3-allyl)$(N_3)(CO)_2$(bpy) (**30**).

For 1,3-dipolar cycloadditions, electron-deficient alkyne components are required. Dimethylacetylene dicarboxylate (DMAD) was chosen because it is known to readily react with metal azide complexes to give the corresponding triazolate complexes and moreover, offers two methyl ester groups for further functionalization. However, DMAD is also reactive towards nucleophiles such as primary amines or hydroxyl groups which

react with the alkyne triple-bond in a Michael-addition reaction. Thus, it is not possible to use DMAD itself as a linker in solid-phase peptide synthesis or other bioconjugation protocols. Therefore, the triple bond was masked by reacting DMAD with furan in a [4+2] Diels-Alder reaction to give the substituted oxanorbornadiene **28**, which does not undergo Michael-addition reactions.[100] In order to allow for *N*-terminal coupling of the oxanorbornadiene building block to a peptide, one methyl ester group of **28** was selectively hydrolyzed using one equivalent of sodium hydroxide in aqueous tetrahydrofuran to give the monoacid **29** (Fig. 3.56).

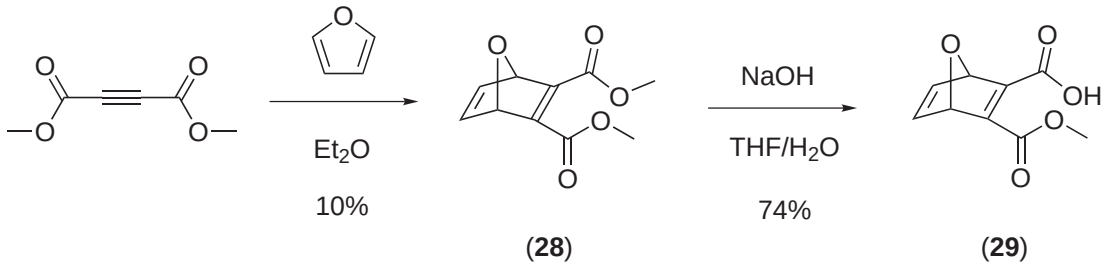

Fig. 3.56: Synthesis of 3-(methoxycarbonyl)-7-oxa-bicyclo[2.2.1]hepta-2,5-diene-2-carboxylic acid (**29**).

In order to evaluate the reactivity of [Mo(η^3-allyl)(N_3)$(CO)_2$(bpy)] (**30**) towards electron-deficient alkynes in a model system, the complex was reacted in a 1:1 ratio with DMAD in dichloromethane at room temperature for 48 h to give the triazolate complex **31** in moderate yield (47%). The progress of the reaction could easily be monitored by IR spectroscopy, following the decrease of the azide vibrational band at 2036 cm^{-1}. To assess whether the oxanorbornadiene **28** still has the same reactivity towards azide complexes as DMAD itself, **30** was also reacted with **28** in dichloromethane for 36 h at room temperature, which gave **31** in 77% yield (Fig. 3.57). Analytical data of the compound obtained from this reaction were in full accordance with those from the product obtained from the reaction with DMAD itself. No product resulting from a reaction with the unsubstituted double-bond of the oxanorbornadiene was observed. The material obtained from the reaction of **30** with **28** crystallized as deep-red needles after slow diffusion of *n*-hexane into a dichloromethane solution of complex after three days in the dark.

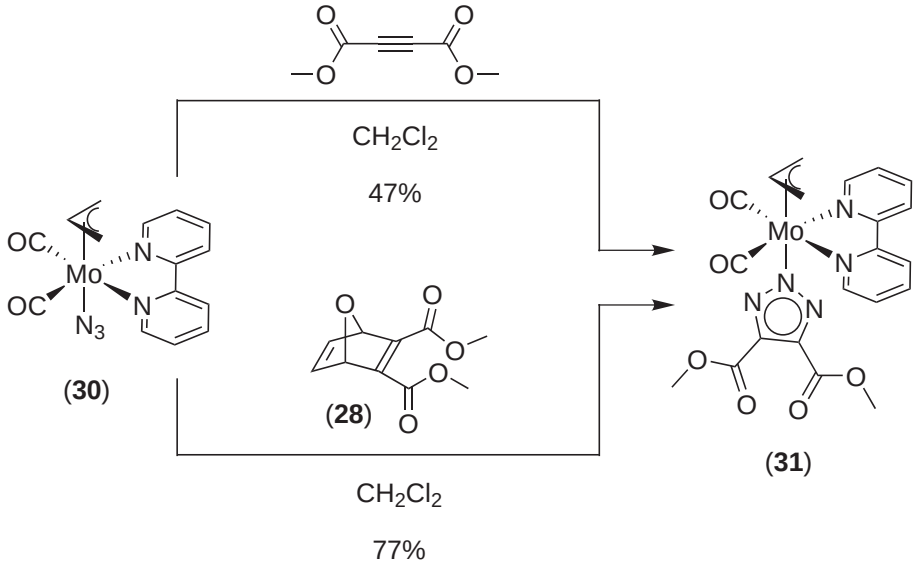

Fig. 3.57: Synthesis of [Mo(η^3-allyl)$(CO)_2$(bpy)$(N_3C_2(COOCH_3)_2)$] (**31**).

Single crystal X-ray diffraction revealed that the complex **31** crystallizes in the monoclinic space group $P2_1/c$. The molybdenum center is located in an octahedral coordination environment with the η^3-coordinated allyl ligand and the triazolate in axial positions whereas the *cis*-carbonyl ligands and the 2,2'-bipyridine ligand occupy the equatorial positions. The plane formed by the carbon atoms of the carbonyl ligands and the molybdenum center (C1-Mo1-C2) is not co-planar with the plane formed by N1-Mo1-N2, but tilted by 8.2(2)° towards the triazolate ligand. The angles of the *cis* ligands range from 72.6(2)° (N2-Mo1-N1) to 104.4(2)° (C1-Mo-N2) while the angles for the *trans* ligands vary from 170.01(2)° (C1-Mo1-N1) to 167.4(2)° (C2-Mo1-N2). The allyl ligand is in an *exo*-conformation with C15 and C13 in ecliptical position relative to the carbonyl ligands C1 and C2 while the dihedral angle (C15-C14-C13) is 116.4(6)°. Moreover, the aromatic rings of the bipyridine ligand are slightly distorted, with a torsion angle of 6.2(8)° for N1-C8-C7-N2. The Mo1-C1 and Mo1-C2 distances (1.982(5) and 1.959(6) Å) are comparable to those found in [Mo(η^3-C_3H_5)$(CO)_2$(dppe)$(N_3C_2(COOCH_3)_2)$][135] (1.950(3) and 1.977(3) Å). The triazolate ligand is bound via the nitrogen atom in 2-position (N4) to the metal center and the Mo1-N4 bond distance is 2.216(5) Å, which is in good agreement with the literature value of 2.2228(18) Å reported for the corresponding bond in [Mo(η^3-C_3H_5)$(CO)_2$(dppe)$(N_3C_2$-$(COOCH_3)_2)$].[135] The bond distances of the five-membered triazolate ring range from 1.330(7) (N4-N5) to 1.382(7) (C17-C18). Thus, they are comparable to the values found for the triazolate ring in [Mo(η^3-C_3H_5)$(CO)_2$(dppe)$(N_3C_2(COOCH_3)_2)$], which vary from 1.327(3) to 1.387(3) Å. It has also been reported that the complex with the N-1-coordinated triazolate ligand (N3) is considered to be a thermodynamic product, while the N-2-coordinated (N4) isomer is a kinetic product.[136]

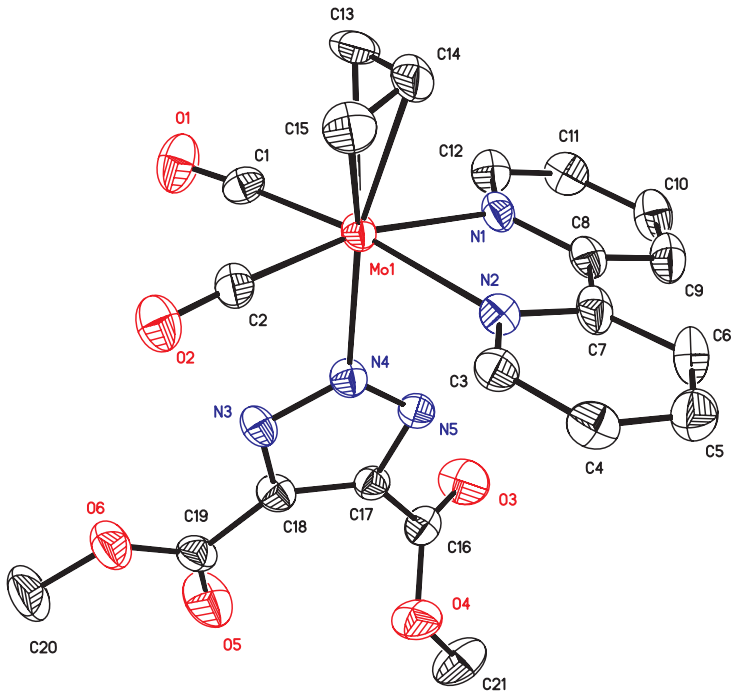

Fig. 3.58: Molecular structure of **31** in the solid state as determined by single crystal X-ray diffraction; thermal ellipsoids are drawn at the 50% probability level, hydrogen atoms are omitted for clarity. Selected interatomic distance (Å), angles (°) and torsion angles (°): Mo1-N1 2.244(4), Mo1-N4 2.216(5), Mo1-N2 2.247(5), Mo1-C1 1.982(5), Mo1-C2 1.959(6), Mo1-C13 2.320(7), Mo1-C14 2.220(7), Mo1-C15 2.350(7), N4-N3 1.344(6), N4-N5 1.330(7), N3-C18 1.350(8), N5-C17 1.344(8), C17-C18 1.382(7), C1-Mo1-C2 80.3(2), C1-Mo1-N2 104.4(2), C2-Mo1-N1 100.8(2), C2-Mo1-N4 86.9(2), N1-Mo1-N4 84.4(2), N2-Mo1-N1 72.6(2), N4-Mo1-C1 85.7(2), N4-Mo1-N2 81.9(2), C13-C14-C15 116.4(6), N1-C7-C8-N2 6.2(8).

Since oxanorbornadiene **28** could successfully be reacted with **30** giving the desired triazolate complex **31**, the oxanorbornadiene acid **29** was used to link the metal azide complex **30** to a model peptide following an on-resin strategy. The model peptide (H-Gly-Leu-Arg-OH) with oxanorbornadiene acid **29** attached to the *N*-terminus was synthesized on an preloaded Fmoc-Arg(Pbf)-Wang resin under the conditions of manual solid-phase peptide synthesis as described below. The conditions applied for the coupling of **29** were the same as described for the other amino acids. For the click-reaction, the ONBD-Gly-Leu-Arg(Pbf)-Wang resin was allowed to swell in dichloromethane prior to use and subsequently shaken with a solution of [Mo(η^3-allyl)(N_3)$(CO)_2$(bpy)] (**30**) in a 1:1 molar ratio in dichloromethane for 24 h while excluded from light. In a control experiment, ONBD-Gly-Leu-Arg(Pbf)-Wang resin was also shaken together with a solution of chlorido complex [Mo(η^3-allyl)Cl$(CO)_2$(bpy)] (**15**) under the same conditions as applied for the azido complex.

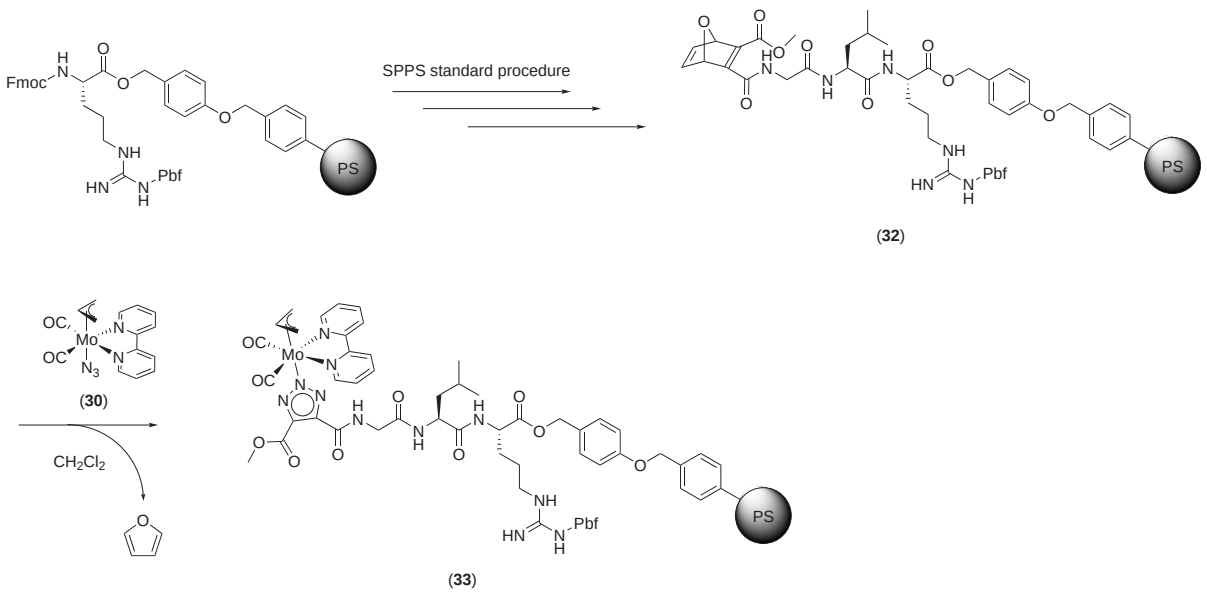

Fig. 3.59: Synthesis of [Mo(η^3-allyl)$(CO)_2$(bpy)(N_3C_2(COOMe)(CO-Gly-Leu-Arg(Pbf)-Wang resin))] (**33**) via copper-free strain-promoted alkyne-azide cycloaddition (SPAAC).

H-Gly-Leu-Arg(Pbf)-Wang (**10a**) and ONBD-Gly-Leu-Arg(Pbf)-Wang resin (**32**) as well as the resins obtained from the reaction of ONBD-Gly-Leu-Arg(Pbf)-Wang resin with the azido (**33**) and the chlorido complex **15** were characterized by light microscopy as well as ATR-IR spectroscopy. Beads of the H-Gly-Leu-Arg(Pbf)-Wang resin (**10a**) were almost colorless and transparent (Fig. 3.60) and the IR spectrum shows C=O vibrational bands for the ester group of the Wang linker at 1739 cm^{-1} and for the amide groups at 1662 cm^{-1} (Fig. 3.61). After *N*-terminal coupling of the oxanorbornadiene acid **29**, the resin turned brownish (Fig. 3.62) and the IR spectrum again shows the amide band at 1660 cm^{-1} and a C=O vibrational band for the ester group of the oxanorbornadiene moiety at 1725 cm^{-1} in addition to that of the Wang-linker at 1739 cm^{-1} (Fig. 3.63). After reaction of [Mo(η^3-allyl)(N_3)$(CO)_2$(bpy)] (**30**) with ONBD-Gly-Leu-Arg(Pbf)-Wang resin (**32**), the resin beads have a bright-red color (Fig. 3.64) which persisted after extensive washing with DMF and dichloromethane. In addition to the C=O vibrational bands at 1734 and 1664 cm^{-1}, two new bands at 1945 and 1863 cm^{-1} appear (Fig. 3.65). These can be assigned to the carbonyl ligands of a *cis*-dicarbonyl unit and therefore demonstrate, together with the absence of the azide vibrational band and the persistent bright-red color of the molybdenum complex, a successful coupling of the metal compound to the ONBD-Gly-Leu-Arg(Pbf)-Wang resin. The control experiment was carried out to investigate whether there is any non-covalent or covalent interaction between the ONBD-Gly-Leu-Arg(Pbf)-Wang resin and a neutral [Mo(η^3-allyl)X$(CO)_2$(bpy)] type complex in general that might also cause persistent coloring. After shaking the resin with a solution of [Mo(η^3-allyl)Cl$(CO)_2$(bpy)] (**15**) followed by extensive washing with DMF and dichloromethane, the resin was obtained with the brownish color as observed before addition of the metal complex (Fig. 3.66) and the IR

spectrum was identical to that of ONBD-Gly-Leu-Arg(Pbf)-Wang resin itself, showing no vibrational bands for the carbonyl ligands (Fig. 3.67). Thus, there is no evidence for a non-covalent or covalent interaction between the ONBD-Gly-Leu-Arg(Pbf)-Wang resin and a neutral [Mo(η^3-allyl)X(CO)$_2$(bpy)] type complex and the red color of the resin exclusively results from the reaction of the azide complex with the oxanorbornadiene moiety coupled to the resin.

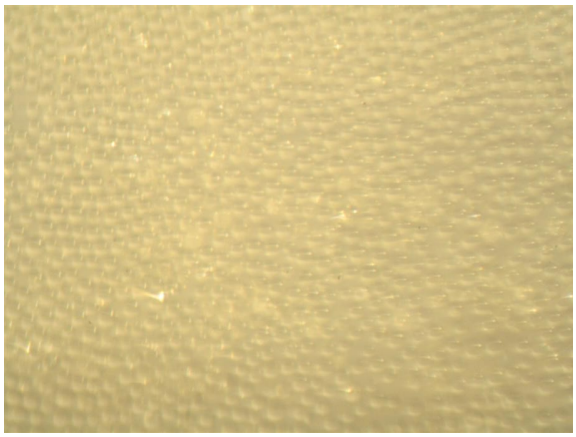

Fig. 3.60: Microscopy picture of H-Gly-Leu-Arg(Pbf)-Wang resin beads (20x magnification).

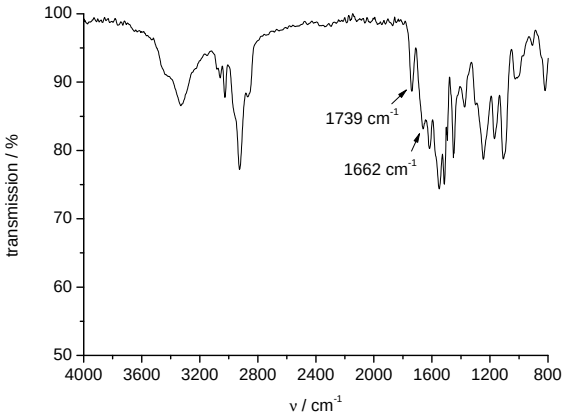

Fig. 3.61: ATR-IR spectrum of H-Gly-Leu-Arg(Pbf)-Wang resin beads (**10a**).

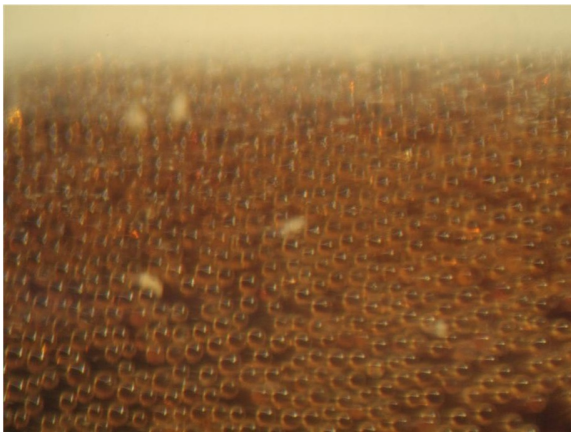

Fig. 3.62: Microscopy picture of ONBD-Gly-Leu-Arg(Pbf)-Wang resin beads (20x magnification).

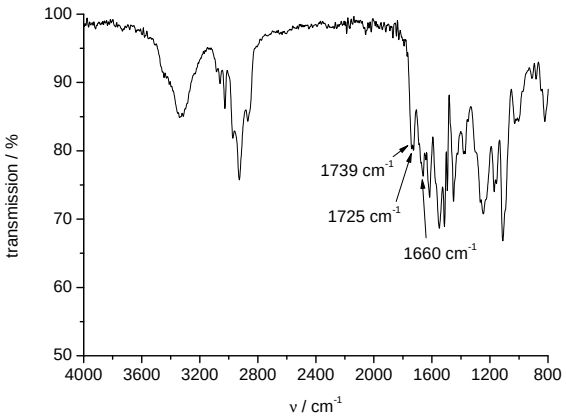

Fig. 3.63: ATR-IR spectrum of ONBD-Gly-Leu-Arg(Pbf)-Wang resin beads (**32**).

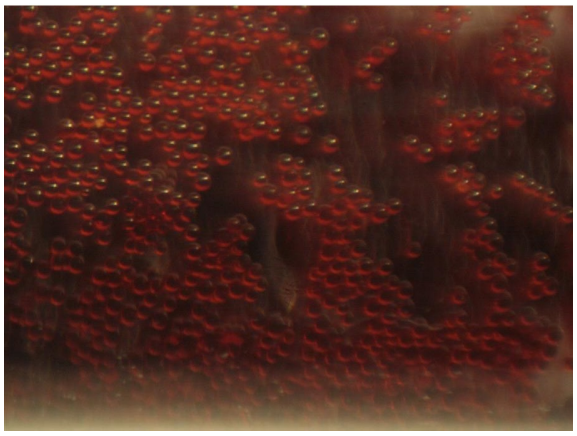

Fig. 3.64: Microscopy picture of ONBD-Gly-Leu-Arg(Pbf)-Wang resin beads after reaction with [Mo(η^3-allyl)(N_3)$(CO)_2$(bpy)] (**33**) (20x magnification).

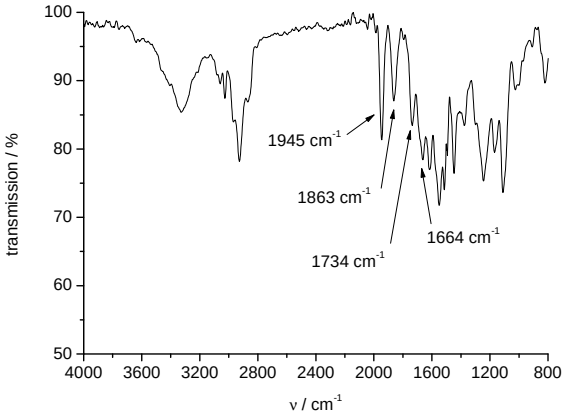

Fig. 3.65: ATR-IR spectrum of ONBD-Gly-Leu-Arg(Pbf)-Wang resin beads after reaction with [Mo(η^3-allyl)(N_3)$(CO)_2$(bpy)] (**33**).

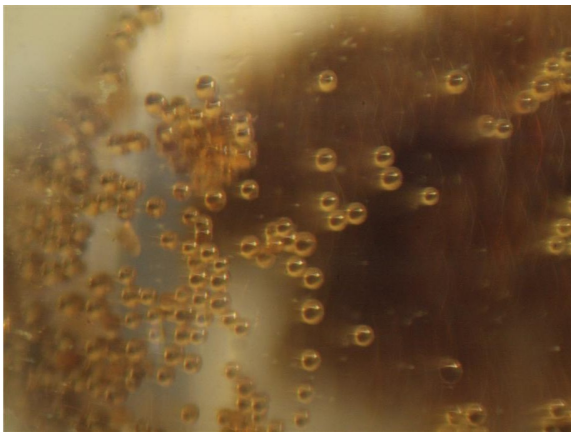

Fig. 3.66: Microscopy picture of ONBD-Gly-Leu-Arg(Pbf)-Wang resin beads after reaction with [Mo(η^3-allyl)Cl$(CO)_2$(bpy)] (20x magnification).

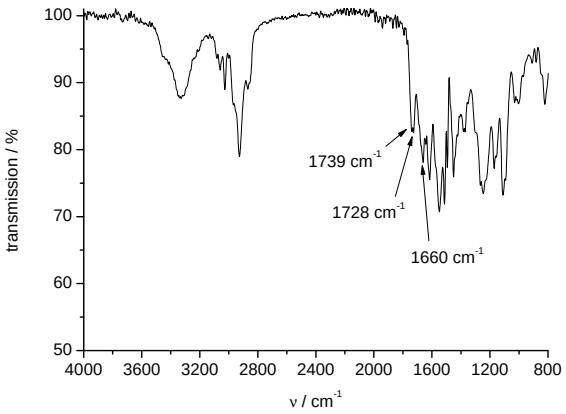

Fig. 3.67: ATR-IR spectrum of ONBD-Gly-Leu-Arg(Pbf)-Wang resin beads after reaction with [Mo(η^3-allyl)Cl$(CO)_2$(bpy)].

After [Mo(η^3-allyl)(N_3)$(CO)_2$(bpy)] (**30**) was sucessfully coupled to the ONBD-Gly-Leu-Arg peptide sequence on-resin, as confirmed by light-microscopy and IR spectroscopy, it was tried to cleave the conjugate from the resin using a mixture of TFA, TIS and water (95:2.5:2.5, v/v). The formation of a dark brown solution during the cleavage procedure indicated that the cleavage of the conjugate from the resin was not successful but led to decomposition of the molybdenum carbonyl moiety. HPLC analysis of the residue obtained after precipitation and lyophilization, combined with UV/Vis monitoring, did not show any presence of species having a MLCT absorption at 450 nm, as it would be expected for an intact [Mo(η^3-allyl)X$(CO)_2$(bpy)] moiety.

Therefore, in a second approach, a post-labelling strategy was employes utilizing the cycloaddition of [Mo(η^3-allyl)(N_3)$(CO)_2$(bpy)] (**30**) and ONBD-Gly-Leu-Arg-OH in solution. Thus, the peptide was cleaved from the resin under standard conditions using a mixture of TFA, TIS and water and the off-white solid obtained after precipitation and lyphilization was used in the next step without further HPLC purification. The cycloaddition reaction was carried out in a mixture of methanol and dichloromethane

(1:1, v/v) which provided optimal solubility for both reactants. After 24 h, the solvent was removed and HPLC analysis of the crude product revealed that no reaction had taken place and the only species having an absorption at 450 nm was the unreacted azide complex **30**. This was confirmed by comparison with the analytical HPLC chromatogram of pure **30**. Since the cycloaddition could successfully be carried out with the peptide still attached to the resin, but did not succeed in solution, it is assumed that the peptide decomposed in the cleavage step.

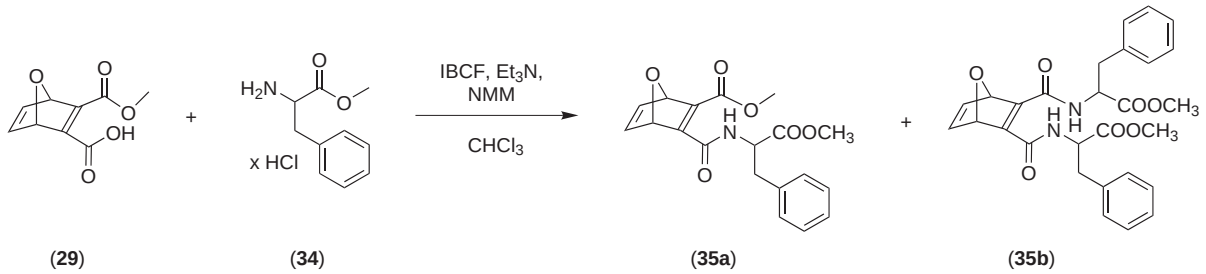

Fig. 3.68: Synthesis of ONBD-CO-Phe-OMe (**35a**) and ONBD-(CO-Phe-OMe)$_2$(**35b**).

In order to evaluate the reactivity of the oxanorbonadiene acid (**29**) towards primary amines, it was coupled to phenylalanine methylester (**34**) in solution using isobutyl chloroformate (IBCF) as the coupling reagent as shown in Fig. 3.68. After purification by column chromatography, two products were obtained in a 1:1 ratio. One was identified as the oxanorbornadiene with one phenylalanine methylester attached to the free acid, while the other one is the oxanorbornadiene with two phenylalanine methylester groups attached to the free acid as well as the hydrolyzed ester group. Thus, it was concluded that if the same reaction occurs when the oxanorbonadiene acid (**29**) is coupled to the *N*-terminus of a peptide in a solid-phase synthesis, the coupling to two peptide strands might be unfavourable in the cleavage step and lead to decomposition of the oxanorbonadiene moiety.

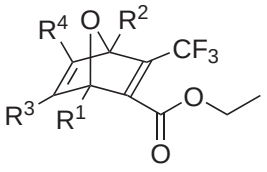

A: R^1 = H, R^2 = H, R^3 = H, R^4 = H
B: R^1 = CH_3, R^2 = CH_3, R^3 = H, R^4 = H
C: R^1 = H, R^2 = H, R^3 = CH_3, R^4 = H
D: R^1 = H, R^2 = H, R^3 = H, R^4 = CH_3

Fig. 3.69: Methyl-substituted derivatives A, B, C, and D of 3-Trifluoromethyl-7-oxa-bicyclo[2.2.1]hepta-2,5-diene-2-carboxylic acid ethyl ester.

In order to avoid such double-coupling reactions, oxanorbonadienes with just one acid functionality should be used as a linker. Trifluoromethyl-substituted oxanorbornadienes (Fig. 3.69), as reported by van Berkel *et al.*,[100–102,137] meet this demand as they

incorporate just one acid group, while the electron deficiency of the double bond is preserved by the electron-withdrawing trifluoromethyl group. Moreover, they are known to be stable towards concentrated TFA, as used in common cleavage mixtures. Therefore, trifluoromethyl-substituted oxanorbornadienes should be considered in further studies of a synthetic route towards peptides *N*-terminally functionalized with oxanorbornadiene moieties to avoide the problem of a double-coupling.

4 Conclusion

The aim of the present work was to synthesize $Mo(CO)_4$ and $Mo(allyl)(CO)_2$ complexes and study the modulation of their biological activity by variation of the coligands as well as methods for their conjugation to carrier peptides via catalyst-free bioorthogonal coupling methods.

In the first part, a molybdenum tetracarbonyl complex with an aldehyde-functionalized N-N coligand was synthesized using a new microwave-assisted procedure which enabled reaction times in the range of minutes, while the product was obtained in high yield and purity. This allowed use of an optimized oxime ligation protocol with an aminoxy acetic acid-terminated peptide derived from the tumor growth factor TGF-β_1 binding sequence to improve the bioavailability and target-specificition of the otherwise neutral compound. The peptide conjugate was studied for its CO release behaviour in the dark and with photoactivation using the myoglobin assay to evaluated the use of light as a trigger for its biological activity. Some CO release of 1.5 equivalents with a half-life time of 2 h was already observed in the dark in phosphate buffer, but was accelerated about 2.5-fold upon irradiation at 468 nm. Mechanistic studies of the CO release using ESI mass spectrometry as well as UV/Vis and IR spectroscopy support the intermediate formation of a *fac*-tricarbonyl molybdenum(0) species by displacement of one axial carbonyl ligand. This compound is oxidized under aerobic conditions, which then triggers loss of the whole molybdenum carbonyl unit from the bidentate ligand. These compounds might serve as photoactivatable CO releasing molecules (PhotoCORMs), although the dark-stability has to be further improved.

In the second part of this thesis, a series of seven molybdenum allyl dicarbonyl complexes with different bidentate polypyridyl coligands was synthesized following a two-step approach. The lipophilictiy of the complexes well as their cytotoxicity on adherent human HT-29 colon cancer and MCF-7 breast cancer cells was found to increase with the size of the bidentate ligand. IC_{50} values of the most active compounds are in the range of 2 to 5 μM, which is comparable to that of the reference drug cisplatin on both cell lines. When tested on non-adherent NALM-6 leukemia cells, the cytotoxicity, induction of apoptosis, and inhibition of cell proliferation was also found to increase with the ligand size. However, compared to the ligand alone, only a minor difference in activity was observed for the complexes in this case. Results from a DNA fragmentation assay as well as apoptosis induction studies carried out for a representative compound on MCF-7 cells revealed a caspase-3 independent pathway as the main mode of activity. This is remarkable since it is normally assumed that the expression of caspase-3 is necessary for DNA fragmentation as a hallmark of apoptosis. Thus, cationic molybdenum allyl dicarbonyl complexes with bidentate polypyridyl ligands of different size have significant cytotoxic activity on different human cancer cell lines with induction of apop-

tosis as the main mode of action. Further studies should attempt to eludicate the exact pathway of the caspase-3 independent apoptosis induction.
To further improve the bioavailability and targeting of the compounds, a novel conjugation method was for the first time applied to bioactive metal complexes. Thus, a molybdenum-coordinated azide was reacted in the metal coordination sphere with masked electron-deficient alkynes such as oxanorbornadiene diesters to form metal-bound triazoles. A X-ray crystal structure showed that the triazolate ligand coordinates to the metal center via the N(2) nitrogen atom of the heterocycle. The methodology was further extended to link the molybdenum azido complex to an oxanorbornadiene-terminated model peptide in an "on-resin" strategy. However, cleavage of the conjugate from the resin led to decomposition of the molybdenum dicarbonyl unit under the conditions tried so far. Therefore, further attempts should follow a "post-labelling" strategy in which the azido complex and the functionalized peptide are coupled in solution.

In summary, molybdenum carbonyl complexes with different polypyridyl coligands were prepared and conjugated to peptides by mild bioorthogonal coupling reactions like the oxime ligation and a catalyst-free azide-alkyne click reaction utilized for the first time in such a context. The biological activity of some of the new complexes and conjugates, including their CO release properties, cytoxicity on human cancer cells, and mode of induction of cell death was studied. Further investigations on these compounds should include in-depth studies of the biological activity, focusing on their exact pathways of induction of apoptosis.

Zusammenfassung

Ziel der vorliegenden Arbeit war die Synthese von $Mo(CO)_4$ und $Mo(allyl)(CO)_2$ Komplexen und die Untersuchung der Veränderung ihrer biologischen Eigenschaften durch Variation der Coliganden als auch die Entwicklung geeigneter Methoden zur Konjugation dieser Komplexe mit Carriereptiden mittels katalysatorfreier Kupplungsreaktionen. Im ersten Teil wurde ein Molybdäntetracarbonyl-Komplex mit einem aldehydfunktionalisiertem N-N Coliganden mittels einer neuen mikrowellen-unterstützen Methode synthetisiert die eine Verkürzung der Reaktionszeit auf wenige Minuten ermöglichte wobei der Komplex in hoher Ausbeute und Reinheit erhalten wurde. Dies ermöglichte die Verwendung eines optimierten Oxim-Ligationsprotokolls zur Konjugation einer aminooxyessigsäure-funktionalisierten und an den Tumorwachstumsfaktor TGF-β_1 bindenden Peptidsequenz mit dem ansonsten neutralen Komplex, zur Verbesserung der Bioverfügbarkeit und des spezifischen Targetings. Um die Anwendung von Licht als Auslöser einer biologischen Aktivität zu bewerten, wurde die Möglichkeit aus dem Peptidkonjugat CO freizusetzen im Dunkeln als auch durch Photoaktivierung mit Hilfe des Myoglobinassays untersucht. Dabei wurde beobachtet, dass bereits im Dunkeln 1.5 Equivalente CO mit einer Halbwertszeit von 2 h freigesetzt werden, was aber durch Bestrahlung bei 468 nm um das 2.5-fache beschleunigt werden konnte. Mechanistische Studien zur CO-Freisetzung die mittels ESI Massenspektrometrie, UV/Vis sowie IR Spektroskopie durchgeführt wurden, legen dabei die Bildung einer intermediären *fac*-Tricarbonylmolybdän(0)spezies durch Substitution eines axialen Carbonylliganden nahe. Diese intermediäre Spezies wird unter aeroben Bedinungen oxidiert, was zu einer Freisetzung der gesamten Moylbdäncarbonyleinheit aus dem bidentaten Liganden führt. Diese Verbindungen könnten daher als photoaktivierbare CO releasing molecules (PhotoCORMs) geeignet sein, wobei die Dunkelstabilität aber noch weiter verbessert werden muss.

Im zweiten Teil dieser Arbeit, wurde eine Serie von sieben Molybdän-allyl-dicarbonylkomplexen mit verschiedenen bidentaten Polypyridyl-Coliganden in einer zweistufigen Synthese hergestellt. Bei der Lipophilie dieser Komplexes, als auch bei deren Cytotoxizität auf adhärente menschliche HT-29 Darmkrebs- und MCF-7 Brustkrebszellen wurde ein Anstieg der entsprechenden Werte mit zunehmender Ligandengröße beobachtet. Die IC_{50}-Werte der aktivsten Verbindungen liegen im Bereich von 2 bis 5 μM und sind daher vergleichbar mit denen der Referenzverbindung Cisplatin auf beide Zelllinien. Untersuchungen an nicht-ahärenten NALM-6 Leukämiezellen zeigten in Bezug auf Cytotoxizität, Apoptoseinduktion und Inhibierung der Zellproliferation ebenfalls ansteigende eine Aktivität mit zunehmender Ligandengröße. Jedoch ließ sich in diesem Fall nur ein geringer Aktivitätsunterschied der Komplexe im Vergleich zu den freien Liganden erkennen. Ergebnisse aus DNA-Fragmentierungs- und Apop-

toseinduktionsstudien mit einer repräsentativen Verbindung an MCF-7 Zellen lassen auf einen von Caspase-3 unabhängigen Apoptosemechanismus schließen. Dies ist in sofern bemerkenswert, da normalerweise angenommend wird, dass eine Expression von Caspase-3 für das Auftreten von DNA-Fragmentierung als Merkmal der Apoptose unbedingt erforderlich ist. Somit besitzen kationische Molybdän-allyl-dicarbonyl Komplexe mit bidentaten Polypyridylliganden verschiedener Größe signifikante cytotoxische Aktivität auf verschiedene Krebszelllinien durch Apoptoseinduktion als haupsächlichen Wirkmechanismus. Weiterführende Untersuchungen sollten deshalb die Aufklärung des genauen Verlaufs der Caspase-3 unabhängigen Apoptoseinduktion zum Ziel haben.
Um die Bioverfügbarkeit und das Targeting derartiger Verbindungen zu verbessern, wurde eine neuartige Konjugationsmethode erstmals auf bioaktive Metallkomplexe angewendet. Dazu wurde ein Molybdän-koordiniertes Azid in der Koordinationsumgebung des Metalls mit einem maskierten elektronenarmen Alkin, wie z.B. einem Oxanorbornadiendiester, zu einem metallgebundenen Triazol umgesetzt. Durch Röntgenkristallstrukturanalyse konnte nachgewiesen werden, dass der Triazolatligand über das N(2) Stickstoffatom des Heterozyklus an das Metallzentrum koordiniert ist. Die beschriebene Methode wurde erweitert um den Molybdänazidkomplex einer "on-resin"-Strategie folgend an ein Oxanorbornadien-funktionalisiertes Modellpeptid anzuknüpfen, jedoch führte die Abspaltung des Konjugats vom Harz unter den getesteten Bedingungen zur Zersetzung der Molybdändicarbonyleinheit. Daher sollten weitere Ansätze einer "post-labelling"-Strategie folgen, bei der Azidkomplex und funktionalisiertes Peptid in Lösung gekuppelt werden.

Somit wurden schließlich Molybdäncarbonylkomplexe mit verschiedenen Polypyridyl-Coliganden synthetisiert und erstmalig in diesem Zusammenhang mittels milder bioorthogonaler Kupplungsreaktionen wie der Oxim-Ligation und der katalysatorfreien Azid-Alkin Click-Reaktion mit Peptiden verknüpft. Die biologische Aktivität einiger der neuen Komplexe und Konjugate, wozu deren Fähigkeit CO freizusetzen, die Cytotoxizität auf menschliche Krebszellen und den Modus der Induktion des Zelltods zählen, wurde untersucht. Weiterführende Studien sollten vertiefende Untersuchungen der biologischen Aktivität mit Schwerpunkt auf der Aufklärung des genauen Verlaufs der Apoptoseinduktion zum Gegenstand haben.

5 Experimental Section

5.1 General procedures and instrumentation

General

Reactions were carried out in oven-dried Schlenk glassware under an atmosphere of pure dinitrogen when necessary. Solvents were dried over molecular sieves and degassed prior to use by applying the freeze-pump-thaw method in at least two cycles. All chemicals were obtained from commercial sources and used without further purification.

NMR spectroscopy

NMR spectra were recorded on Bruker Avance 200 or DPX 200 spectrometers (^{1}H at 200.13 MHz, ^{13}C at 50.33 MHz) as well as a DPX 250 spectrometer (^{1}H at 250 MHz, ^{13}C at 63.5 MHz). Chemical shifts in ppm indicate a downfield shift relative to tetramethylsilane (TMS) and were referenced relative to the signal of the solvent.[138] Coupling constants *J* are given in Hz. Individual peaks are marked as singlet (s), doublet (d), triplet (t), quartet (q), multiplet (m), or broad signal (br).

Mass spectrometry

Mass spectra were measured on Bruker Esquire 6000 (ESI), VG Autospec (FAB), and Finnigan MAT 90 (FD) instruments, only characteristic fragments are given for the most abundant isotope peak. The solvent flow rate for the ESI measurements was 4 ml min^{-1} with a nebulizer pressure of 10 psi and a dry gas flow rate of 5 l min^{-1} at a dry gas temperature of 300 °C.

IR spectroscopy

IR spectra of pure solid samples were recorded with a Bruker Tensor 27 IR spectrometer equipped with a Pike MIRacle Micro ATR accessory or a Nicolet 380 FT-IR spectrometer equipped with a SMART iTR ATR unit. IR spectra of liquid samples were recorded with a Jasco FT/IR-4100 spectrometer using a flow-cell holder equipped with calcium fluoride windows (d = 4 mm) and a teflon spacer (d = 0.5 mm).

UV/Vis spectroscopy

The myoglobin assay and photophysical studies were carried out in a quartz cuvette (d = 1 cm) with an Agilent 8453 UV/Vis diode array spectrophotometer as described below. UV/Vis measurements for the determination of log$P_{7.4}$ values were carried out in disposable polystyrene semi-micro cuvettes (1.5 ml, BRAND GmbH & Co KG).

Microanalysis

The elemental composition of the compounds was determined with a vario EL III as well as a vario MICRO cube analyzer from Elementar Analysensysteme GmbH, Hanau. The elemental composition of halogenide-containing compounds was determined with an Euro EA Elementaranalzer from HEKAtech GmbH, Wegberg.

Single crystal X-ray diffraction

The X-ray diffraction measurements as well as crystal structure determination and refinement were carried out by Fabian Schönfeld, Institut für Anorganische Chemie, Universität Würzburg. Crystal and refinement data are summarized in the appendix. Intensity data were collected using 1 ° ω scans and Mo-$K\alpha$ radiation (λ = 0.71073 Å) on a Bruker Apex1 single crystal diffractometer equipped with a CCD camera. Indexing of peaks was carried out using the Bruker AXS Smart-Suite software, integration was done with SAINT+. Absorption corrections were carried out by semi-empirical methods using SADABS. Crystal structures were solved by direct methods using SHELXS 97 and refined using SHELXL 97. Visualisation and rendering of crystal sturctures was performed using XP (version 6.0).[139] Residuals are defined according to Eq. 1 and Eq. 2.

$$R_1 = \frac{\sum \| F_0 | - | F_c \|}{\sum | F_0 |} \tag{1}$$

$$wR_2 = \sqrt{\frac{\sum w(F_0^2 - F_c^2)^2}{\sum w(F_0^2)^2}} \tag{2}$$

High-pressure liquid chromatography (HPLC)

The analytical and preparative HPLC measurements were preformed on two different HPLC systems. System A: Knauer Smartline HPLC instrument equipped with a ReproSil 70 column (C_{18}, 5 μm, diameter 4.6 mm, 250 mm length) for analytical purposes using a mixture of water and acetonitrile containing trifluoroacetic acid (0.1%, v/v)as the eluent, using a linear gradient of 5-95% acetonitrile over 22 min at a flow rate of 1 ml min^{-1}. Purifications on a semipreparative scale on system A were performed using a Varian Dynamax Microsorb column (C_{18}, diameter 10 mm, 250 mm length) System B: Dionex Ultimate 3000 HPLC system equipped with a ReproSil 100 column (C_{18}, 5 μm, 4.6 mm or 10 mm diameter, 250 mm length) using a linear gradient gradient of 5-90% acetonitrile over 40 min at a flow rate of 0.6 ml min^{-1} for analytical and 3.0 ml min^{-1} for preparative chromatography, respectively. Thus, retention times obtained with the two different HLPC systems are not comparable.

5.1.1 Solid-phase peptide synthesis (SPPS)

Peptides were either prepared on an automated CEM Liberty peptide synthesizer or manually in a filter syringe according to the method described by Kirin *et al.*,[140] both using the Fmoc-strategy and a pre-loaded Fmoc-Arg(Pbf)-Wang or a pre-loaded H-*L*-His(Trt)-2CT resin as the solid support. All amino acids were used in their *L*-configuration. Deprotection of the Fmoc-protected amino acids was done with a solution of piperidine in *N,N*-dimethylformamide (30%, v/v). For each coupling step, five or ten equivalents of Fmoc amino acid (0.65 M in DMF) and coupling reagent solution (HOBT/TBTU, 0.65 M in DMF) were used. Diisopropylethylamine (DIPEA) served as the activator base. When carried out manually, the completeness of each coupling step was monitored by the Kaiser test.[141] For this test, a few resin beads are incubated for 5 min at 90 °C with one or two drops of each of the following reagents: a) a solution of ninhydrine in ethanol (5%, w/v), b) a solution of phenol in ethanol (80%, w/v), and c) a mixture of an aqueous potassium cyanide solution (1 mM) and pyridine (2%, v/v). Blue-violet staining due to the formation of Ruhemann's violet of the resin beads indicates incomplete coupling. Clevage of the peptide from the solid support was performed manually in a filter syringe at room temperature, using a solution of TFA/TIS/H_2O (95:2.5:2.5, v/v), unless otherwise stated. The peptide was isolated by precipitation with cold diethylether (-20 °C) and repeated cycles of washing with diethylether, centrifugation, and decanting. The remaining residue was dissolved in an acetonitrile/water mixture (1:1, v/v) and lyophilized to give the desired peptides as white to off-white solid.

5.1.2 Myoglobin assay

In a quartz cuvette, horse skeletal muscle myoglobin (Sigma Aldrich) dissolved in 0.1 M phosphate buffer (890 μl, pH = 7.4) and degassed by bubbling with dinitrogen, was reduced by addition of an excess of buffered sodium dithionite solution (10 mM, 100 μl) in the same solvent to give a total volume of 990 μl. To this solution, 10 μl of the complex or the peptide conjugate dissolved in DMSO was added to give a final concentration of 10 μM of metal complex, 1 mM sodium dithionite and 50 μM of myoglobin with $A_{557\,nm} < 1$. Solutions were irradiated for up to 180 min under dinitrogen either with a custom-made 15 LED cluster at 468 nm (Kingbright Elec. Co., 3800 to 5000 mcd, part-no. BL0106-15-410) or an UV hand lamp at 365 nm (LF-206.LS, 6 W, UVITEC Cambridge), both positioned perpendicular to the cuvette at a distance of 3 cm. Irradiations were interrupted in regular intervals to take UV/Vis spectra on a Agilent 8453

UV/Vis diode-array spectrophotometer. Dark control experiments were performed under the same conditions over a period of 12 h. In this case, UV/Vis spectra were automatically recorded in 15 min intervals. The concentration of carboxy-myoglobin (MbCO) was calculated from changes in the absorption of the Q-band at 540 nm according to Eq. 3 with ϵ_{540nm}(MbCO) = 15.4 l·mmol^{-1}·cm^{-1}.[142] Absorptions at 540 nm were corrected against deviations at the isosbestic point at 510 nm for A(t=0) according to the method reported by Fairlamb *et al.*[143] Half-life times and CO equivalents released were obtained by a non-linear fit from a plot of c(MbCO) versus irradation time.

$$c(MbCO) = \left[\frac{A(t)}{l} - \frac{A(t=0)}{l}\right] \cdot \frac{1}{\epsilon_{540nm}(MbCO) - \frac{A(t=0)}{c_0(Mb)\cdot l}} \tag{3}$$

5.1.3 Determination of the *n*-octanol/water partition coefficient

Log$P_{7.4}$ values were determined by applying the "shake-flask" method reported by Kunz *et al.*[69] Equal volumes of phosphate buffer (10 mM, pH 7.4) and *n*-octanol were shaken together on a lab shaker (IKA KS 130 basic) for 72 h prior to use to allow saturation of both phases. In the experiment, 750 μl of each phase and 10 μl of a complex stock solution (1 to 2 mg of complex dissolved in 100 to 200 μl DMSO) were combined in an Eppendorf tube and shaken on a lab vortexer (VWR Analogue Vortexer) for 15 min followed by centrifugation (5 min, 3000 rpm) to separate the two phases. UV/Vis absorptions of each phase were determined at 300 nm from aliquots of 500 μl. Samples were diluted 2- to 4-fold with the corresponding phase prior to measurement if necessary ($A_{300\,nm}$ < 1). Log$P_{7.4}$ values were calculated according to Eq. 4, f_{dil} represents the diliution factor. Given values and standard deviations were derived from three independent experiments.

$$logP_{7.4} = log\left(\frac{A_{octanol(300nm)} \cdot f_{dil}}{A_{buffer(300nm)} \cdot f_{dil}}\right) \tag{4}$$

5.1.4 Photolysis experiments monitored by UV/Vis spectroscopy

Photolysis of complexes and conjugates as well as dark control experiments were carried out in a quartz cuvette in pure DMSO under aerobic or anaerobic conditions at a concentration of 125 μM ($A_{490/468\,nm}$ < 1). Solutions were irradiated at 468 nm using the LED cluster described above. In experiments involving anaerobic conditions, DMSO

solutions of the corresponding compound were saturated with carbon monoxide or argon prior to the experiments. Calculations of the rate constants and half-life times were based on the changes in absorption of the MLCT band at 468 nm for **12**, 490 nm for **5** and 387 nm for both compounds.

5.1.5 Photolysis experiments monitored by IR spectroscopy

Photolysis experiments as well as dark controls were monitored by IR spectroscopy on solutions of complexes or peptide conjugates in pure DMSO (1 mM) on a Jasco FT/IR-4100 spectrometer using an IR flow cell equipped with calcium fluoride windows (d = 4 mm) and a teflon spacer (d = 0.5 mm). Background corrections were made against the pure solvent. The irradiations were carried out at 468 nm using the LED cluster described above with the flow cell positioned at a distance of 3 cm. IR spectra were recorded at 0, 15, 30, 60, 90, 120, 150, and 180 min during the irradiation as well as the dark control experiments. Calculations of rate constants and half-lifes were based on changes in absorption of the carbonyl vibrational bands at 2010, 1898, 1873, and 1828 cm^{-1}. All experiments were performed as duplicates.

5.1.6 Buffer stabilitiy tests

The conjugate **12** was incubated in a acetonitrile/phosphate buffer (0.1 M, pH 7.4) mixture (1:1, v/v) under aerobic conditions with exclusion of light for 7 h. Samples were taken directly from the solution in 1 h intervals and analyzed by RP-HPLC (System A) without any further workup. Dominant species were identified by HPLC-ESI-MS as well as continous UV/Vis absoption monitoring using the diode array detector of the HPLC system (results not shown for the latter method). The intact peptide conjugate was identified by its charateristic MLCT transition at 468 nm. Integrals were calculated using the HPLC trace recorded at 254 nm, assuming similar absorption coefficients for all species carrying bipyridine moietes.

5.2 Synthetic procedures

5.2.1 Synthesis of 4,4'-dimethyl-2,2'-bipyridine

USC-PF067, literature:[144]

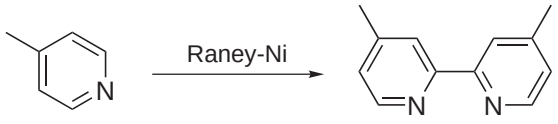

(**1**)

C_6H_7N
93.13 g/mol

$C_{12}H_{12}N_2$
184.24 g/mol

Raney-nickel (9.8 g, 0.17 mol) was transferred into a flask under a dinitrogen atmosphere. Then, freshly distilled anhydrous 4-picoline (50 ml, 47.9 g, 0.51 mol) was added via syringe and the mixture was heated to 130 °C for 3 d. The mixture solidified upon cooling to room temperature and therefore, toluene (100 ml) was added to dissolve the solid. Remaining Raney-nickel was filtered off under a dinitrogen atmosphere and the residue was washed with chloroform (2 x 50 ml). The solvent and unreacted 4-picoline were completely removed under vacuum to give a light brown solid which was dried under vaccum at 80°C for 12 h. Yield: 50 % (based on Raney-Ni), (16.1 g, 87 mmol). MS (FAB^+): *m/z* 185 $[M + H]^+$; IR (ATR, cm^{-1}): 3056 (w), 1591 (s), 1457 (m), 823 (s), 670 (m); ^{1}H-NMR (200 MHz, $CDCl_3$): δ 8.50 (d, 2H, $H_{6,6'}$), 8.20 (s, 2H, $H_{3,3'}$), 7.09 (d, 2H, $H_{5,5'}$), 2.41 (s, 6H, CH_3); ^{13}C-NMR (50 MHz, $CDCl_3$): δ 159.29 (C-2,2'), 149.11 (C-6,6'), 148.23 (C-4,4'), 124.80 (C-3,3'), 122.19 (C-5,5'), 21.34 (CH_3).

5.2.2 Synthesis of 4'-methyl-2,2'-bipyridine-4-carboxaldehyde

USC-PF035, literature:[145]

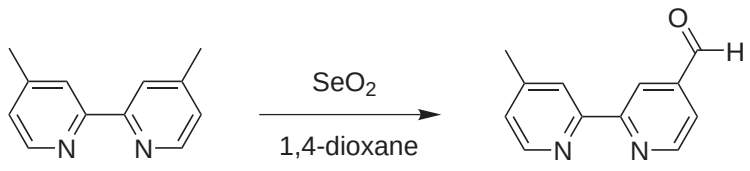

(**1**)
$C_{12}H_{12}N_2$
184.24 g/mol

(**2**)
$C_{12}H_{10}N_2O$
198.22 g/mol

Selenium dioxide (0.36 g, 3.2 mmol) was added to a solution of 4,4'-dimethyl-2,2'-bipyridine (**1**) (0.50 g, 2.7 mmol) in 1,4-dioxane (30 ml) and heated to reflux for 40 h. Over the course of the reaction, the mixture became intense yellow and selenium metal precipitated as black solid. After cooling to room temperature, the selenium metal was filtered off and the filtrate was rotary evaporated to dryness to yield a beige solid. The residue was suspended in ethyl acetate (100 ml), stirred for 30 min and filtered to remove the remaining brown solid. The now slightly yellow filtrate was extracted with 1.0 M sodium carbonate solution (2 x 125 ml) and afterwards with 0.3 M sodium metabisulfite solution (2 x 125 ml). The combined bisulfite extracts were adjusted to pH 10 with solid sodium carbonate and extracted with dichloromethane (5 x 100 ml). After drying over magnesium sulfate and removal of the solvent, the product was obtained as a white solid. Yield: 41% (215 mg, 1.1 mmol). IR (ATR, cm^{-1}): 1701 (s) ν(CO), 1594 (m), 1557 (m), 1461 (s), 1353 (s), 1250 (m), 1149 (s), 990 (m), 824 (s), 751 (m), 667 (s); MS (ESI^+, acetone): m/z 199 $[M+H]^+$, 221 $[M+Na]^+$; ^{1}H-NMR (200.13 MHz, $CDCl_3$): δ 10.15 (d, 1H, 4-CHO, $^4J_{H\text{-}6,CHO}$ = 0.6 Hz), 8.87 (ddd, 1H, H-6, $^3J_{H\text{-}5,H\text{-}6}$ = 5.0 Hz, $^4J_{H\text{-}6,CHO}$ = 0.6 Hz, $^5J_{H\text{-}3,H\text{-}6}$ = 0.9 Hz), 8.80 (dd, 1H, H-3, $^4J_{H\text{-}3,H\text{-}5}$ = 1.6 Hz, $^5J_{H\text{-}3,H\text{-}6}$ = 0.9 Hz), 8.55 (dd, 1H, H-6', $^3J_{H\text{-}5',H\text{-}6'}$ = 5.0 Hz, $^5J_{H\text{-}6',H\text{-}3'}$ = 0.7 Hz), 8.25 (dq, 1H, H-3', $^4J_{H\text{-}3',H5'}$ = 1.6 Hz, $^4J_{H\text{-}3',CH_3}$ = 0.7 Hz), 7.69 (dd, 1H, H-5, $^3J_{H\text{-}5,H\text{-}6}$ = 5.0 Hz, $^4J_{H\text{-}3,H\text{-}5}$ = 1.6 Hz), 7.17 (ddq, 1H, H-5', $^3J_{H\text{-}5',H\text{-}6'}$ = 5.0 Hz, $^4J_{H\text{-}3',H\text{-}5'}$ = 1.6 Hz; $^4J_{H\text{-}5',CH_3}$ = 0.7 Hz), 2.44 (t, 3H, CH_3, $^4J_{H\text{-}5'/3',CH_3}$ = 0.7 Hz); ^{13}C-NMR (50.13 MHz, $CDCl_3$): δ 191.98 (4-CHO), 158.51 (C-4), 154.94 (C-2), 150.51 (C-2'), 149.41 (C-6), 148.62 (C-6'), 142.86 (C-4'), 125.60 (C-3'), 122.29 (C-5'), 121.59 (C-3), 120.78 (C-5), 21.43 (4'-CH_3) ppm.

5.2.3 Synthesis of [Mo(CO)$_4$(phen)]

USC-PF030, literature:[107]

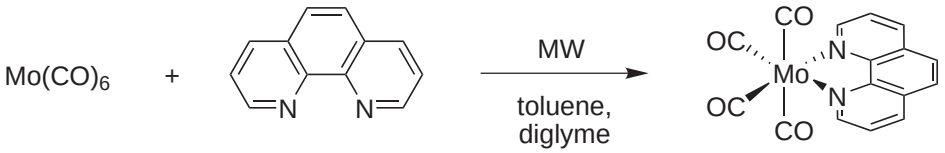

(**3**)

C_6MoO_6	$C_{12}H_8N_2$	$C_{16}H_8MoN_2O_4$
264.00 g/mol	180.22 g/mol	388.19 g/mol

Molybdenum hexacarbonyl (132 mg, 0.50 mmol) and 1,10-phenanthroline (110 mg, 0.55 mmol) were suspended in a mixture of diglyme/toluene (v/v, 1:2.5, 6 ml) in a 10 ml microwave pressure tube. The tube was placed in a CEM Discover microwave reactor and heated to 180 °C for 5 min. After cooling to room temperature, a red precipitate formed. The mixture was further cooled down to -20 °C for 4 h and the precipitate that formed was filtered off, washed with *n*-hexane (2 x 5 ml) and dried under vacuum. Yield: 62% (119 mg, 0.31 mmol). IR (ATR, cm^{-1}): 2005 (s) ν(CO), 1858 (s) ν(CO), 1820 (s) ν(CO), 1422 (m), 1413 (m), 1142 (m), 843 (s), 723 (s), 642 (s); ^{1}H-NMR (400.13 MHz, DMSO-d$_6$): δ 9.38 (dd, 2H, H-1, $^3J_{H\text{-}1,H\text{-}2}$ = 5.0 Hz, $^4J_{H\text{-}1,H\text{-}3}$ = 1.4 Hz), 8.82 (dd, 2H, H-3, $^3J_{H\text{-}2,H\text{-}3}$ = 8.2 Hz, $^4J_{H\text{-}1,H\text{-}3}$ = 1.4 Hz), 8.24 (s, 2H, H-4), 8.00 (dd, 2H, H-2, $^3J_{H\text{-}2,H\text{-}3}$ = 8.2 Hz, $^3J_{H\text{-}1,H\text{-}2}$ = 5.0 Hz), ^{13}C-NMR (100.13 MHz, DMSO-d$_6$): δ 223.01 (CO_{ax}), 206.06 (CO_{eq}), 153.96 ($C_{2,9}$), 145.93 ($C_{10a,10b}$), 138.70 ($C_{5,6}$), 130.76 ($C_{4,7}$), 128.18 ($C_{4a,6a}$), 126.13 ($C_{3,8}$) ppm.

5.2.4 Synthesis of [Mo(CO)$_4$(bpy)]

USC-PF034, literatur:[107]

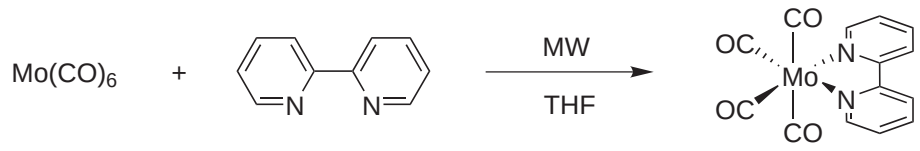

(**4**)

C_6MoO_6	$C_{10}H_8N_2$	$C_{14}H_{10}MoN_2O_4$
264.00 g/mol	156.18 g/mol	366.18 g/mol

The following procedure was applied for four batches with a total of 2.56 mmol, referred to 2,2'-bipyridine: Molybdenum hexacarbonyl (253 mg, 0.96 mmol) and 2,2'-bipyridine (100 mg, 0.64 mmol) were mixed in tetrahydrofuran (6 ml) in a sealed tube (10 ml) The tube was placed in a CEM Discover microwave reactor and heated to 130 °C for 15 min. After cooling to room temperature, the four batches were combined and poured into *n*-pentane (200 ml). The orange precipitate was filtered off, washed with *n*-pentane (50 ml) and dried under vacuum. Yield: 88% (820 mg, 2.24 mmol). IR (ATR, cm^{-1}): 2007 (s) ν(CO), 1831 (s) ν(CO), 1820 (s) ν(CO), 1597 (m), 1467 (m), 1439 (m), 1314 (w), 1241 (w), 964 (w), 759 (s), 733 (m), 639 (m); ^{1}H-NMR (200.13 MHz, DMSO-d$_6$): δ 8.98 (ddd, 2H, H-6, $^5J_{H\text{-}6,H\text{-}3}$ = 1.0 Hz, $^4J_{H\text{-}6,H\text{-}4}$ = 1.6 Hz, $^3J_{H\text{-}6,H\text{-}5}$ = 5.4 Hz), 8.66 (ddd, 2H, H-3, $^5J_{H\text{-}6,H\text{-}3}$ = 1.0 Hz, $^4J_{H\text{-}3,H\text{-}5}$ = 1.2 Hz, $^3J_{H\text{-}3,H\text{-}4}$ = 8.1 Hz), 8.20 (ddd, 2H, H-4, $^4J_{H\text{-}6,H\text{-}4}$ = 1.6 Hz, $^3J_{H\text{-}3,H\text{-}4}$ = 8.1 Hz, $^3J_{H\text{-}4,H\text{-}5}$ = 7.6 Hz), 7.68 (ddd, 2H, H-5, $^4J_{H\text{-}3,H\text{-}5}$ = 1.2 Hz, $^3J_{H\text{-}4,H\text{-}5}$ = 7.6 Hz, $^3J_{H\text{-}6,H\text{-}5}$ = 5.4 Hz) ppm; ^{13}C-NMR (50.68 MHz, DMSO-d$_6$): δ 222.19 (CO_{ax}), 205.08 (CO_{eq}), 154.26 (C-2), 152.54 (C-6), 138.90 (C-4), 126.34 (C-5), 123.57 (C-3) ppm.

5.2.5 Synthesis of [Mo(CO)$_4$(bpy^{CH_3,CHO})]

USC-PF048

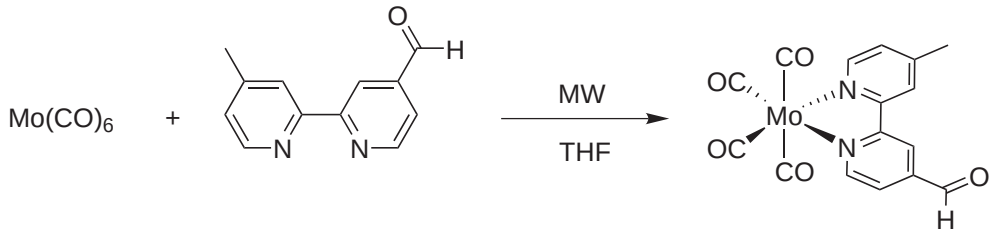

	(**2**)	(**5**)
264.00 g/mol	$C_{12}H_{10}N_2O$ 198.22 g/mol	$C_{16}H_{10}MoN_2O_5$ 406.23 g/mol

The procedure described below was sequentially performed with four batches of equal quantity which were pooled before workup. Molybdenum hexacarbonyl (200 mg, 0.75 mmol, 1.5 eq, in total: 3 mmol) and 4'-methyl-2,2'-bipyridine-4-carboxaldehyde (**2**) (100 mg, 0.50 mmol, 1.0 eq, in total: 2 mmol) werde mixed in tetrahydrofuran (6 ml) and heated under microwave irradiation in a CEM Discover instrument for 15 min at 130 °C. The deep purple solutions of each batch were pooled and poured into *n*-pentane (200 ml). The resulting violet precipitate was filtered off, washed with *n*-pentane, dried under vacuum, and subsequently purified by column chromatography on silica with dichloromethane as the eluent. Yield: 62% (505 mg, 1.24 mmol); Elemental analysis (%): calc. $C_{16}H_{10}MoN_2O_5$: C 47.31, H 2.48, N 6.90, found: C 47.11, H 2.55, N 6.81; MS (FD$^+$): *m/z* 405.2 [M]$^+$; UV-Vis (DMSO): $\lambda_{max}(\epsilon)$ = 387 (4010), 490 nm (6700 l mol^{-1} cm^{-1}); IR (ATR, cm^{-1}): 2011 (s) ν(CO), 1867 (s) ν(CO), 1804 (s) ν(CO), 1709 (s) ν(CHO); ^{1}H-NMR (200 MHz, DMSO-d$_6$): δ 10.16 (s, 1H, 4-CHO), 9.24 (d, 1H, H-6, $^3J_{H\text{-}6,H\text{-}5}$ = 5.5 Hz), 9.02 (d, 1H, H-3, $^4J_{H\text{-}3,H\text{-}5}$ = 1.6 Hz), 8.83 (d, 1H, H-6', $^3J_{H\text{-}6',H\text{-}5'}$ = 5.5 Hz), 8.71 (d, 1H, H-3', $^4J_{H\text{-}3',H\text{-}5'}$ = 1.6 Hz), 7.97 (dd, 1H, H-5, $^3J_{H\text{-}5,H\text{-}6}$ = 5.5 Hz, $^4J_{H\text{-}5,H\text{-}3}$ = 1.6 Hz), 7.53 (dd, 1H, H-5', $^3J_{H\text{-}5',H\text{-}6'}$ = 5.5 Hz, $^4J_{H\text{-}5',H\text{-}3'}$ = 1.6 Hz), 2.54 (s, 3H, CH_3); ^{13}C-NMR (62.5 MHz, DMSO-d$_6$): δ 222.60 (CO_{eq}), 221.73 (CO_{eq}), 204.88 (CO_{ax}), 191.45 (CHO), 155.93 (C-4), 153.77 (C-2), 153.32 (C-2'), 151.94 (C-6), 150.80 (C-6'), 142.84 (C-4'), 127.56 (C-3'), 124.85 (C-5), 123.75 (C-3), 122.06 (C-5'), 20.74 (CH_3).

5.2.6 Synthesis of dimethylketoxime

USC-PF052, literature:[111]

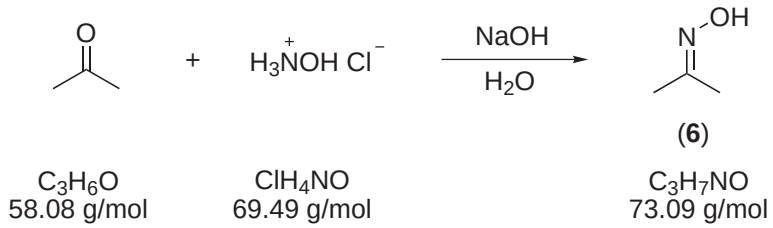

(**6**)

C_3H_6O
58.08 g/mol

ClH_4NO
69.49 g/mol

C_3H_7NO
73.09 g/mol

Hydroxylamine hydrochloride (30.0 g, 0.43 mol) was dissolved in water (60 ml) and an aqueous solution (30 ml) of sodium hydroxide (18.5 g, 0.46 mol) was added over the course of 10 min under cooling with an ice bath. Subsequently acetone (21 ml, 26.6 g, 0.46 mol) was added via a dropping funnel over 30 min. During that time, a white recipitate formed, but dissolved upon more intense stirring. Later, precipitation started again. After 30 min of further stirring, the pH of the solution was adjusted to 6 by addition of concentrated hydrochloric acid. The mixture was stirred for one additional hour (pH 7.5) and extracted with diethylether (4 x 100 ml), dried over magnesium sulfate. Then the solvent was removed by evaporation to give a white residue which was dried *in vacuo*. Yield: 56% (17.5 g, 0.24 mol). IR (ATR, cm^{-1}): 3197 (s), 3136 (s), 2923 (s), 2891 (s), 1679 (s) ν(C=O), 1496 (s), 1428 (s), 1368 (s), 1269 (s), 1069 (s), 957 (s), 790 (s); ^{1}H-NMR (200.13 MHz, DMSO-d_6): δ 10.17 (s, 1H, OH), 1.76 (s, 3H, (*E*/*Z*)-CH_3), 1.76 (s, 3H, (*E*/*Z*)-CH_3) ppm; ^{13}C-NMR (50.13 MHz, DMSO-d_6): δ 152.10 (C=N), 21.40 ((*E*/*Z*)-CH_3), 14.56 ((*E*/*Z*)-CH_3) ppm.

5.2.7 Synthesis of dimethylketoxime-*O*-acetic acid

USC-PF051, literature:[112]

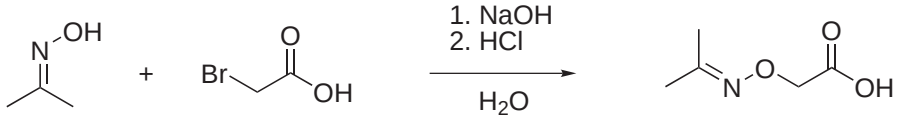

(**6**)

C_3H_7NO
73.09 g/mol

$C_2H_3BrO_2$
138.95 g/mol

(**7**)

$C_5H_9NO_3$
131.13 g/mol

Bromoacetic acid (6.66 g, 48 mmol) was dissolved in water (10 ml) and cooled to 0°C. Then, an aqueous solution of sodium hydroxoide (3.5 ml, 40% w/w, 50 mmol) was

added dropwise while keeping the temperature below 20°C. Subsequently, a solution of dimethylketoxime (**6**) (3.14 g, 43 mmol) in water (15 ml) was added, again followed by an aqueous solution of sodium hydroxide (3.0 ml, 40% w/w, 43 mmol). The resulting mixture was allowed to warm to room temperature while stirring overnight. The alkaline mixture was extracted with diethylether (1 x 50 ml), then acidified to pH 1 with concentrated hydrochloric acid and again extracted with diethylether (4 x 50 ml). The latter extracts were combined and dried over magnesium sulfate. Evaporation of the solvent gave the title compound as an off-white solid. Yield: 42% (2.40 g, 18 mmol). MS (ESI$^+$, MeOH): *m/z* 154 $[M+Na]^+$; IR (ATR, cm^{-1}): 2926 (m), 2580 (m), 1723 (s), 1406 (m), 1366 (m), 1256 (s), 1107 (s), 1021 (m), 874 (m); ^{1}H-NMR (200.13 MHz, DMSO-d_6): δ 12.59 (s, 1H, COOH), 4.44 (s, 2H, CH_2), 1.82 (s, 3H, (*E*/*Z*)-CH_3), 1.79 (s, 3H, (*E*/*Z*)-CH_3) ppm; ^{13}C-NMR (50.13 MHz, DMSO-d_6): δ 171.40 (C=O), 152.10 (C=N), 69.58 (CH_2), 21.19 ((*E*/*Z*)-CH_3), 15.52 ((*E*/*Z*)-CH_3) ppm.

5.2.8 Synthesis of aminooxyacetic acid hemi hydrochloride

USC-PF053, literature:[113]

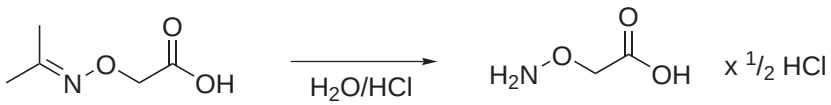

(**7**)
$C_5H_9NO_3$
131.13 g/mol

(**8**)
$C_2H_5NO_3$ x $^1/_2$ HCl
109.30 g/mol

Dimethylketoxime-*O*-acetic acid (**7**) (6.1 g, 47 mmol) was dissolved in water (60 ml) and concentrated hydrochloric acid (4.6 ml) was added. The mixture was then heated to 95°C for 4 h in an open flask with a stream of nitrogen passing through. The volume was reduced to about 5 ml over the course of the reaction. After cooling to room temperature, the residue was treated with isopropanol (30 ml) followed by diethylether (120 ml) and stored at -25°C overnight. The crystalline precipitate that formed was filtered off, washed with diethylether and dried under vacuum to give a white solid. The product was isolated as the hemi hydrochloride. Yield: 72% (3.7 g, 34 mmol). Elemental analysis (%): calc. $C_2H_5NO_3 \cdot 1/2$ HCl: C 21.98, H 5.07, N 12.82, found: C 21.52, H 5.01, N 12.73; MS (ESI$^+$, MeOH): *m/z* 92 $[M+H]^+$; IR (ATR, cm^{-1}): 2858 (s), 2683 (s), 2019 (m), 1715 (vs), 1521 (s), 1442 (s), 1400 (s), 1212 (s), 1057 (s), 1009 (s), 913 (m), 889 (s), 800 (vs), 669 (s); ^{1}H-NMR (200.13 MHz, DMSO-d_6): δ 4.64 (s, 2H, CH_2) ppm; ^{13}C-NMR (50.13 MHz, DMSO-d_6): δ 169.21 (C=O), 70.06 (CH_2) ppm.

5.2.9 Synthesis of *N*-(9-fluorenylmethoxycarbonyl)aminooxyacetic acid (Fmoc-Aoa-OH)

USC-PF054, literature:[114]

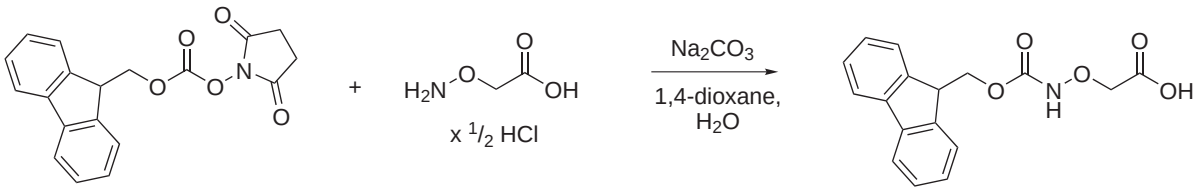

(**8**)
$C_2H_5NO_3$ x $^1/_2$ HCl
109.30 g/mol

(**9**)
$C_{17}H_{15}NO_5$
313.30 g/mol

$C_{19}H_{15}NO_5$
337.33 g/mol

Aminooxyacetic acid hemi hydrochloride (**8**) (3.5 g, 32 mmol) was dissolved in a 1,4-dioxane/water mixture (200 ml, v/v 60:40) and solid sodium carbonate (8.5 g, 80 mmol) was added. The mixture was cooled to 0 °C and a solution of 9-fluorenylmethoxycarbonyl-*N*-succinimidyl carbonate (10.8 g, 32 mmol) in 1,4-dioxane (50 ml) was added while stirring. The resulting mixture was stirred for 2 h at about 0 °C and the white precipitate that formed was filtered off. The filtrate was concentrated under vacuum and the viscous residue was re-dissolved in water (200 ml). Addition of concentrated hydrochloric acid gave a white precipitate which was filtered off, washed with diluted hydrochloric acid and subsequently lyophilized. Yield: 84% (8.6 g, 27 mmol). RP-HPLC (system B): t_R = 27.73 min; MS (ESI$^+$, MeOH): *m/z* 336 [M+Na]$^+$; IR (ATR, cm^{-1}): 3268 (w), 1714 (vs), 1448 (m), 1254 (m), 1122 (s), 738 (vs); ^{1}H-NMR (200.13 MHz, DMSO-d_6): δ 12.88 (s, 1H, COOH), 10.69 (s, 1H, NH), 7.89 (d(br), 2H, Fmoc-H(5,8),^3J = 6.8 Hz), 7.70 (d(br), 2H, Fmoc-H(1,4),^3J = 7.3 Hz), 7.42 (dt, 2H, Fmoc-H(7,6),^3J = 7.3 Hz, ^4J = 1.0 Hz), 7.32 (dt, 2H, Fmoc-H(2,3),^3J = 7.3 Hz, ^4J = 1.3 Hz), 4.37 (d, 2H, Fmoc-CH_2, ^3J = 7.0 Hz), 4.26 (s, 2H, Aoa-CH_2, overlapping), 4.27-4.20 (t, 1H, Fmoc-H(9), ^3J = 7.0 Hz, overlapping) ppm; ^{13}C-NMR (50.13 MHz, DMSO-d_6): δ 170.06 (Aoa, C=O), 156.93 (Fmoc, C=O), 143.57 (Fmoc, C-9a,8a), 140.74 (Fmoc, C-4a,4b), 127.71 (Fmoc, C-1,8), 127.09 (Fmoc, C-2,7), 125.24 (Fmoc, C-4,5), 120.13 (Fmoc, C-3,6), 72.05 (Aoa, CH_2), 66.12 (Fmoc, CH_2), 46.50 (Fmoc, C-9) ppm.

5.2.10 Synthesis of Aoa-Gly-Leu-Arg-OH

USC-PF075

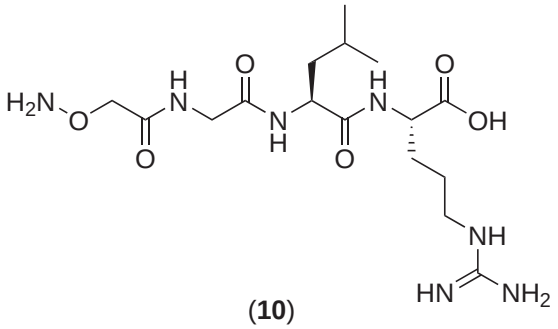

(**10**)

$C_{16}H_{31}N_7O_6$
417.46 g/mol

The peptide was prepared on a 0.189 mmol scale on a Fmoc-Arg(Pbf)-Wang resin (300 mg, 0.63 mmol/g) using the amino acids Fmoc-Leu-OH, Fmoc-Gly-OH and Fmoc-Aoa-OH (**9**) under the conditions of microwave-assisted solid-phase peptide synthesis as described above. Cleavage time: 100 min. The product was obtained as a white solid. Yield: 85% (67 mg, 0.161 mmol). RP-HPLC (system A): t_R = 5.17 min; MS (ESI^+, MeOH): *m/z* 418 $[M+H]^+$; IR (ATR, cm^{-1}): 1649 (s), 1542 (s), 1138 (s), 1046 (s).

5.2.11 Synthesis of Aoa-Leu-Pro-Leu-Gly-Asn-Ser-His-OH (Aoa-TGF-β_1-OH)

USC-PF138

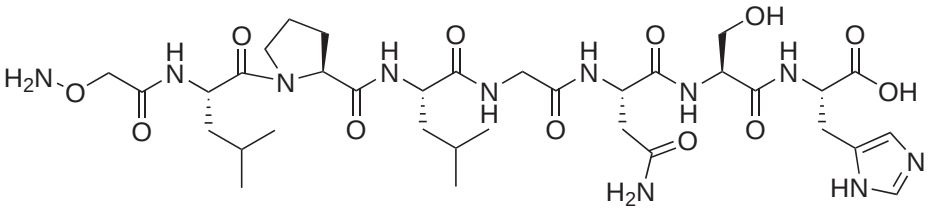

(**11**)

$C_{34}H_{55}N_{11}O_{12}$
809.87 g/mol

The TGF-β_1 peptide was prepared on a 0.156 mmol scale on a preloaded H-*L*-His(Trt)-2CT resin (200 mg, 0.78 mmol/g) using the amino acids Fmoc-Ser(tBu)-OH, Fmoc-Asn(Trt)-OH, Fmoc-Gly-OH, Fmoc-Leu-OH, and Fmoc-Pro-OH under the conditions of manual solid phase peptide synthesis as described above. Coupling of Fmoc-Aoa-OH

(**9**) was carried out using a small portion (100 mg, 0.078 mmol) of the TGF-β_1-2CT resin. Three repeated couplings with 10 eq. of amino acid were required to achieve complete coupling of Fmoc-Aoa-OH, indicated by a negative Kaiser test. Cleavage time: 3 h (TFA/TIS/H_2O, 90:5:5, v/v). The product was obtained as an off-white solid. Yield: 46% (30 mg, 0.037 mmol). RP-HPLC (system B): t_R = 14.59 min; MS (ESI$^+$, MeOH): *m/z* 832.4 $[M+Na]^+$; IR (ATR, cm^{-1}): 3291 (m), 2961 (m), 1659 (s), 1535 (s), 1434 (m), 1194 (s), 1133 (s), 835 (w), 799 (w).

5.2.12 Synthesis of $[Mo(CO)_4(bpy^{CH_3,CH=Aoa\text{-}Gly\text{-}Leu\text{-}Arg\text{-}OH})]$

USC-PF076

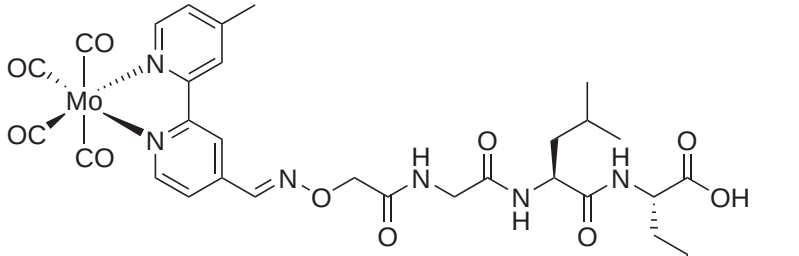

(**12**)
$C_{32}H_{39}MoN_9O_{10}$
805.64 g/mol

$[Mo(CO)_4(bpy^{CH_3,CHO})]$ (**5**) (20 mg, 0.049 mmol, 1 eq.) and Aoa-Gly-Leu-Arg-OH (**10**) (31 mg, 0.074 mmol, 1.5 eq.) were dissolved in a mixture of tetrahydrofuran (5 ml) and sodium phosphate buffer (5 ml, 100 mM, pH 5.2). The clear red solution was desoxygenated by purging with pure dinitrogen for 15 min and stirred for 3 h at room temperature under a dinitrogen atmosphere with exclusion of light. The solvent was removed by lyophization and the residue was dissolved in a acetonitrile/water mixture (v/v, 10:90) and loaded on a pre-conditioned reversed phase column (Waters SepPak C-18, 5 g). After washing the column with pure water (5 x 10 ml), the product was eluated using a acetonitrile/water mixture (v/v, 50:50) and subsequently lyophilized to give an orange-red solid which was purified by preparative HPLC (system A). Yield: 25% (10 mg, 0.012 mmol). RP-HPLC (system A): t_R = 8.69 min; MS (ESI$^+$, MeOH): *m/z* 808 $[M+H]^+$; UV-Vis (DMSO): $\lambda_{max}(\epsilon)$ = 387 (3330), 468 nm (4620 l mol^{-1} cm^{-1}); IR (ATR, cm^{-1}): 2014 (vs) ν(CO), 1861 (vs) ν(CO), 1815 (vs) ν(CO), 1655 (s), 1536 (m).

5.2.13 Synthesis of [Mo(CO)$_4$(bpy$^{CH_3,CH=Aoa\text{-}TGF\text{-}\beta_1\text{-}OH}$)]

USC-PF144

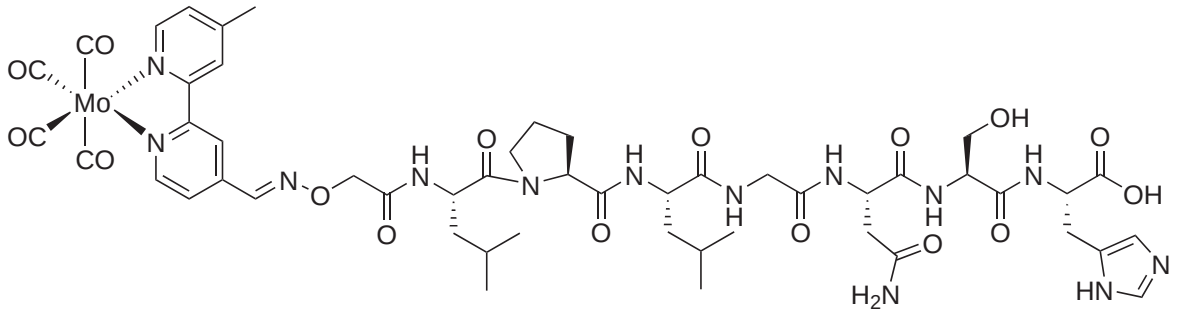

(**13**)

$C_{50}H_{63}MoN_{13}O_{16}$
1198.05 g/mol

[Mo(CO)$_4$(bpy^{CH_3,CHO})] (**5**) and H-Aoa-TGF-β_1-OH (**11**) were dissolved in a mixture (4 ml, v/v, 50:50) of tetrahydrofuran (2 ml) and sodium phosphate buffer (2 ml, 100 mM, pH 5.2). The clear red solution was stirred for 4 h while excluded from light. The solvent was removed under vacuum and the residue was suspended in a water/acetonitrile mixture (v/v, 90:10) and loaded on a reversed phase column (Waters SepPak C-18, 5 g). After washing the column with pure water (5 x 10 ml) and water/acetonitrile (2 x 10 ml, v/v, 50:50), the product was eluated using a water/acetonitrile mixture (v/v, 30:70) and subsequently lyophilized to give an orange-red solid which was purified by preparative HPLC (system B). Yield: 30% (4 mg, 0.003 mmol). RP-HPLC (system B): t_R = 30.26 min; MS (ESI$^-$, MeOH): *m/z* 1198.4 [M-H]$^-$, 1172.2 [M-CO+H]$^+$; IR (ATR, cm^{-1}): 3301 (m), 2959 (m), 2015 (vs) ν(CO), 1861 (vs) ν(CO), 1812 (vs) ν(CO), 1661 (s), 1533 (m), 1533 (w), 1198 (m).

5.2.14 Synthesis of [Mo(η^3-methallyl)Cl(CO)$_2$(bpy)]

USC-PF042

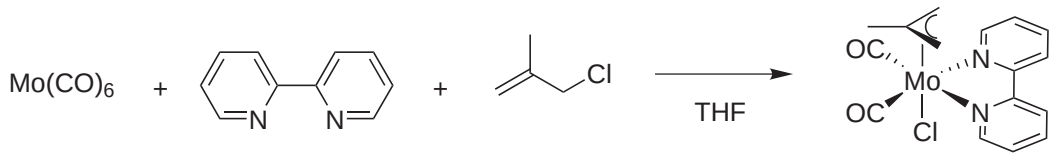

(**14**)

C_6MoO_6	$C_{10}H_8N_2$	C_4H_7Cl	$C_{16}H_{15}ClMoN_2O_2$
264.00 g/mol	156.18 g/mol	90.55 g/mol	398.69 g/mol

Molybdenum hexacarbonyl (1.5 g, 5.7 mmol), 2,2'-bipyridine (0.89 g, 5.7 mmol), and β-methallylchloride (3.6 ml, 5.2 g, 57 mmol) were mixed under a nitrogen atmosphere in anhydrous and degassed tetrahydofuran and heated to reflux for 5 h. The initially colorless solution turned dark red after a few minutes and a dark precipitate formed. The reaction mixture was cooled to room temperature and after overnight storage at -20°C, more precipitate had formed. The precipitate was filtered off and washed with *n*-pentane until the filtrate was colorless (2 x 5 ml) and dried under vacuum to give a dark red-brown solid. Unreacted molybdenum hexacarbonyl was removed by sublimation at 50°C and about $5.5 \cdot 10^{-2}$ mbar. Yield: 49% (1.11 g, 2.8 mmol). Elemental analysis (%): calc. $C_{16}H_{15}ClMoN_2O_2$: C 48.20, H 3.79, N 7.03, found: C 48.07, H 3.83, N 6.69; MS (FAB$^+$): *m/z* 365 [M - Cl]$^+$; IR (ATR, cm^{-1}): 3074 (w), 2977 (w) 1925 (s) ν(CO), 1850 (s) ν(CO), 1601 (m), 1472 (m), 1444 (m), 1313 (m), 1160 (w), 1027 (m), 765 (s), 737 (m); ^{1}H-NMR (250.13 MHz, DMSO-d$_6$): δ 8.77 (dd, 2H, bpy$_{H\text{-}6}$, $^4J_{H\text{-}6,H\text{-}4}$ = 1.5 Hz, $^3J_{H\text{-}6,H\text{-}5}$ = 5.5 Hz), 8.61 (dt, 2H, bpy$_{H\text{-}3}$, $^4J_{H\text{-}3,H\text{-}5}$ = 0.9 Hz, $^3J_{H\text{-}3,H\text{-}4}$ = 8.0 Hz), 8.19 (td, 2H, bpy$_{H\text{-}4}$, $^4J_{H\text{-}6,H\text{-}4}$ = 1.5 Hz, $^3J_{H\text{-}3,H\text{-}4}$ = 8.0 Hz, 7.66 (ddd, 2H, bpy$_{H\text{-}5}$, $^4J_{H\text{-}3,H\text{-}5}$ = 0.9 Hz, $^3J_{H\text{-}4,H\text{-}5}$ = 7.6 Hz, $^3J_{H\text{-}6,H\text{-}5}$ = 5.5 Hz), 2.83 (s, 2H, allyl-H$_{syn}$), 1.23 (s, 2H, allyl-H$_{anti}$), 0.95 (s, 2H, CH$_3$-allyl) ppm; ^{13}C-NMR (62.86 MHz, DMSO-d$_6$): δ 227.27 (CO), 153.24 (C-2), 151.68 (C-6), 139.23 (C-4), 126.34 (C-5), 123.13 (C-3), 80.26 (C$_q$-allyl), 52.57 (CH$_2$-allyl), 18.64 (CH$_3$-allyl) ppm.

5.2.15 Synthesis of [Mo(η^3-allyl)Cl(CO)$_2$(bpy)]

USC-PF095

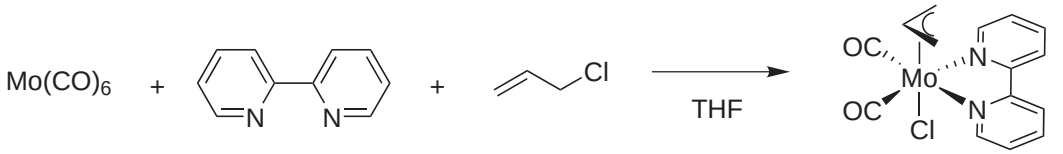

(**15**)

C_6MoO_6	$C_{10}H_8N_2$	C_3H_5Cl	$C_{15}H_{13}ClMoN_2O_2$
264.00 g/mol	156.18 g/mol	76.52 g/mol	384.66 g/mol

To a degassed mixture of anhydrous tetrahydrofuran (20 ml) and allylchloride (1.6 ml, 1.5 g, 19.6 mmol) molybdenum hexacarbonyl (500 mg, 1.89 mmol) and 2,2'-bipyridine (265 mg, 1.70 mmol) were added under a dinitrogen atmosphere and the mixture was heated to reflux for 18 h. The resulting red precipitate was filtered from the purple solution, washed with *n*-hexane (4 x 25 ml) and dried under vaccum to give a bright red powder. Yield: 74% (486 mg, 1.26 mmol). Elemental analysis (%): calc. $C_{15}H_{13}ClMoN_2O_2$: C 46.84, H 3.41, N 7.28, found: C 46.55, H 3.48, N 7.15; IR (ATR, cm^{-1}): 3063 (w), 2985 (w) 1925 (s) ν(CO), 1831 (s) ν(CO), 1600 (m), 1468 (m), 1442 (m), 1310 (w), 1152 (w), 769 (m); ^{1}H-NMR (200.13 MHz, DMSO-d_6): δ isomer A: 9.06 (d, 2H, $bpy_{H\text{-}6}$, ^3J = 3.8 Hz), 8.65 (d, 2H, $bpy_{H\text{-}3}$, $^3J_{H\text{-}3,H\text{-}4}$ = 8.3 Hz), 8.26 (d, 2H, $bpy_{H\text{-}4}$, $^3J_{H\text{-}3,H\text{-}4}$ = 8.3 Hz), 7.79 (t, 2H, $bpy_{H\text{-}5}$, ^3J = 6.3 Hz), 3.91-3.79 (m, 1H, allyl-H_{meso}), 3.51 (d, 2H, allyl-H_{syn},$^3J_{H\text{-}syn,H\text{-}meso}$ = 6.2 Hz), 1.36 (d, 2H, allyl-H_{anti},$^3J_{H\text{-}anti,H\text{-}meso}$ = 9.4 Hz), isomer A*: 8.77 (d, 2H, $bpy_{H\text{-}6}$, ^3J = 4.9 Hz), 8.56 (d, 2H, $bpy_{H\text{-}3}$, $^3J_{H\text{-}3,H\text{-}4}$ = 8.0 Hz), 8.17 (dt, 2H, $bpy_{H\text{-}4}$, $^3J_{H\text{-}3,H\text{-}4}$ = 8.0 Hz, ^4J = 1.0 Hz), 7.63 (t, 2H, $bpy_{H\text{-}5}$, ^3J = 6.3 Hz), 3.27-3.12 (m, 1H, allyl-H_{meso}), 3.07 (d, 2H, allyl-H_{syn},$^3J_{H\text{-}syn,H\text{-}meso}$ = 6.2 Hz), 1.23 (d, 2H, allyl-H_{anti},$^3J_{H\text{-}anti,H\text{-}meso}$ = 8.7 Hz) ppm; ^{13}C-NMR (50 MHz, DMSO-d_6): isomer A&A* δ 227.13 (CO), 153.30 (C-2), 151.85 (C-6), 139.18 (C-4), 126.27 (C-5), 122.98 (C-3), 70.76 (CH-allyl), 54.00 (CH_2-allyl) ppm.

5.2.16 Synthesis of [Mo(η^3-methallyl)Cl(CO)$_2$(phen)]

USC-PF046

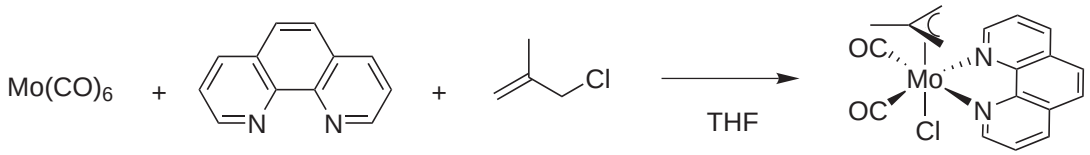

C_6MoO_6	$C_{12}H_8N_2$	C_4H_7Cl	(**16**) $C_{18}H_{15}ClMoN_2O_2$
264.00 g/mol	180.22 g/mol	90.55 g/mol	422.71 g/mol

Molybdenum hexacarbonyl (1.2 g, 4.5 mmol), 1,10-phenanthroline (757 mg, 4.2 mmol) and β-methallyl chloride (2.7 ml, 3.8 g, 42 mmol) were mixed in degassed anhydrous tetrahydrofuran and heated to reflux under a dinitrogen atmosphere for 5 h. Upon heating, the reactants dissolved slowly and the initially colorless solution turned purple after about 15 min. After cooling to room temperature, the precipitate formed was filtered off, washed with *n*-hexane and the excess of molybdenum hexacarbonyl was removed by sublimation at 50 °C and about $3.3 \cdot 10^{-1}$ mbar to give a dark brown solid. Yield: 62% (1.11 g, 2.6 mmol). Elemental analysis (%): calc. $C_{16}H_{15}ClMoN_2O_2$: C 51.14, H 3.58, N 6.63, found: C 50.85, H 3.24, N 6.84; IR (ATR, cm^{-1}): 3042 (w), 2997 (w), 1927 (s) ν(CO), 1852 (s) ν(CO), 1517 (w), 1425 (m), 1149 (w), 1029 (m), 850 (s), 780 (w), 729 (s); ^{1}H-NMR (250.13 MHz, DMSO-d$_6$): δ isomer A: 8.82 (d, 2H, H-4,7, ^3J = 8.0 Hz), 8.21 (s, 2H, H-5,6), 8.01 (d, 2H, H-3,8, ^3J = 8.0 Hz, ^3J = 5.0 Hz); isomer A*: 8.65 (d, 2H, H-4,7, ^3J = 8.0 Hz), 8.09 (s, 2H, H-5,6,), 7.89 (d, 2H, H-3,8, ^3J = 8.0 Hz, ^3J = 5.0 Hz); isomer A & A*: 9.17 (m, 4H, H-2,9), 3.00 (s, 2H, allyl-H$_{syn}$), 1.30 (s, 2H, allyl-H$_{anti}$), 0.67 (s, 2H, CH$_3$-allyl) ppm; ; ^{13}C-NMR (50 MHz, DMSO-d$_6$):δ 226.90 (CO), 152.05 (phen$_{C\text{-}2,9}$), 143.94 (phen$_{C\text{-}10a,10b}$), 138.27 (phen$_{C\text{-}5,6}$), 129.71 (phen$_{C\text{-}4,7}$), 127.31 (phen$_{C\text{-}4a,6a}$), 125.28 (phen$_{C\text{-}3,8}$), 81.57 (allyl-C$_q$), 79.93(allyl-CH$_2$), 18.54 (allyl-CH$_3$)ppm.

5.2.17 Synthesis of [Mo(η^3-allyl)Cl(CO)$_2$(phen)]

USC-PF096

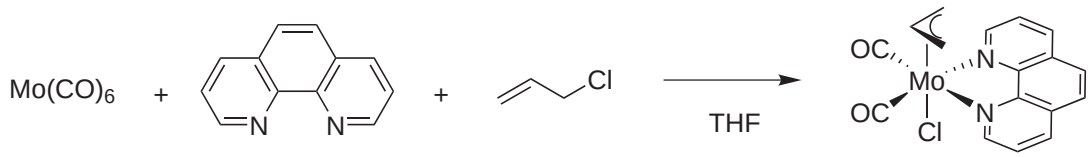

C_6MoO_6	$C_{12}H_8N_2$	C_3H_5Cl	(**17**) $C_{17}H_{13}ClMoN_2O_2$
264.00 g/mol	180.22 g/mol	76.52 g/mol	408.68 g/mol

To a degassed mixture of anhydrous tetrahydrofuran (20 ml) and allyl chloride (1.6 ml, 1.5 g, 19.6 mmol), molybdenum hexacarbonyl (500 mg, 1.89 mmol) and 1,10-phenanthroline (306 mg, 1.70 mmol) were added under dinitrogen atmosphere and the mixture was heated to reflux for 18 h. The resulting red precipitate was filtered from the purple solution, washed with *n*-hexane (4 x 25 ml) and dried under vaccum to give a bright red powder. Yield: 74% (516 mg, 1.26 mmol). Elemental analysis (%): calc. $C_{17}H_{13}ClMoN_2O_2$: C 49.96, H 3.21, N 6.85, found: C 49.61, H 3.38, N 6.76; IR (ATR, cm^{-1}): 3053 (w), 1930 (s) ν(CO), 1842 (s) ν(CO), 1514 (w), 1427 (m), 852 (m), 725 (w); ^{1}H-NMR (200.13 MHz, DMSO-d$_6$): δ isomer A: 9.18 (dd, 2H, H-2,9 $^3J_{H\text{-}2,9,H\text{-}3,8}$ = 5.0 Hz, $^4J_{H\text{-}2,9,H\text{-}4,7}$ = 1.0 Hz), 8.80 (dd, 2H, H-4,7 $^3J_{H\text{-}4,7,H\text{-}3,8}$ = 8.2 Hz, $^4J_{H\text{-}2,9,H\text{-}4,7}$ = 1.0 Hz), 8.19 (s, 2H, H-5,6), 7.98 (dd, 2H, H-3,8 $^3J_{H\text{-}4,7,H\text{-}3,8}$ = 8.2 Hz, $^3J_{H\text{-}2,9,H\text{-}3,8}$ = 5.0 Hz), 3.23 (d, 2H, allyl-H_{syn},$^3J_{H\text{-}syn,H\text{-}meso}$ = 6.2 Hz), 3.15-3.04 (m, 1H, allyl-H_{meso}), 1.30 (d, 2H, allyl-H_{anti},$^3J_{H\text{-}anti,H\text{-}meso}$ = 8.6 Hz), isomer A*: 9.47 (s(br), 2H, H-2,9), 8.88 (d(br), 2H, H-4,7), 8.27 (s, 2H, H-5,6), 8.16-8.11 (m(br), 2H, H-3,8), 4.16-4.00 (m(br), 1H, allyl-H_{meso}), 3.66 (d, 2H, allyl-H_{syn},$^3J_{H\text{-}syn,H\text{-}meso}$ = 6.2 Hz), 1.46 (d, 2H, allyl-H_{anti},$^3J_{H\text{-}anti,H\text{-}meso}$ = 9.3 Hz) ppm; ^{13}C-NMR (50 MHz, DMSO-d$_6$):δ 226.87 (CO), 152.20 (phen$_{C\text{-}2,9}$), 144.03 (phen$_{C\text{-}10a,10b}$), 138.26 (phen$_{C\text{-}5,6}$), 129.62 (phen$_{C\text{-}4,7}$), 127.22 (phen$_{C\text{-}4a,6a}$), 125.17 (phen$_{C\text{-}3,8}$), 70.13 (allyl-CH), 53.97 (allyl-CH_2) ppm.

5.2.18 Synthesis of [Mo(η^3-allyl)Cl(CO)$_2$(dpq)]

USC-PF081

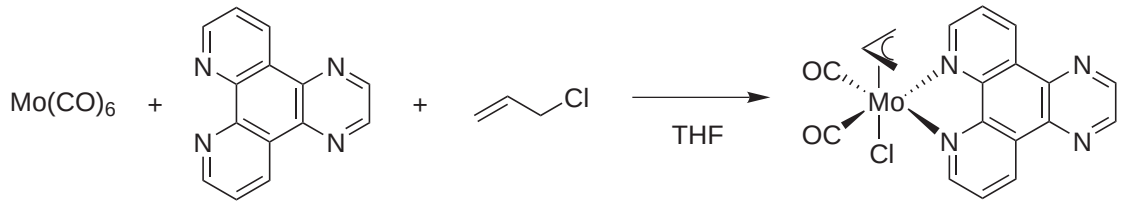

(**18**)

C_6MoO_6	$C_{14}H_8N_4$	C_3H_5Cl	$C_{19}H_{13}ClMoN_4O_2$
264.00 g/mol	232.24 g/mol	79.10 g/mol	460.72 g/mol

Anhydrous tetrahydrofuran (20 ml) and allyl chloride (1.3 ml, 1.27 g, 16.6 mmol) were degassed in a Schlenk-flask by two freeze-pump-thaw cycles and molybdenum hexacarbonyl (438 mg, 1.66 mmol) and dipyido[3,2-*d*:2',3'-*f*]quinoxaline (dpq) (350 mg, 1.51 mmol) were added under a dinitrogen atmosphere. The mixture was heated to reflux for 18 h whereupon the solution turned violet and a red precipitate formed. The precipitate was filtered off, washed with *n*-hexane (4 x 20 ml) and dried under vacuum to give a red-brown solid. Yield: 77% (587 mg, 1.27 mmol). Elemental analysis (%): calc. $C_{19}H_{13}ClMoN_4O_2$: C 49.53 H 2.84 N 12.16, found: C 49.63, H 3.11, N 11.86; IR (ATR, cm^{-1}): 3059 (w), 1932 (s) ν(CO), 1840 (s) ν(CO), 1477 (w), 1400 (m), 1387 (m), 1123 (w), 1081 (w), 824 (m), 734 (m); ^{1}H-NMR (200.13 MHz, DMSO-d$_6$): δ isomer A: 9.62 (dd, 2H, dpq$_{H\text{-}2,11}$, $^3J_{H\text{-}2,11,H\text{-}3,10}$ = 8.3 Hz, $^4J_{H\text{-}2,11,H\text{-}4,9}$ = 1.4 Hz), 9.30 (dd, 2H, dpq$_{H\text{-}4,9}$, $^3J_{H\text{-}4,9,H\text{-}3,10}$ = 5.1 Hz, $^4J_{H\text{-}4,9,H\text{-}2,11}$ = 1.4 Hz), 9.27 (s, 2H, dpq$_{H\text{-}6,7}$), 8.14 (dd, 2H, dpq$_{H\text{-}3,10}$, $^3J_{H\text{-}2,11,H\text{-}3,10}$ = 8.3 Hz, $^4J_{H\text{-}3,10,H\text{-}4,9}$ = 5.1 Hz), 3.44-3.36 (m, 1H, allyl-H$_{meso}$, overlapping with H_2O signal), 3.25 (d, 2H, allyl-H$_{syn}$, $^3J_{H\text{-}meso,H\text{-}syn}$ = 6.4 Hz), 1.34 (d, 2H, allyl-H$_{anti}$, $^3J_{H\text{-}meso,H\text{-}anti}$ = 8.6 Hz), isomer A*: 9.69 (dd, 2H, dpq$_{H\text{-}2,11}$, $^3J_{H\text{-}2,11,H\text{-}3,10}$ = 8.4 Hz, $^4J_{H\text{-}2,11,H\text{-}4,9}$ = 1.0 Hz), 9.34-9.30 (m, 2H, dpq$_{H\text{-}4,9}$, overlapping signals), 9.29 (s, 2H, dpq$_{H\text{-}6,7}$, overlapping signals), 8.30 (dd, 2H, dpq$_{H\text{-}3,10}$, $^3J_{H\text{-}2,11,H\text{-}3,10}$ = 8.4 Hz, $^4J_{H\text{-}3,10,H\text{-}4,9}$ = 5.3 Hz), 4.15-4.01 (m, 1H, allyl-H$_{meso}$), 3.69 (d, 2H, allyl-H$_{syn}$, $^3J_{H\text{-}meso,H\text{-}syn}$ = 6.2 Hz), 1.50 (d, 2H, allyl-H$_{anti}$, $^3J_{H\text{-}meso,H\text{-}anti}$ = 9.1 Hz) ppm; ^{13}C-NMR (50 MHz, DMSO-d$_6$): δ 226.91 (CO), 153.45 (dpq$_{C\text{-}2,11}$), 146.50 (dpq$_{C\text{-}12a,12b}$), 145.77 (dpq$_{C\text{-}6,7}$), 138.77 (dpq$_{C\text{-}4b,8a}$), 134.52 (dpq$_{C\text{-}3,10}$), 128.07 (dpq$_{C\text{-}4a,8b}$), 126.30 (dpq$_{C\text{-}9,4}$), 81.57 (allyl-CH), 57.91 (allyl-CH$_2$) ppm.

5.2.19 Synthesis of [Mo(η^3-allyl)Cl(CO)$_2$(dppz)]

USC-PF084

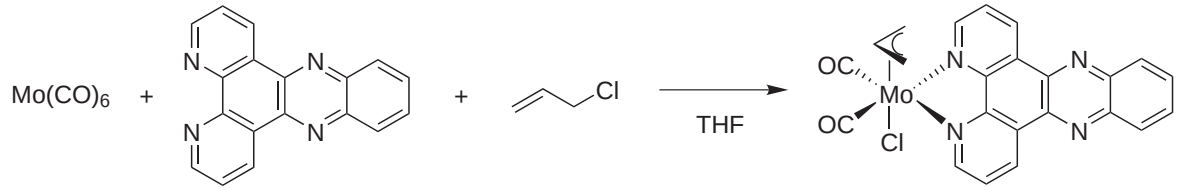

(**19**)

C_6MoO_6	$C_{18}H_{10}N_4$	C_3H_5Cl	$C_{23}H_{15}ClMoN_4O_2$
264.00 g/mol	282.30 g/mol	79.10 g/mol	510.79 g/mol

Molybdenum hexacarbonyl (739 mg, 2.8 mmol) and dipyrido[3,2-*a*:2',3'-*c*]phenazine (dppz) (528 mg, 1.87 mmol) were dissolved in anhydrous tetrahydrofuran (30 ml). Then, allyl chloride (0.75 ml, 705 mg, 9.2 mmol) was added and the mixture was heated to reflux for 6 h under nitrogen atmosphere. The now deep purple solution was stored at -20 °C overnight and the precipitate that formed was filtered off, washed with *n*-pentane, and subsequently with diethylether until the filtrate was colorless to give a deep purple solid that was dried under vacuum. Yield: 68% (650 mg, 1.27 mmol). Elemental analysis (%): calc. $C_{23}H_{15}ClMoN_4O_2$: C 54.08 H 2.96 N 10.97, found: C 53.91, H 3.14, N 11.12; IR (ATR, cm^{-1}): 3072 (w), 3012 (w) 1935 (s) ν(CO), 1859 (s) ν(CO), 1490 (w), 1463 (w), 1417 (m), 1359 (m), 1078 (m), 827 (s), 764 (s), 732 (s), 716 (m). Characterization by NMR spectroscopy was not possible due to insufficient solubility in the deuterated solvents available.

5.2.20 Synthesis of [Mo(η^3-allyl)Cl(CO)$_2$(dppn)]

USC-PF082

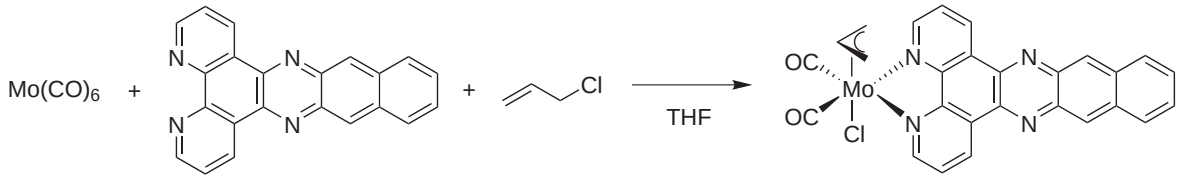

(**20**)

C_6MoO_6	$C_{22}H_{12}N_4$	C_3H_5Cl	$C_{27}H_{17}ClMoN_4O_2$
264.00 g/mol	332.36 g/mol	79.10 g/mol	560.83 g/mol

A mixture of anhydrous tetrahydrofuran (20 ml) and allyl chloride (1.0 ml, 0.94 g, 13.0 mmol) was degassed, and then molybdenum hexacarbonyl (219 mg, 0.83 mmol) and benzo[*i*]dipyrido[3,2-*a*:2',3'-*c*]phenazine (dppn) (250 mg, 0.75 mmol) were added. Upon heating the mixture to reflux for 14 h under a dinitrogen atmosphere, the dppn dissolved very slowly and an almost black precipitate formed. The precipitate was filtered off, washed with *n*-hexane (3 x 20 ml) and dried under vacuum to give an almost black powder. Yield: 72% (302 mg, 0.54 mmol). Elemental analysis (%): calc. $C_{23}H_{15}ClMoN_4O_2 \cdot H_2O$: C 56.91 H 3.18 N 9.83, found: C 56.68, H 3.18, N 9.71; IR (ATR, cm^{-1}): 3053 (w), 1935 (s) ν(CO), 1865 (s) ν(CO), 1457 (w), 1413 (m), 1391 (w), 881 (m), 823 (w), 739 (w). Characterization by NMR spectroscopy was not possible due to insufficient solubility in the deuterated solvents available.

5.2.21 Synthesis of [Mo(η^3-methallyl)$(CO)_2$(bpy)(py)]PF_6

USC-PF-045

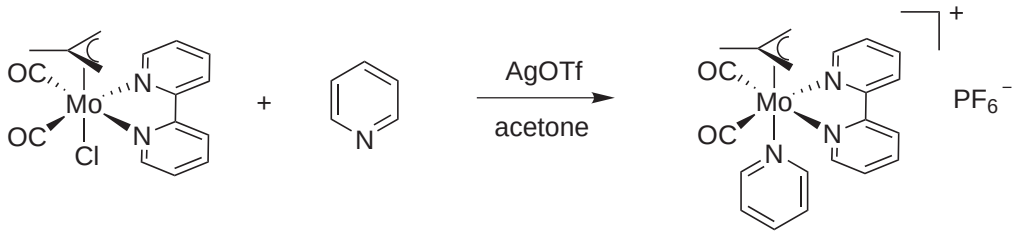

(**14**)
$C_{16}H_{15}ClMoN_2O_2$
398.69 g/mol

C_5H_5N
79.10 g/mol

(**21**)
$C_{21}H_{20}F_6MoN_3O_2P$
587.30 g/mol

[Mo(η^3-methallyl)Cl$(CO)_2$(bpy)] (**14**) (500 mg, 1.25 mmol) was partially dissolved in anhydrous and degassed acetone (30 ml). Upon addition of silver triflate (308 mg, 1.2 mmol), silver chloride formed as a white precipitate and the suspension was stirred for 2 h under a dinitrogen atmosphere with exclusion of light. The resulting clear dark-red solution was transferred via canula to a new flask and then, pyridine (500 μl, 509 mg, 6.43 mmol) was added and allowed to react for another 2 h at room temperature. Subsequently, a solution of potassium hexafluorophosphate (1.15 g, 6.25 mmol) in water (25 ml) was added, giving a red micro-crystalline precipitate, which was filtered off, washed with *n*-pentane (3 x 5 ml) and dried in vacuo. Yield: 76% (568 mg, 0.95 mmol). Elemental analysis (%): calc. $C_{21}H_{20}F_6MoN_3O_2P$: C 42.95, H 3.43, N 7.15, found: C 42.07, H 3.43, N 6.95; MS (ESI$^+$, acetone): *m/z* 444 [M - PF_6]$^+$; UV-Vis (10% DMSO/water): $\lambda_{max}(\epsilon)$ = 416 (1471), 299 (12306), 238 nm (12264 l mol^{-1} cm^{-1}); IR (ATR, cm^{-1}): 1944 (m) ν(CO), 1860 (m) νCO), 1603 (w), 1441 (w), 830 (s) ν(P-F), 758 (s), 700 (w); ^{1}H-NMR (250.13 MHz, DMSO-d_6): δ 8.99 (d, 2H, bpy, ^3J = 5.0 Hz), 8.60 (d, 2H, py, ^3J = 8.0 Hz), 8.59-8.56 (m, 2H, bpy, overlapping signal), 8.29 (dt, 2H, bpy, ^3J = 7.9 Hz, ^4J = 1.2 Hz), 7.82-7.75 (tt, 1H, py, ^4J = 7.8 Hz, ^4J = 1.6 Hz), 7.78-7.73 (m, 2H, bpy, overlapping signal), 7.41-7.35 (ddd, 2H, py, ^3J = 7.8 Hz, ^3J = 4.3 Hz, ^4J = 1.5 Hz), 3.16 (s, 2H, allyl-H_{syn}), 1.29 (s, 2H, allyl-H_{anti}), 1.01 (s, 3H, allyl-CH_3) ppm; ^{13}C-NMR (62.53 MHz, DMSO-d_6): δ 225.93 (CO) 153.22, 152.11, 149.63, 140.57, 136.15, 127.12, 123.93, 123.51, 82.78 (C_q-allyl), 56.00 (CH_2-allyl), 19.46 (CH_3-allyl) ppm.

5.2.22 Synthesis of [Mo(η^3-allyl)$(CO)_2$(bpy)(py)]PF_6

USC-PF043

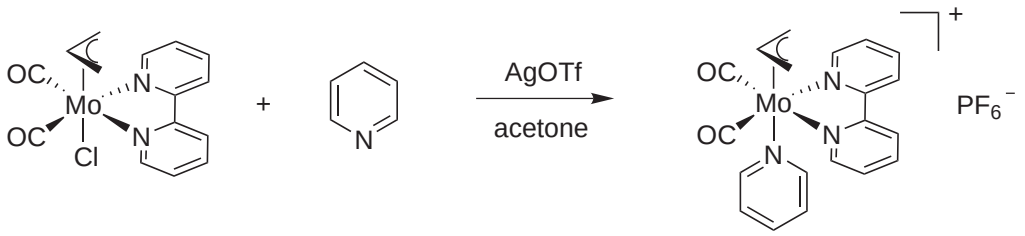

(**15**)
$C_{15}H_{13}ClMoN_2O_2$
384.66 g/mol

C_5H_5N
79.10 g/mol

(**22**)
$C_{20}H_{18}F_6MoN_3O_2P$
573.27 g/mol

[Mo(η^3-allyl)Cl$(CO)_2$(bpy)] (**15**) (500 mg, 1.3 mmol) was dissolved in anhydrous and degassed acetone (20 ml) to give a deep red solution. Upon addition of silver triflate (334 mg, 1.3 mmol) silver chloride formed as a white precipitate and the resulting suspension was strirred for 2 h under a dinitrogen atmosphere with exclusion of light. The solution was then transfered into another Schlenk-flask via teflon kanula and pyridine (524 μl, 6.5 mmol) was added via syringe. The mixture was stirred for 2.5 h at room temperature with exclusion of light and subsequently a solution of potassium hexafluorophosphate (1.19 g, 6.5 mmol) in water (30 ml) was added and the mixture was stored overnight at -20°C. The precipitate that formed was filtered off, washed with diethylether (3 x 10 ml) and dried in vacuo to give orange needles. Yield: 85% (615 mg, 1.1 mmol). Elemental analysis (%): calc. $C_{20}H_{18}F_6MoN_3O_2P$: C 41.90, H 3.16, N 7.33, found: C 41.66, H 3.13, N 7.19; MS (ESI$^+$, acetone): *m/z* 430 [M - PF_6]$^+$; UV-Vis (2% DMSO/water): $\lambda_{max}(\epsilon)$ = 447 (1720), 300 nm (15323 l mol^{-1} cm^{-1}); IR (ATR, cm^{-1}): 3129 (w), 2992 (w) 1944 (s) ν(CO), 1841 (s) ν(CO), 1599 (m), 1447 (m), 1315 (m), 1225 (m), 1160 (w), 827 (s), 774 (s), 749 (s), 693 (s); ^{1}H-NMR (400.13 MHz, DMSO-d_6): δ isomer A: 9.21 (d, 2H, bpy_{H-6}, $^3J_{H-6,H-5}$ = 5.5 Hz), 8.71 (d, 2H, bpy_{H-3}, $^3J_{H-3,H-4}$ = 8.1 Hz), 8.36 (td, 2H, bpy_{H-4}, ^4J = 1.3 Hz, $^3J_{H-4,H-3}$ = 8.1 Hz), 7.90 (t, 2H, bpy_{H-5}, $^4J_{H-5,H-6}$ = 5.5 Hz), 4.01 (tt, 1H, allyl-H_{meso}, $^3J_{H-meso,H-syn}$ = 6.5 Hz, $^3J_{H-meso,H-anti}$ = 9.5 Hz), 3.63 (d, 2H, allyl-H_{syn}, $^3J_{H-meso,H-syn}$ = 6.5 Hz, 1.58 (d, 2H, allyl-H_{anti}, $^3J_{H-meso,H-anti}$ = 9.5 Hz); isomer A*: 8.96 (dd, 2H, bpy_{H-6}, $^4J_{H-6,H-4}$ = 1.6 Hz, $^3J_{H-6,H-5}$ = 5.5 Hz), 8.56 (d, 2H, bpy_{H-3}, $^3J_{H-3,H-4}$ = 8.0 Hz, overlapping), 8.26 (td, 2H, bpy_{H-4}, $^4J_{H-6,H-4}$ = 1.6 Hz, $^3J_{H-5,H-4}$ = 8.0 Hz), 7.72 (tt, 2H, bpy_{H-5}, ^4J = 1.1 Hz, $^3J_{H-5,H-6}$ = 5.5 Hz, $^3J_{H-5,H-4}$ = 8.0 Hz), 3.38 - 3.27 (m, 3H, allyl-$H_{meso,syn}$, overlapping of H_2O signal), 1.32 (d, 2H, allyl-H_{anti}, $^3J_{H-meso,H-anti}$ = 8.5 Hz); isomer A & A*: 8.57 (dd, 2H, $py_{H-1,5}$, $^4J_{H-3,H-1,5}$ = 1.8 Hz, $^3J_{H-5,H-4}$ = 6.0 Hz, overlapping); 7.78 (tt, 1H, py_{H-3}, $^4J_{H-3,H-1,5}$ = 1.8 Hz, $^3J_{H-3,H-2,4}$ = 7.6 Hz), 7.38 (m, 2H, $py_{H-2,4}$) ppm; ^{13}C-NMR (100.13 MHz, DMSO-d_6): δ isomer A: 225.73 (CO), 153.47

(bpy_{C-1}), 152.90 (bpy_{C-6}), 140.78 (bpy_{C-4}), 127.67 (bpy_{C-5}), 123.77 (bpy_{C-3}); isomer A*: 225.59 (CO), 153.47 (bpy_{C-1}), 152.18 (bpy_{C-6}), 140.38 (bpy_{C-4}), 126.97 (bpy_{C-5}), 123.28 (bpy_{C-3}); isomer A & A*: 149.62 ($py_{C-2,6}$), 136.15 (py_{C-4}), 123.92 ($py_{C-3,5}$), 74.00 ($allyl_{CH}$), 71.29 ($allyl_{CH}$), 57.43 ($allyl_{CH2}$) ppm.

5.2.23 Synthesis of [Mo(η^3-methallyl)$(CO)_2$(phen)(py)]PF_6

USC-PF047

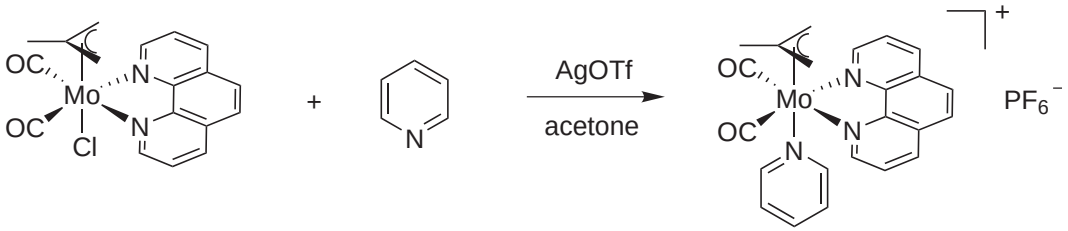

(**16**)
$C_{18}H_{15}ClMoN_2O_2$
422.71 g/mol

C_5H_5N
79.10 g/mol

(**23**)
$C_{23}H_{20}F_6MoN_3O_2P$
611.32 g/mol

To a suspension of [Mo(η^3-methallyl)Cl$(CO)_2$(phen)] (**16**) (500 mg, 1.18 mmol) in anhydrous and degassed acetone (30 ml), silver triflate (303 mg, 1.18 mmol) was added, resulting in a clear deep-red solution containing a white precipitate. The resulting mixture was stirred for 2 h at room temperature under a dinitrogen atmosphere with exclusion of light and the solution was then transferred via canula into another flask already charged with pyridine (500 μl, 509 mg, 6.43 mmol). It was stirred for another 2 h under the same conditions as before. Then, a solution of potassium hexafluorophosphate (1.09 g, 5.9 mmol) in water (25 ml) was added and the aqueous mixture was stored at 4 °C to give bright red crystalls that were filtered off, washed with water (2 x 10 ml), and diethylether (2 x 10 ml), and dried in vacuo. Yield: 44% (315 mg, 0.52 mmol). Elemental analysis (%): calc. $C_{23}H_{20}F_6MoN_3O_2P{\cdot}H_2O$: C 43.90, H 3.52, N 6.68, found: C 43.56, H 3.07, N 6.53; MS (ESI$^+$, acetone): *m/z* 468 [M - PF_6]$^+$; IR (ATR, cm^{-1}): 1938 (s) ν(CO), 1870 (m) ν(CO), 1847 (s) ν(CO), 1443 (w), 1427 (w), 833 (s) $\nu(PF_6)$, 775 (m), 727 (m), 702 (m); ^{1}H-NMR (200.13 MHz, acetone-d_6): δ 9.83 (dd, 2H, $phen_{H\text{-}2,9}$, $^3J_{H\text{-}2,9,H\text{-}3,8}$ = 5.0 Hz, $^4J_{H\text{-}2,9,H\text{-}4,7}$ = 1.0 Hz), 8.96 (dd, 2H, $phen_{H\text{-}4,7}$, $^3J_{H\text{-}4,7,H\text{-}3,8}$ = 8.2 Hz, $^4J_{H\text{-}4,7,H\text{-}2,9}$ = 1.0 Hz), 8.38 (td, 2H, $py_{H\text{-}2,6}$, $^3J_{H\text{-}2,6,H\text{-}3,5}$ = 5.0 Hz, $^4J_{H\text{-}2,6,H\text{-}4}$ = 1.4 Hz), 8.29 (td, 2H, $phen_{H\text{-}3,8}$, $^3J_{H\text{-}3,8,H\text{-}4,7}$ = 8.2 Hz, $^4J_{H\text{-}3,8,H\text{-}2,9}$ = 5.0 Hz), 8.22 (s, 2H, $phen_{H\text{-}5,6}$), 7.72 (tt, 1H, $py_{H\text{-}4}$, $^3J_{H\text{-}4,H\text{-}3,5}$ = 7.6 Hz, $^4J_{H\text{-}4,H\text{-}2,6}$ = 1.4 Hz), 7.27 (ddd, 1H, $py_{H\text{-}3,5}$, $^3J_{H\text{-}3,5,H\text{-}4}$ = 7.6 Hz, $^3J_{H\text{-}3,5,H\text{-}2,6}$ = 5.0 Hz, ^4J = 1.4 Hz), 3.61 (s, 2H, allyl-H_{syn}), 1.85 (s, 2H, allyl-H_{anti}), 0.85 (s, 3H, allyl-CH_3) ppm; ^{13}C-NMR (62.86 MHz, DMSO-d_6): δ 225.57 (CO), 152.75 ($phen_{C\text{-}2,9}$), 149.60 ($py_{C\text{-}2,6}$), 143.68 ($phen_{C\text{-}10,10b}$), 139.58 ($phen_{C\text{-}5,6}$), 136.14 ($py_{C\text{-}4}$), 129.79 ($phen_{C\text{-}4,7}$), 127.56 ($phen_{C\text{-}4a,6a}$), 125.85 ($phen_{C\text{-}3,8}$), 123.91 ($py_{C\text{-}3,5}$), 82.02 (C_q-allyl), 55.31 (CH_2-allyl), 18.84 (CH_3-allyl) ppm.

5.2.24 Synthesis of [Mo(η^3-allyl)(CO)$_2$(phen)(py)]PF$_6$

USC-PF044

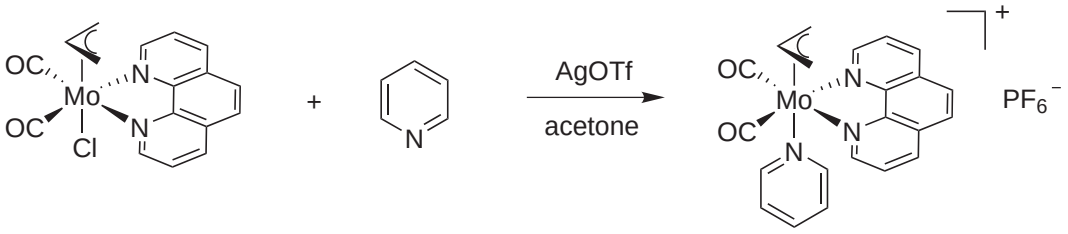

(**17**)
$C_{17}H_{13}Cl_1MoN_2O_2$
408.68 g/mol

C_5H_5N
79.10 g/mol

(**24**)
$C_{22}H_{18}F_6MoN_3O_2P$
597.29 g/mol

[Mo(η^3-allyl)Cl(CO)$_2$(phen)] (**17**) (500 mg, 1.2 mmol) was dissolved in anhydrous and degassed acetone (20 ml) to give a deep red solution. Upon addition of silver triflate (308 mg, 1.2 mmol), silver chloride formed as a white precipitate and the resulting suspension was strirred for 2 h under a dinitrogen atmosphere with exclusion of light. The solution was then transfered into another Schlenk-flask via a teflon canula and pyridine (566 μl, 6.0 mmol) was added via syringe. The mixture was stirred for 2 h at room temperature with exclusion of light and subsequently, a solution of potassium hexafluorophosphate (1.1 g, 6.0 mmol) in water (20 ml) was added and the mixture was stored overnight at 4 °C. Some crystals that formed were filtered off, washed with diethylether (4 x 10 ml), and dried in vacuo to give deep-red prismatic crystals. Yield: 77% (550 mg, 0.9 mmol). Elemental analysis (%): calc. $C_{22}H_{18}F_6MoN_3O_2P$: C 44.24, H 3.04, N 7.04, found: C 44.10, H 3.08, N 6.96; MS (ESI$^+$, acetone): *m/z* 454 [M - PF$_6$]$^+$; UV-Vis (2% DMSO/water): $\lambda_{max}(\epsilon)$ = 451 (1967), 370 (2193), 273 nm (28198 l mol^{-1} cm^{-1}); IR (ATR, cm^{-1}): 1938 (s) ν(CO), 1869 (sh) ν(CO), 1845 (s) ν(CO), 1630 (w), 1519 (w), 1466 (m), 1429 (m), 829 (s) ν(P-F), 764 (s), 725 (s), 701 (s); ^{1}H-NMR (400.13 MHz, DMSO-d$_6$): δ isomer A: 9.64 (d, 2H, phen$_{H\text{-}2}$, ^3J = 4.4 Hz), 8.99 (d, 2H, phen$_{H\text{-}3}$, ^3J = 8.1 Hz), 8.33 (s, 2H, phen$_{H\text{-}5,6}$), 8.24 (m, 2H, phen$_{H\text{-}4}$), 3.50 (d, 2H, allyl-H$_{syn}$, $^3J_{H\text{-}meso,H\text{-}syn}$ = 6.4 Hz), 3.22 (tt, 1H, allyl-H$_{meso}$, $^3J_{H\text{-}meso,H\text{-}syn}$ = 6.4 Hz, $^3J_{H\text{-}meso,H\text{-}anti}$ = 9.4 Hz), 1.39 (d, 2H, allyl-H$_{anti}$, $^3J_{H\text{-}meso,H\text{-}anti}$ = 9.4 Hz); isomer A*: 9.37 (dd, 2H, phen$_{H\text{-}2}$, $^3J_{H\text{-}1,H\text{-}2}$ = 5.0 Hz, $^4J_{H\text{-}1,H\text{-}3}$ = 1.1 Hz), 8.88 (dd, 2H, phen$_{H\text{-}4}$, $^3J_{H\text{-}3,H\text{-}4}$ = 8.2 Hz, $^3J_{H\text{-}1,H\text{-}3}$ = 1.1 Hz), 8.21 (s, 2H, phen$_{H\text{-}5,6}$), 8.05 (dd, 2H, phen$_{H\text{-}3}$, $^3J_{H\text{-}3,H\text{-}2}$ = 5.0 Hz, $^3J_{H\text{-}2,H\text{-}3}$ = 8.2 Hz), 4.22 (tt, 1H, allyl-H$_{meso}$, $^3J_{H\text{-}meso,H\text{-}syn}$ = 6.4 Hz, $^3J_{H\text{-}meso,H\text{-}anti}$ = 9.4 Hz), 3.78 (d, 2H, allyl-H$_{syn}$, $^3J_{H\text{-}meso,H\text{-}syn}$ = 6.4 Hz), 1.66 (d, 2H, allyl-H$_{anti}$, $^3J_{H\text{-}meso,H\text{-}anti}$ = 9.3 Hz); isomer A* & A: 8.57 (dd, 2H, py$_{H\text{-}2,6}$, $^4J_{H\text{-}4,H\text{-}2,6}$ = 1.5 Hz, $^3J_{H\text{-}2,6,H\text{-}5}$ = 5.7 Hz), 7.78 (tt, 1H, py$_{H\text{-}4}$, $^4J_{H\text{-}4,H\text{-}2,6}$ = 1.5 Hz, $^3J_{H\text{-}4,H\text{-}3,5}$ = 7.6 Hz), 7.38 (ddd, 2H, py$_{H\text{-}3,5}$, $^3J_{H\text{-}4,H\text{-}3,5}$ = 7.6 Hz, ^3J = 4.4 Hz, ^4J = 1.5 Hz) ppm; ^{13}C-NMR (100.13 MHz, DMSO-d$_6$): δ isomer A:

144.01 ($phen_{C\text{-}2,9}$), 139.94 ($phen_{C\text{-}3,8}$), 129.87 ($phen_{C\text{-}5,6}$), 127.43 ($phen_{C\text{-}4,8}$); isomer A^*: 152.78 ($phen_{C\text{-}2,9}$), 139.43 ($phen_{C\text{-}3,8}$), 129.69 ($phen_{C\text{-}5,6}$), 125.69 ($phen_{C\text{-}4,8}$); isomer A & A^*: 225.48 (CO), 149.62 ($py_{C\text{-}2,6}$), 136.16 ($py_{C\text{-}4}$), 123.92 ($py_{C\text{-}3,5}$), 73.96 (allyl-CH), 70.86 (allyl-CH), 57.46 (allyl-CH_2) ppm.

5.2.25 Synthesis of [Mo(η^3-allyl)(CO)$_2$(dpq)(py)]PF$_6$

USC-PF083

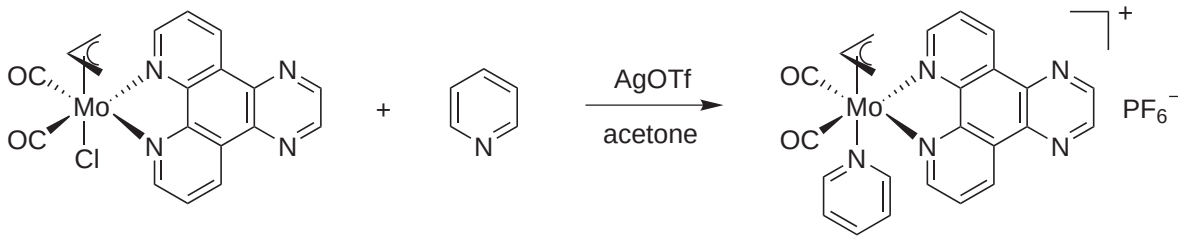

(**18**)
$C_{19}H_{13}ClMoN_4O_2$
460.72 g/mol

C_5H_5N
79.10 g/mol

(**25**)
$C_{24}H_{18}F_6MoN_5O_2P$
649.33 g/mol

[Mo(η^3-allyl)Cl(CO)$_2$(dpq)] (**18**) (400 mg, 0.87 mmol) was suspended in degassed acetone (50 ml), silver triflate (224 mg, 0.87 mmol) was added and the mixture was stirred for 16 h at room temperature under a dinitrogen atmosphere with exclusion of light to give deep red solution containing a white precipitate. After separation of the solution from the solid via canula, pyridine (350 μl, 344 mg, 4.35 mmol) was added and the clear mixture was again stirred for 3 h under a dinitrogen atmosphere while protected from light. Subsequently, an aqueous solution (30 ml) of potassium hexafluorophosphate (800 mg, 4.35 mmol) was added and after storage at -25 °C overnight the resulting precipitate was filtered off. It was washed with water (2 x 25 ml), ethanol (1 x 5 ml), and plenty of diethylether, and the brick-red solid then dried under vacuum. Yield: 43% (240 mg, 0.37 mmol). Elemental analysis (%): calc. $C_{24}H_{18}F_6MoN_5O_2P{\cdot}H_2O$: C 43.19, H 3.02, N 10.49, found: C 43.42, H 3.04, N 10.28; MS (ESI$^+$, acetone): *m/z* 506 [M - PF_6]$^+$; IR (ATR, cm^{-1}): 3108 (w), 1948 (s) ν(CO), 1861 (s) ν(CO), 1476 (w), 1445 (w), 1403 (m), 1390 (m), 832 (s) ν(P-F), 735 (m); ^{1}H-NMR (200.13 MHz, DMSO-d_6): δ isomer A: 9.70 (d(br), 2H, $dpq_{H\text{-}2,11}$, $^3J_{H\text{-}2,11,H\text{-}3,10}$ = 8.0 Hz), 9.49 (d(br), 2H, $dpq_{H\text{-}4,9}$, $^3J_{H\text{-}4,9,H\text{-}3,10}$ = 5.0 Hz), 9.31 (s, 2H, $dpq_{H\text{-}6,7}$), 8.21 (d, 2H, $dpq_{H\text{-}3,10}$, $^3J_{H\text{-}2,11,H\text{-}3,10}$ = 8.0 Hz, $^3J_{H\text{-}4,9,H\text{-}3,10}$ = 5.0 Hz), 3.51-3.41 (m, 3H, allyl-$H_{syn,meso}$, overlapping with H_2O signal), 1.43 (d, 2H, allyl-H_{anti}, $^3J_{H\text{-}anti,H\text{-}meso}$ = 8.1 Hz), isomer A*: 9.78 (d(br), 2H, $dpq_{H\text{-}2,11,H\text{-}4,9}$, $^3J_{H\text{-}2,11,H\text{-}3,10}$ = 8.0 Hz), 9.34 (s, 2H, $dpq_{H\text{-}6,7}$), 8.38 (dd(br), 2H, $dpq_{H\text{-}3,10}$, $^3J_{H\text{-}2,11,H\text{-}3,10}$ = 8.3 Hz, $^3J_{H\text{-}4,9,H\text{-}3,10}$ = 5.3 Hz), 4.25-4.16 (m, 1H, allyl-H_{meso}), 3.81 (d, 2H, allyl-H_{syn}, $^3J_{H\text{-}syn,H\text{-}meso}$ = 5.6 Hz), 1.71 (d, 2H, allyl-H_{anti}, $^3J_{H\text{-}anti,H\text{-}meso}$ = 9,3 Hz), isomer A&A*: 8.61 (d(br), 2H, $py_{H\text{-}2,6}$), 7.87 (d(br), 1H, $py_{H\text{-}4}$), 7.45 (d(br), 2H, $py_{H\text{-}3,5}$) ppm.

5.2.26 Synthesis of [Mo(η^3-allyl)(CO)$_2$(dppz)(py)]PF$_6$

USC-PF079

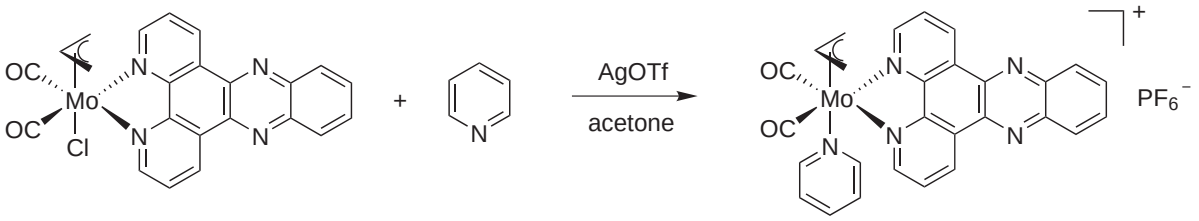

(**19**)
$C_{23}H_{15}ClMoN_4O_2$
510.79 g/mol

C_5H_5N
79.10 g/mol

(**26**)
$C_{28}H_{20}F_6MoN_5O_2P$
699.39 g/mol

[Mo(η^3-allyl)Cl(CO)$_2$(dppz)] (**19**) (500 mg, 1.02 mmol) was suspended in degassed acetone (70 ml) and stirred for 15 min. Then, silver triflate (262 mg, 1.02 mmol) was added and stirring under a dinitrogen atmosphere with exclusion of light was continued. Over the course of 2.5 h, the dark suspension turned into a deep red solution and a white precipitate formed. The red solution was transferred into another flask via canula and pyridine was added (411 μl, 403 mg, 5.1 mmol), and the mixture allowed to react for 2 h. Subsequently an aqueous solution (30 ml) of potassium hexafluorophosphate (939 mg, 5.1 mmol) was added and the mixture was stored overnight at -25 °C to give a red-brown precipitate which was filtered off, washed with ethanol (5 ml) followed by plenty of diethylether and dried under vacuum. Yield: 56% (396 mg, 0.57 mmol). Elemental analysis (%): calc. $C_{28}H_{20}F_6MoN_5O_2P{\cdot}H_2O$: C 46.88, H 3.09, N 9.76, found: C 46.44, H 2.90, N 9.68; MS (ESI$^+$, acetone): *m/z* 556 [M - PF_6]$^+$; IR (ATR, cm^{-1}): 3094 (w), 1948 (s) ν(CO), 1860 (s) ν(CO), 1494 (m), 1419 (m), 1361 (m), 1080 (w), 832 (s) ν(P-F), 761 (m), 733 (m); ^{1}H-NMR (200.13 MHz, DMSO-d$_6$): δ 9.76 (d(br), 2H, dppz$_{H\text{-}2,12}$, ^3J = 7.8 Hz), 9.46 (d(br), 2H, dppz$_{H\text{-}3,11}$, ^3J = 4.1 Hz), 8.58 (d(br), 2H, py$_{H\text{-}2,6}$, $^3J_{H\text{-}2,6,H\text{-}3,5}$ = 4.2 Hz), 8.48-8.43 (m(br), 2H, dppz$_{H\text{-}(6,7),(8,9)}$, overlapping signals), 8.24-8.12 (m, 4H, dppz$_{H\text{-}(6,7),(8,9)}$/dppz$_{H\text{-}4,10}$), 7.82 (td, 1H, py$_{H\text{-}4}$, $^3J_{H\text{-}4,H\text{-}3,5}$ = 7.7 Hz, $^4J_{H\text{-}4,H\text{-}2,6}$ = 1.4 Hz), 7.41 (ddd, 2H, py$_{H\text{-}3,5}$, $^3J_{H\text{-}4,H\text{-}3,5}$ = 7.7 Hz, $^3J_{H\text{-}2,6,H\text{-}3,5}$ = 4.2 Hz, ^4J = 1.4 Hz), isomer A: 4.22 (m, 1H, allyl-H$_{meso}$), 3.81 (d, 2H, allyl-H$_{syn}$, $^3J_{H\text{-}meso,H\text{-}syn}$ = 6.2 Hz), 1.72 (d, 2H, allyl-H$_{anti}$, $^3J_{H\text{-}meso,H\text{-}anti}$ = 8.9 Hz), isomer A*: 3.47-3.18 (m, 3H, allyl-H$_{meso/anti}$, overlapping signals), 1.45 (d, 2H, allyl-H$_{anti}$, $^3J_{H\text{-}meso,H\text{-}anti}$ = 7.8 Hz) ppm.

5.2.27 Synthesis of [Mo(η^3-allyl)(CO)$_2$(dppn)(py)]PF$_6$

USC-PF080

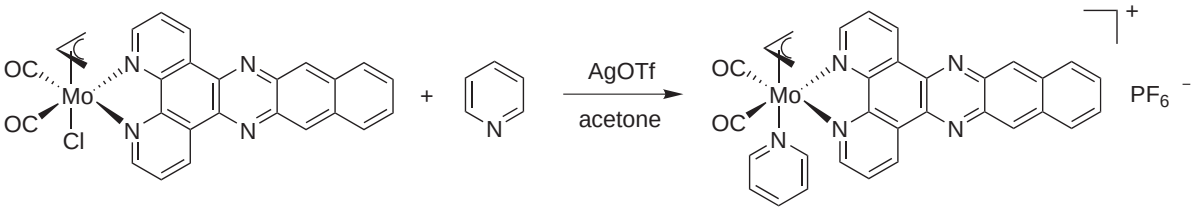

(**20**)
$C_{27}H_{17}ClMoN_4O_2$
560.83 g/mol

C_5H_5N
79.10 g/mol

(**27**)
$C_{32}H_{22}F_9MoN_5O_2P$
749.45 g/mol

[Mo(η^3-allyl)Cl(CO)$_2$(dppn)] (**20**) (250 mg, 0.45 mmol) was suspended in degassed acetone (70 ml), silver triflate (116 mg, 0.45 mmol) was added, and the mixture was stirred at room temperature under a dinitrogen atmosphere with exclusion of light for 20 h. The dark red solution was separated from the white precipitate that formed and pyridine (182 μl, 178 mg, 2.25 mmol) was added to the solution. After a reaction time of 2.5 h, a solution of potassium hexafluorophosphate (414 mg, 2.25 mmol) in deionized water (20 ml) was added and the volume of the aqueous mixture was reduced to one half under vacuum. Precipitation was completed by addition of water (50 ml The resulting solid was filtered off, washed with plenty of distilled water, ethanol (5 ml) and finally with diethylether (3 x 10 ml), and dried under vacuum to give a brick-red solid. Yield: 51% (174 mg, 0.23 mmol). Elemental analysis (%): calc. $C_{32}H_{22}F_6MoN_5O_2P{\cdot}H_2O$: C 50.08, H 3.15, N 9.13, found: C 49.90, H 3.20, N 8.97; MS (ESI$^+$, acetone): *m/z* 606 [M - PF_6]$^+$; IR (ATR, cm^{-1}): 3067 (w), 1948 (s) ν(CO), 1858 (s) ν(CO), 1417 (m), 1360 (w), 1076 (w), 1047 (w), 834 (s) ν(P-F), 752 (w); ^{1}H-NMR (200.13 MHz, DMSO-d_6): δ isomer A: 9.75 (d(br), 2H, dppn$_{H\text{-}2,15}$, ^3J = 8.1 Hz), 9.44 (d(br), 2H, dppn$_{H\text{-}4,13}$, ^3J = 3.9 Hz), 9.17 (s, 2H, dppn$_{H\text{-}6,11}$), 8.20 (dd, 2H, dppn$_{H\text{-}3,14}$, ^3J = 5.0 Hz, ^3J = 7.4 Hz), 8.43-8.32 (m(br), 4H, dppn$_{H\text{-}7,10}$, overlapping signals with isomer A*), 7.76 (d(br), 2H, dppn$_{H\text{-}8,9}$, ^3J = 5.2 Hz), 3.55 (s(br), 3H, allyl-H$_{meso,syn}$, overlapping signals), 1.47 (d, 2H, allyl-H$_{anti}$, $^3J_{H\text{-}meso,H\text{-}anti}$ = 7.2 Hz), isomer A*: 9.81 (d(br), 2H, dppn$_{H\text{-}2,15,H\text{-}4,13}$, ^3J = 8.3 Hz), 8.43-8.32 (m(br), 4H, dppn$_{H\text{-}4,13}$, overlapping signals with isomer A), 4.25-4.19 (m, 1H, allyl-H$_{meso}$), 3.83 (d, 2H, allyl-H$_{syn}$, $^3J_{H\text{-}meso,H\text{-}syn}$ = 6.0 Hz), 1.75 (d, 2H, allyl-H$_{anti}$, $^3J_{H\text{-}meso,H\text{-}anti}$ = 9.1 Hz), isomer A&A*: 8.66 (d(br), 2H, py$_{H\text{-}2,6}$, $^3J_{H\text{-}3,5,H\text{-}2,6}$ = 5.0 Hz), 7.99 (t(br), 1H, py$_{H\text{-}4}$, $^3J_{H\text{-}4,H\text{-}3,5}$ = 7.5 Hz), 7.56 (dd, 2H, py$_{H\text{-}3,5}$, $^3J_{H\text{-}3,5,H\text{-}2,6}$ = 5.0 Hz, $^3J_{H\text{-}3,5,H\text{-}4}$ = 7.4 Hz) ppm.

5.2.28 Synthesis of dimethyl-7-oxa-bicyclo[2.2.1]hepta-2,5-diene-2,3-dicarboxylate

USC-PF109, literature:[100]

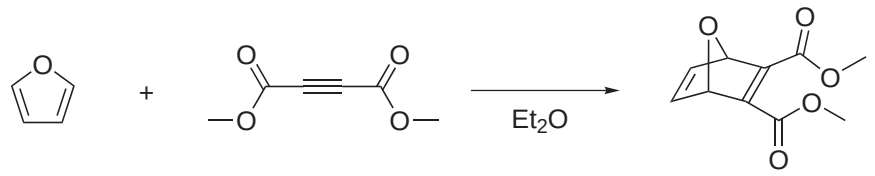

(**28**)

C_4H_4O	$C_6H_6O_4$	$C_{10}H_{10}O_5$
68.07 g/mol	142.11 g/mol	210.18 g/mol

Furan (2.70 g, 39.7 mmol) and dimethylacetylene dicarboxylate (5.64 g, 39.7 mmol) were dissolved in diethylether (15 ml) and stirred at room temperature for 7 d under exclusion of light. Water (25 ml) was added and the phases were separated. The aqueous phase was then extracted with diethylether (25 ml). The combined organic phases were washed with brine, dried over magnesium sulfate and concentrated in vacuo. The yellow liquid obtained was purified by column chromatography on silica 60 using ethyl acetate/hexane in a gradient of 4:1 to 1:1 to give the desired product as a colorless liquid. Yield: 10% (774 mg, 3.6 mmol). IR (ATR, cm^{-1}): 2959 (w), 1710 (s), 1640 (m), 1434 (m), 1259 (s), 1210 (s), 1108 (s), 878 (m); ^{1}H-NMR (200.13 MHz, $CDCl_3$): δ 7.21 (t, 2H, H-5,6, $^3J_{H\text{-}5,6,H\text{-}1,4}$ = 1.0 Hz), 5.67 (t, 2H, H-1,4, $^3J_{H\text{-}5,6,H\text{-}1,4}$ = 1.0 Hz), 3.81 (s, 6H, CH_3) ppm; ^{13}C-NMR (50.32 MHz, $CDCl_3$): δ 163.37 (C=O), 153.45 (C-2,3), 143.39 (C-5,6), 85.21 (C-1,4), 52.49 (CH_3) ppm.

5.2.29 Synthesis of 3-(methoxycarbonyl)-7-oxa-bicyclo[2.2.1]hepta- 2,5-diene-2-carboxylic acid

USC-PF114, literature:[100]

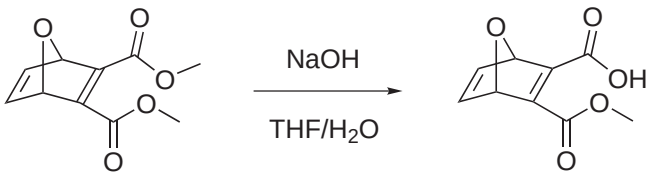

(**28**)
$C_{10}H_{10}O_5$
210.18 g/mol

(**29**)
$C_9H_8O_5$
196.16 g/mol

Dimethyl-7-oxa-bicyclo[2.2.1]hepta-2,5-diene-2,3-dicarboxylate (**28**) (643 mg, 3.0 mmol) was dissolved in tetrahydrofuran (15 ml) and cooled to 0 °C. An aqueous solution of sodium hydroxide (32 ml, 0.25 M, 3.0 mmol) was added dropwise and the mixture was stirred at this temperature for 1 h, then warmed to room temperature and stirred for another 1 h. Then, the reaction was quenched by addition of aqueous hydrochloric acid (10 ml, 1 M). The clear brown mixture was extracted with ethyl acetate (2 x 25 ml) and the combined extracts were dried over magnesium sulfate. Concentration *in vacuo* gave a brownish oil which was re-dissolved in ethyl acetate (15 mL) and added dropwise to *n*-hexane (150 mL). The dark-brown solid that formed was filtered off and the clear filtrate was evaporated to dryness to give the product as an off-white sticky solid. Yield: 74% (438 mg, 2.2 mmol). IR (ATR, cm^{-1}): 2961 (w), 2656 (w), 1722 (vs), 1619 (vs), 1473 (m), 1328 (s), 1247 (vs), 874 (s); ^{1}H-NMR (200.13 MHz, $CDCl_3$): δ 7.28 (dd, 1H, H-5, $^3J_{H\text{-}5,H\text{-}6}$ = 5.3 Hz, $^3J_{H\text{-}4,H\text{-}5}$ = 1.8 Hz), 7.19 (dd, 1H, H-6, $^3J_{H\text{-}5,H\text{-}6}$ = 5.3 Hz, $^3J_{H\text{-}1,H\text{-}6}$ = 1.8 Hz), 5.83 (t, 1H, H-1, $^3J_{H\text{-}6,H\text{-}1}$ = 1.8 Hz), 5.79 (t, 1H, H-4, $^3J_{H\text{-}4,H\text{-}5}$ = 1.8 Hz), 3.90 (s, 3H, CH_3) ppm; ^{13}C-NMR (50.32 MHz, $CDCl_3$): δ 166.59 (C=O, acid), 162.22 (C=O, ester), 161.49 (C-3), 151.91 (C-2), 142.75 (C-5,6), 142.95 (C-5,6), 85.48 (C-4), 84.45 (C-1), 54.29 (CH_3) ppm.

5.2.30 Synthesis of [Mo(η^3-allyl)(N_3)($CO)_2$(bpy)]

USC-PF099

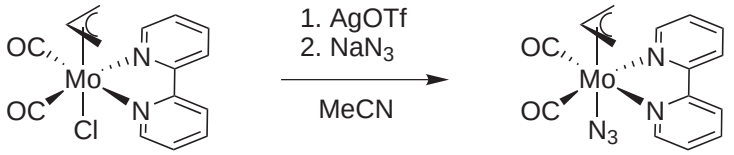

(**15**)
$C_{15}H_{13}ClMoN_2O_2$
384.66 g/mol

(**30**)
$C_{15}H_{13}MoN_5O_2$
391.23 g/mol

[Mo(η^3-allyl)Cl($CO)_2$(bpy)] (**15**) (450 mg, 1.17 mmol) was suspended in degassed acetonitrile (30 ml). Upon addition of silver triflate (301 mg, 1.17 mmol), a white precipitate appeared and the resulting suspension was stirred for 2 h under a dinitrogen atmosphere with exclusion of light. The clear red solution was transferred with a teflon cannula into another flask containing sodium azide (152 mg, 2.34 mmol) and stirred at room temperature for 19 h while protected from light. The resulting precipitate was filtered off, first washed with plenty of water to remove excess sodium azide, and then with ethanol (2 x 5 ml) followed by diethylether (2 x 10 ml) and subsequently dried in vacuo to give the complex as a bright red solid. Yield: 56% (258 mg, 0.66 mmol). Elemental analysis (%): calc. $C_{15}H_{13}MoN_5O_2$: C 45.05, H 3.35, N 17.90, found: C 45.09, H 3.41, N 18.02; IR (ATR, cm^{-1}): 3083 (w), 2036 (s) $\nu(N_3)$, 1928 (s) ν(CO), 1836 (s) ν(CO), 1600 (m), 1469 (m), 1440 (m), 1310 (w), 1172 (w), 757 (m), 733 (w); ^{1}H-NMR (200.13 MHz, DMSO-d_6): δ isomer A: 9.05 (d(br), 2H, bpy_{H-6}), 8.69 (d(br), 2H, bpy_{H-3}), 8.26 (d(br), 2H, bpy_{H-4}), 7.83 (m, 2H, bpy_{H-5}), 3.89-3.71 (m, 1H, allyl-H_{meso}), 3.20 (d, 2H, allyl-H_{syn}, $^3J_{H\text{-}syn,H\text{-}meso}$ = 8.1 Hz), overlapping signals), 1.36 (d, 2H, allyl-H_{anti}, $^3J_{H\text{-}anti,H\text{-}meso}$ = 9.0 Hz, overlapping signals), isomer A*: 8.80 (dd, 2H, bpy_{H-6}, $^3J_{H\text{-}6,H\text{-}5}$ = 5.3 Hz, $^4J_{H\text{-}6,H\text{-}4}$ = 0.9 Hz), 8.57 (d(br), 2H, bpy_{H-3}, $^3J_{H\text{-}3,H\text{-}4}$ = 8.2 Hz), 8.20 (dt, 2H, bpy_{H-4}, $^3J_{H\text{-}3,H\text{-}4}$ = 7.9 Hz, $^4J_{H\text{-}4,H\text{-}6}$ = 1.2 Hz), 7.66 (ddd, 2H, bpy_{H-5}, $^3J_{H\text{-}5,H\text{-}4}$ = 7.9 Hz, $^3J_{H\text{-}5,H\text{-}6}$ = 5.4 Hz, $^3J_{H\text{-}5,H\text{-}3}$ = 1.1 Hz), 3.23-3.18 (m, 1H, allyl-H_{meso}), 3.14 (d, 2H, allyl-H_{syn}, $^3J_{H\text{-}syn,H\text{-}meso}$ = 6.7 Hz, overlapping signals), 1.29 (d, 2H, allyl-H_{anti}, $^3J_{H\text{-}anti,H\text{-}meso}$ = 8.9 Hz) ppm; ^{13}C-NMR (50 MHz, DMSO-d_6): isomer A&A* δ 227.20 (CO), 153.27 (C-2), 151.85 (C-6), 139.48 (C-4), 126.56 (C-5), 123.04 (C-3), 72.54 (CH-allyl), 55.78 (CH_2-allyl) ppm.

5.2.31 Synthesis of [Mo(η^3-allyl)(CO)$_2$(bpy)(N$_3$C$_2$(COOMe)$_2$)], method A

USC-PF111

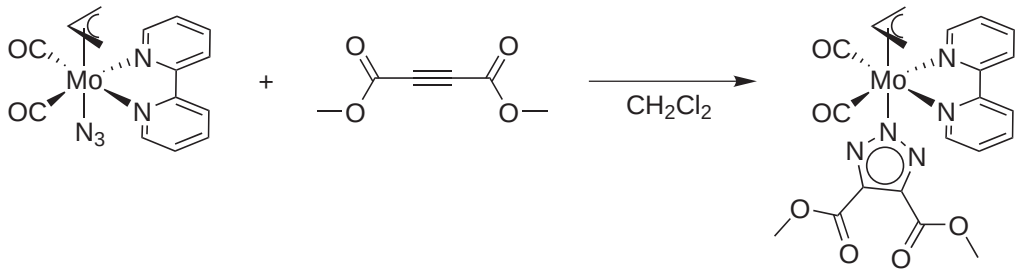

(**30**)
$C_{15}H_{13}MoN_5O_2$
391.23 g/mol

$C_6H_6O_4$
142.11 g/mol

(**31**)
$C_{21}H_{19}MoN_5O_6$
533.34 g/mol

[Mo(η^3-allyl)(N$_3$)(CO)$_2$(bpy)] (**30**) (44 mg, 0.11 mmol) and dimethylacetylene dicarboxylate (DMAD, 17 μl, 20 mg, 0.14 mmol) were dissolved in dichloromethane (15 ml) and stirred for 36 h at room temperature with exclusion of light. The resulting red solution was filtered through Celite and after concentration in vacuo layered with *n*-hexane for crystallization. After 3 d in the dark, the red needles obtained were filtered off, washed with *n*-hexane and dried under vacuum. Yield: 47% (28 mg, 0.05 mmol). Elemental analysis (%): calc. $C_{21}H_{19}MoN_5O_6$: C 47.29, H 3.59, N 13.13, found: C 47.41, H 3.52, N 12.95; IR (ATR, cm^{-1}): 3071 (w), 2957 (w) , 1931 (s) ν(CO), 1858 (s) ν(CO), 1723 (s) ν(C=O, ester), 1438 (m), 1300 (m), 1220 (m), 1165 (m), 1091 (m), 763 (m); ^{1}H-NMR (200.13 MHz, DMSO-d$_6$): δ isomer A: 9.20 (s(br), 2H, bpy$_{H\text{-}6}$), 8.58-8.53 (m(br), 2H, bpy$_{H\text{-}3}$, overlapping signals), 8.26-8.17 (m(br), 2H, bpy$_{H\text{-}4}$, overlapping signals), 7.84-7.78 (m, 2H, bpy$_{H\text{-}5}$), 4.15-4.05 (m, 1H, allyl-H$_{meso}$), 3.60 (s, 6H, CH$_3$), 3.45 (d, 2H, allyl-H$_{syn}$, $^3J_{H\text{-}syn,H\text{-}meso}$ = 6.4 Hz), 1.54-1.48 (m, 2H, allyl-H$_{anti}$, overlapping signals), isomer A*: 8.92 (dd, 2H, bpy$_{H\text{-}6}$, $^3J_{H\text{-}6,H\text{-}5}$ = 5.5 Hz, $^4J_{H\text{-}6,H\text{-}4}$ = 1.7 Hz), 8.54 (d(br), 2H, bpy$_{H\text{-}3}$, $^3J_{H\text{-}3,H\text{-}4}$ = 8.0 Hz), 8.17 (dt, 2H, bpy$_{H\text{-}4}$, $^3J_{H\text{-}3,H\text{-}4}$ = 8.0 Hz, $^4J_{H\text{-}4,H\text{-}6}$ = 1.6 Hz), 7.58 (ddd, 2H, bpy$_{H\text{-}5}$, $^3J_{H\text{-}5,H\text{-}4}$ = 7.9 Hz, $^3J_{H\text{-}5,H\text{-}6}$ = 5.5 Hz, $^3J_{H\text{-}5,H\text{-}3}$ = 1.6 Hz), 3.63 (s, 6H, CH$_3$), 3.33-3.31 (m, 2H, allyl-H$_{syn}$, overlapping H$_2$O signal), 3.21-3.08 (m, 1H, allyl-H$_{meso}$), 1.49 (d, 2H, allyl-H$_{anti}$, $^3J_{H\text{-}anti,H\text{-}meso}$ = 9.1 Hz) ppm; ^{13}C-NMR (50 MHz, DMSO-d$_6$): isomer A&A* δ 226.13 (CO), 162.40 (C=O, ester), 154.49 (C-2), 152.24 (C-6), 139.56 (C-4), 138.37 (C$_q$, triazol), 126.36 (C-5), 122.76 (C-3), 81.58 (CH-allyl), 57.52 (CH$_2$-allyl), 51.64 (CH$_3$) ppm.

5.2.32 Synthesis of [Mo(η^3-allyl)(CO)$_2$(bpy)(N$_3$C$_2$(COOMe)$_2$)], method B

USC-PF111

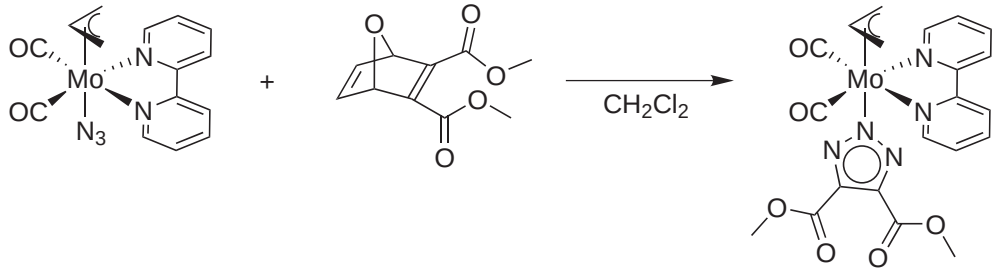

(**30**)
$C_{15}H_{13}MoN_5O_2$
391.23 g/mol

(**28**)
$C_{10}H_{10}O_5$
210.18 g/mol

(**31**)
$C_{21}H_{19}MoN_5O_6$
533.34 g/mol

[Mo(η^3-allyl)(N$_3$)(CO)$_2$(bpy)] (**30**) (62 mg, 0.16 mmol) and dimethyl-7-oxa-bicyclo[2.2.1]hepta-2,5-diene-2,3-dicarboxylate (**28**) (50 mg, 0.24 mmol) were dissolved in dichloromethane (20 ml) and stirred for 48 h at room temperature with exclusion from light. The solvent was evaporated under vacuum and the red residue was washed with ethyl acetate (3 x 5 ml) followed by *n*-hexane (3 x 5 ml) and subsequently dried under vacuum to give a bright red powder. Crystals suitable for X-ray analysis were grown by diffusion of *n*-hexane into a concentrated solution in dichloromethane to give fine red needles after 3 d. Yield: 77% (65 mg, 0.12 mmol). Elemental analysis (%): calc. $C_{21}H_{19}MoN_5O_6$: C 47.29, H 3.59, N 13.13, found: C 47.03, H 3.58, N 13.14; IR (ATR, cm^{-1}): 3071 (w), 2957 (w) , 1931 (s) ν(CO), 1856 (s) ν(CO), 1723 (s) ν(C=O, ester), 1439 (m), 1301 (m), 1220 (m), 1163 (m), 1090 (m), 764 (m); ^{1}H-NMR (200.13 MHz, DMSO-d$_6$): δ isomer A: 9.19 (s(br), 2H, bpy$_{H\text{-}6}$), 8.57-8.52 (m(br), 2H, bpy$_{H\text{-}3}$, overlapping signals), 8.25-8.18 (m(br), 2H, bpy$_{H\text{-}4}$, overlapping signals), 7.84-7.77 (m, 2H, bpy$_{H\text{-}5}$), 4.14-4.05 (m, 1H, allyl-H$_{meso}$), 3.62 (s, 6H, CH$_3$), 3.45 (d, 2H, allyl-H$_{syn}$,$^3J_{H\text{-}syn,H\text{-}meso}$ = 6.3 Hz), 1.54-1.47 (m, 2H, allyl-H$_{anti}$, overlapping signals), isomer A*: 8.97 (dd, 2H, bpy$_{H\text{-}6}$, $^3J_{H\text{-}6,H\text{-}5}$ = 5.5 Hz, $^4J_{H\text{-}6,H\text{-}4}$ = 1.6 Hz), 8.54 (d(br), 2H, bpy$_{H\text{-}3}$, $^3J_{H\text{-}3,H\text{-}4}$ = 8.0 Hz), 8.16 (dt, 2H, bpy$_{H\text{-}4}$, $^3J_{H\text{-}3,H\text{-}4}$ = 8.0 Hz, $^4J_{H\text{-}4,H\text{-}6}$ = 1.6 Hz), 7.58 (ddd, 2H, bpy$_{H\text{-}5}$, $^3J_{H\text{-}5,H\text{-}4}$ = 8.0 Hz, $^3J_{H\text{-}5,H\text{-}6}$ = 5.5 Hz, $^3J_{H\text{-}5,H\text{-}3}$ = 1.6 Hz), 3.63 (s, 6H, CH$_3$), 3.33-3.31 (m, 2H, allyl-H$_{syn}$, overlapping H$_2$O signal), 3.21-3.06 (m, 1H, allyl-H$_{meso}$), 1.49 (d, 2H, allyl-H$_{anti}$,$^3J_{H\text{-}anti,H\text{-}meso}$ = 9.0 Hz) ppm; ^{13}C-NMR (50 MHz, DMSO-d$_6$): isomer A&A* δ 226.31 (CO), 162.38 (C=O, ester), 154.49 (C-2), 152.24 (C-6), 139.55 (C-4), 138.34 (C$_q$, triazol), 126.36 (C-5), 122.76 (C-3), 81.58 (CH-allyl), 57.56 (CH$_2$-allyl), 51.64 (CH$_3$) ppm.

5.2.33 Synthesis of ONBD-Gly-Leu-Arg(Pbf)-Wang resin

USC-PF125

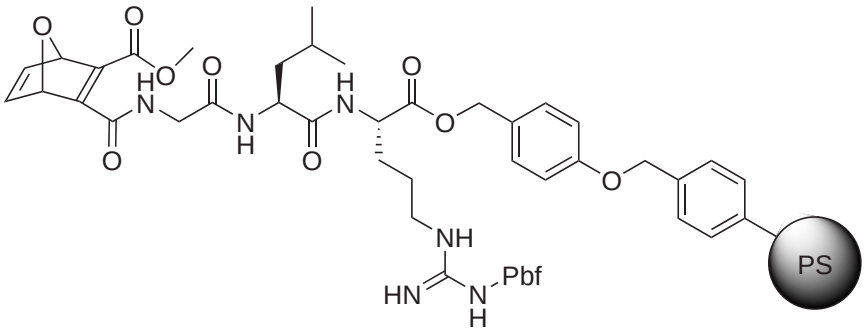

(**32**)

The peptide was prepared on a 0.189 mmol scale on a Fmoc-Arg(Pbf)-Wang resin (300 mg, 0.63 mmol/g) using the amino acids Fmoc-Leu-OH and Fmoc-Gly-OH applying the manual peptide synthesis conditions as described above. 3-(methoxycarbonyl)-7-oxabicyclo[2.2.1]hepta-2,5-diene-2-carboxylic acid (**29**) was also coupled under the conditions applied for the other amino acids. The peptide was not cleaved from the resin and used, after drying, in the next step without further modifications. IR (ATR, cm^{-1}): 3339 (m), 3060 (w) , 3027 (w), 2927 (s), 1739 (s) ν(C=O, ester), 1727 (s) ν(C=O, ester), 1660 (s) ν(C=O, amide), 1616 (s) ν(C=O, amide), 1559 (s), 1513(s), 1451 (s), 1246 (s), 1171 (m), 1111 (s), 758 (m);

5.2.34 Synthesis of [Mo(η^3-allyl)(CO)$_2$(bpy)(N$_3$C$_2$(COOMe)(CO-Gly-Leu-Arg(Pbf)-Wang resin))]

USC-PF126

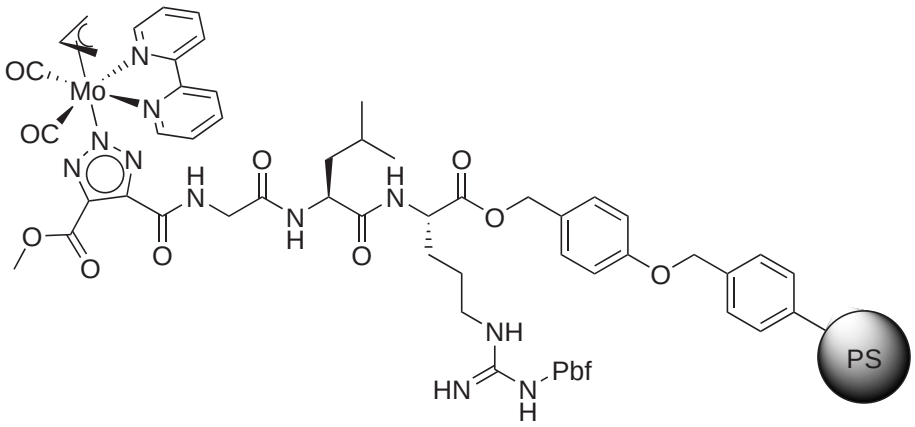

(**33**)

ONBD-Gly-Leu-Arg(Pbf)-Wang resin (**32**) (44 mg, 0.05 mmol) was allowed to swell in dichloromethane (3 ml) for 1 h prior to use. [Mo(η^3-allyl)(N$_3$)(CO)$_2$(bpy)] (**30**) (20 mg, 0.05 mmol) was dissolved in dichloromethane (3 ml) and shaken together with the ONBD-Gly-Leu-Arg(Pbf)-Wang resin in a filter syringe under exclusion from light for 24 h. The resin was washed with dimethylformamide (5 x 3 ml) followed by dichloromethane (5 x 3 ml), and diethylether (5 x 3 ml), and subsequently dried under vacuum to give a light solid. IR (ATR, cm^{-1}): 3338 (m), 3060 (w) , 3027 (m), 2926 (s), 1945 (m) ν(CO), 1863 (m) ν(CO), 1734 (s) ν(C=O, ester), 1664 (s) ν(C=O, amide), 1616 (s) ν(C=O, amide), 1550 (s), 1515 (s), 1447 (s), 1246 (s), 1169 (m), 1110 (s), 760 (m);

5.2.35 Synthesis of *DL*-phenylalanine methylester hydrochloride

USC-PF016

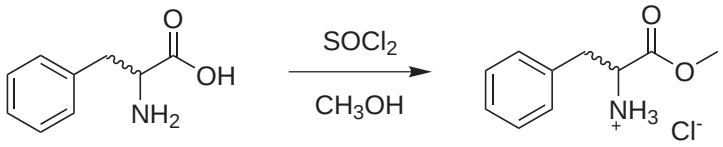

(**34**)

$C_9H_{11}NO_2$
165.19 g/mol

$C_{10}H_{14}ClNO_2$
215.68 g/mol

Thionylchloride (10.0 ml, 16.4 g, 0.14 mol) was added dropwise into methanol (60 ml) under ice cooling. Subsequently a suspension of *DL*-phenylalanine (5.0 g, 30.0 mmol) in methanol (30 ml) was added under ice cooling and the resulting mixture was heated to reflux for 14 h. After cooling to room temperature the solvent was removed under vacuum and the remaining white residue was re-desolved in a minimal volume of methanol and added dropwise into diethylether (250 ml). The white precipitate that formed was filtered, washed with diethylether (3 x 25 ml) and dried under vacuum to give the product as a white solid. Yield: 90% (5.80 g, 27.0 mmol). Elemental analysis (%): calc. $C_{10}H_{14}ClNO_2$ (%): C 55.69, H 6.54, N 6.49, found: C 55.39, H 6.57, N 6.48; MS (ESI$^+$, CH_3OH): m/z 180 [M - Cl]$^+$; IR (ATR, cm^{-1}): 2914 (s) ν_{NH}, 2840 (s) ν_{NH}, 2620 (m), 1744 (s) $\nu_{C=O}$, 1238 (s), 741 (s), 701(s); ^{1}H-NMR (200.13 MHz, DMSO-d$_6$): δ 8.78 (s, 2H, NH_2), 7.35 - 7.23 (m, 5H, H_{Ar}), 4.22 (dd, 1H, H-α, $^3J_{\alpha,\beta}$ = 5.7 Hz, $^3J_{\alpha,\beta'}$ = 7.5 Hz), 3.65 (s, 3H, CH_3), 3.22 (dd, 1H, H-β, $^3J_{\alpha,\beta}$ = 5.7 Hz, $^2J_{\beta,\beta'}$ = 14.0 Hz), 3.10 (dd, 1H, H-β', $^3J_{\alpha,\beta'}$ = 7.5 Hz, $^2J_{\beta,\beta'}$ = 14.0 Hz) ppm; ^{13}C-NMR (50.62 MHz, DMSO-d$_6$): δ 169.27 (C=O), 134.71 (C-1), 129.33 (C-3, C-5), 128.52 (C-2, C-6), 127.19 (C-4), 53.22 (C-α), 52.45 (OCH_3), 35.79 (C-β) ppm.

5.3 Biological assays

The following experiments were carried out in collaboration with members of the DFG-funded Forschergruppe 630 (FOR 630) "Biological function of organometallic compounds". Cytotoxicity measurements on HT-29 and MCF-7 cancer cells were performed by Johanna Niesel, Universität Würzburg, in collaboration with the group of Prof Dr Nils Metzler-Nolte, Ruhr-Universität Bochum and the group Prof Dr Ingo Ott, Technische Universität Braunschweig. Proliferation inhibition, LDH release as well as DNA fragmentation assays on NALM-6 leukemia cells and MCF-7 (+/-) cancer cells were carried out by the group of Dr Aram Prokop, AG Experimentelle Onkologie, Kliniken der Stadt Köln GmbH.

5.3.1 Cell culture conditions

MCF-7 human breast adeno carcinoma and HT-29 human colon carcinoma cells were maintained in 10% (v/v) fetal calf serum containing Dulbecco's Modified Eagle's cell culture medium (PAA, high glucose, without phenol red, supplemented with penicillin and streptomycine) at 37 °C: 5% CO_2 and passaged twice a week according to standard procedures.

MCF-7 (+/-) (human breast adeno carcinoma cells, (+) caspase-3 expressing/(-)non--expressing), and NALM-6 cells (human B cell precursor leukemia cells) were subcultured every 3-4 days by dilution of the cells to a concentration of $1{\cdot}10^5$ cells/ml. All experiments were performed in RPMI 1640 cell culture medium (GIBCO, Invitrogen) supplemented with 10% heat inactivated fetal calf serum, 100 U/ml penicillin, 100 μg/ml streptomycin and 0.56 g/l *L*-glutamine. Twenty-four hours before the assay was set up, cells were cultured at a concentration of $3{\cdot}10^5$ cells/ml to attain standardized growth conditions. For apoptosis assays, the cells were then diluted to a concentration of $1{\cdot}10^5$ cells/ml immediately before addition of the different compounds.[146]

5.3.2 Cytotoxicity measurements

The cytotoxic of the complexes were determined by using the crystal violet assay (CV-assay), following an established procedure.[129] Cells were suspended in cell culture medium (HT-29: 3000 cells/ml, MCF-7: 10000 cells/ml), and 100 μl aliquots thereof were seeded in 96 well microtiter plates and incubated at 37 °C with 5% CO_2 for 48 h (HT-29) or 72 h (MCF-7). Stock solutions of the compounds in DMSO were freshly prepared and diluted with cell culture medium to the desired concentrations (final DMSO

concentration: 1% v/v). The medium in the plates was replaced with medium containing the compounds in different concentrations (six replicates). Wells containing DMSO (1%, v/v) were used as a control (twelve replicates). After further incubation for 72 h (HT-29) or 96 h (MCF-7), the medium was removed, the cells were washed with 100 μl PBS and fixed with 1% glutardialdehyd. Cell biomass was determined by crystal violet staining. The fixing solution was removed and 100 μl of a Triton X-100 (0.1%) solution was added to each well. Cells were then stained with a solution (0.04%, w/v) of crystal violet in ethanol (4%, v/v) for 30 min and subsequently washed with water. The crystal violet was extracted with ethanol (96%, v/v) by shaking for 4 h and the absorbance was determined at 570 nm with a Tecan Saphire2 microplate reader. IC_{50} values were determined by non-linear curve fitting as those concentrations causing 50% inhibition of cell proliferation. Results were calculated from two independent experiments.

5.3.3 LDH-release assay

Cytotoxicity of the different compounds on NALM-6 and MCF-7 (+/-) cells was measured by the release of lactate dehydrogenase (LDH). After incubation with different concentrations of complexes and ligands for 1 h, the amount of LDH released by NALM-6 and MCF-7 (+/-) cells was measured in the cell culture supernatants using the Cytotoxicity Detection Kit from Boehringer Mannheim® (Mannheim, Germany). The supernatants were centrifuged at 1500 rpm for 5 min. 20 μl of cell-free supernatants were diluted with 80 μl phosphate-buffered saline (PBS) and 100 μl reaction mixture containing 2-(4-iodophenyl)-3-(4-nitrophenyl)-5-phenyltetrazolium chloride (INT), sodium lactate, NAD^+ and diaphorase were added. Then, time-dependent formation of the reaction product was quantified photometrically at 490 nm. The maximum amount of LDH released by the cells was determined after lysis of the cells using 0.1% Triton X-100 in culture medium and set to represent 100% of cell death.[146]

5.3.4 DNA fragmentation assay

Apoptotic cell death in NALM-6 and MCF-7 (+/-) cells was determined by a modified cell cycle analysis, which detects DNA fragmentation on the single cell level. Cells were seeded at a density of $1 \cdot 10^5$ cells/ml and treated with different concentrations of compounds. After a 72 h incubation period at a temperature of 37 °C, cells were collected by centrifugation at 1500 rpm for 5 min, washed with PBS at 4 °C and fixed in PBS/ 2% formaldehyde (v/v) on ice for 30 min. After fixation, cells were pelleted, incubated with ethanol/PBS (2:1, v/v) for 15 min, pelleted and resuspended in PBS containing 40 μg/ml RNase. RNA was digested for 30 min at a temperature of 37 °C,

after which the cells were pelleted again and finally resuspended in PBS containing 50 μg/ml propidium iodide. Nuclear DNA fragmentation was quantified by flow cytometric determination of hypodiploid DNA. Data were collected and analyzed using a FACScan 3-colour flow cytometry analyzer (Becton Dickinson, Heidelberg, Germany) equipped with CELL Quest software. Data are given in percent hypoploidy (sub-G_1), which reflects the number of apoptotic cells.[146]

5.3.5 Proliferation inhibition assay

Cell viability of NALM-6 and MCF-7 (+/-) cells was measured following an established procedure. In proliferation inhibition experiments, it was determined using the CASY Cell Counter and Analyzer System from Innovatis (Bielefeld, Germany). Settings were specifically defined for the requirements of the cells used. With this system, the cell concentration can be analyzed simultaneously in three different size ranges: cell debris, dead cells, and viable cells. Cells were seeded at a density of $1 \cdot 10^5$ cells/ml and treated with various concentrations of compounds; non-treated cells served as controls. After a 24 h incubation period at 37 °C, cells were re-suspended properly and 100 μl of each well was diluted in 10 mL CASYton (ready-to-use isotonic saline solution) for an immediate automated counting of the cells.[147]

6 References

[1] G. Jaouen, A. Vessières, I. S. Butler, *Acc. Chem. Res.* **1993**, *26*, 361–369.

[2] M. Frey, *ChemBioChem* **2002**, *3*, 153–160.

[3] G. Gasser, I. Ott, N. Metzler-Nolte, *J. Med. Chem.* **2011**, *54*, 3–25.

[4] O. Novakova, H. Chen, O. Vrana, A. Rodger, P. J. Sadler, V. Brabec, *Biochemistry* **2003**, *42*, 11544–11554.

[5] Y. K. Yan, M. Melchart, A. Habtemariam, P. J. Sadler, *Chem. Commun.* **2005**, *38*, 4764–4776.

[6] R. E. Aird, J. Cummings, A. A. Ritchie, M. Muir, R. E. Morris, H. Chen, P. J. Sadler, D. I. Jodrell, *Br. J. Cancer* **2002**, *86*, 1652–1657.

[7] W. H. Ang, E. Daldini, C. Scolaro, R. Scopelliti, L. Juillerat-Jeannerat, P. J. Dyson, *Inorg. Chem.* **2006**, *45*, 9006–9013.

[8] P. J. Dyson, G. Sava, *Dalton Trans.* **2006**, *35*, 1929–1933.

[9] H. Köpf, P. Köpf-Meier, *Angew. Chem. Int. Ed.* **1979**, *18*, 477–478.

[10] P. Köpf-Meier, H. Köpf, *J. Organomet. Chem.* **1988**, *342*, 167–176.

[11] K. Mross, P. Robben-Bathe, L. Edler, J. Baumgart, W. E. Berdel, H. Fiebig, C. Unger, *Onkologie* **2000**, *23*, 576–579.

[12] M. Tacke, L. T. Allen, L. Cuffe, W. M. Gallagher, Y. Lou, O. Mendoza, H. Müller-Bunz, F. J. K. Rehmann, N. Sweeney, *J. Organomet. Chem.* **2004**, *689*, 2242–2249.

[13] K. Strohfeldt, M. Tacke, *Chem. Soc. Rev.* **2008**, *37*, 1174–1187.

[14] M. Guo, Z. Guo, P. J. Sadler, *J. Biol. Inorg. Chem.* **2001**, *6*, 698–707.

[15] G. Mokdsi, M. M. Harding, *J. Inorg. Biochem.* **2001**, *83*, 205–209.

[16] C. V. Cristodoulou, A. G. Eliopoulos, L. S. Young, L. Hodgkins, D. R. Ferry, D. J. Kerr, *Br. J. Cancer* **1998**, *77*, 2088–2097.

[17] A. Nguyen, A. Vessières, E. A. Hillard, S. Top, P. Pigeon, G. Jaouen, *Chimia* **2007**, *61*, 716–724.

[18] G. Jaouen, S. Top, A. Vessières, G. Leclercq, M. J. McGlinchey, *Curr. Med. Chem.* **2004**, *11*, 2505–2517.

[19] U. Schatzschneider, N. Metzler-Nolte, *Angew. Chem. Int. Ed.* **2006**, *45*, 1504–1507.

[20] E. Hillard, A. Vessières, L. Thouin, G. Jaouen, C. Amatore, *Angew. Chem. Int. Ed.* **2006**, *45*, 285–290.

[21] J. Debreczeni, A. Bullock, G. Atilla, D. Williams, H. Bregman, S. Knapp, E. Meggers, *Angew. Chem. Int. Ed.* **2006**, *45*, 1580–1585.

[22] D. S. Williams, G. E. Atilla, H. Bregman, A. Arzoumanian, P. S. Klein, E. Meggers, *Angew. Chem. Int. Ed.* **2005**, *44*, 1984–1987.

[23] A. Wilbuer, D. H. Vlecken, D. J. Schmitz, K. Kräling, K. Harms, C. P. Bagowski, E. Meggers, *Angew. Chem. Int. Ed.* **2010**, *49*, 3839–3842.

[24] L. Zhang, P. Carroll, E. Meggers, *Org. Lett.* **2004**, *6*, 521–523.

[25] I. Ott, *Coord. Chem. Rev.* **2009**, *253*, 1670–1681.

[26] J. L. Hickey, R. A. Ruhayel, P. J. Barnard, M. V. Baker, S. J. Berners-Price, A. Filipovska, *J. Am. Chem. Soc.* **2008**, *130*, 12570–12571.

[27] M. M. Jellicoe, S. J. Nichols, B. A. Callus, M. V. Baker, P. J. Barnard, S. J. Berners-Price, J. Whelan, G. C. Yeoh, A. Filipovska, *Carcinogenesis* **2008**, *29*, 1124–1133.

[28] L. Messori, G. Marcon, M. A. Cinellu, M. Coronnello, E. Mini, C. Gabbiani, P. Orioli, *Bioorg. Med. Chem.* **2004**, *12*, 6039–6043.

[29] S. S. Jurisson, J. D. Lydon, *Chem. Rev.* **1999**, *99*, 2205–2218.

[30] R. Alberto, R. Schibli, A. Egli, A. Schubiger, U. Abram, T. Kaden, *J. Am. Chem. Soc.* **1998**, *120*, 7987–7988.

[31] R. Alberto, K. Ortner, N. Wheatley, R. Schibli, A. P. Schubiger, *J. Am. Chem. Soc.* **2001**, *123*, 3135–3136.

[32] R. Alberto, J. K. Pak, D. van Staveren, S. Mundwiler, P. Benny, *Biopolymers* **2004**, *76*, 324–333.

[33] J. Pak, P. Benny, B. Spingler, K. Ortner, R. Alberto, *Chem. Eur. J.* **2003**, *9*, 2053–2061.

[34] T. Storr, Y. Sugai, C. Barta, Y. Mikata, M. Adam, S. Yano, C. Orvig, *Inorg. Chem.* **2005**, *44*, 2698–2705.

[35] R. Motterlini, L. E. Otterbein, *Nat. Rev. Drug Discovery* **2010**, *9*, 728–743.

[36] C. C. Romão, W. A. Blättler, J. D. Seixas, G. J. L. Bernardesw, *Chem. Soc. Rev.* **2012**.

[37] R. Foresti, G. Bani-Hani Mohamed, R. Motterlini, *Intensive Care Med.* **2008**, *34*, 649–658.

[38] B. Wegiel, B. Y. Chin, L. E. Otterbein, *Cell Cycle* **2008**, *7*, 1379–1384.

[39] B. E. Mann, *Top. Organomet. Chem.* **2010**, *32*, 247–285.

[40] S. Hou, S. H. Heinemann, T. Hoshi, *Physiology* **2009**, *24*, 26–35.

[41] R. Motterlini, P. Sawle, J. Hammad, S. Bains, R. Alberto, R. Foresti, J. Green Colin, *FASEB J.* **2005**, *19*, 284–286.

[42] T. S. Pitchumony, B. Spingler, R. Motterlini, R. Alberto, *Chimia* **2008**, *62*, 277–279.

[43] T. S. Pitchumony, B. Spingler, R. Motterlini, R. Alberto, *Org. Biomol. Chem.* **2010**, *8*, 4849–4854.

[44] T. R. Johnson, B. E. Mann, J. E. Clark, R. Foresti, C. J. Green, R. Motterlini, *Angew. Chem. Int. Ed.* **2003**, *42*, 3722–3729.

[45] R. Motterlini, J. E. Clark, R. Foresti, P. Sarathchandra, B. E. Mann, C. J. Green, *Circul. Res.* **2002**, *90*, 17–24.

[46] R. Foresti, J. Hammad, J. E. Clark, T. R. Johnson, B. E. Mann, A. Friebe, C. J. Green, R. Motterlini, *Br. J. Pharmacol.* **2004**, *142*, 453–460.

[47] R. A. Motterlini, B. E. Mann (Northwick Park Institute for Medical Research; UK; University of Sheffield), *patent WO 2002092075,* **2002**.

[48] U. Hasegawa, A. J. van der Vlies, E. Simeoni, C. Wandrey, J. A. Hubbell, *J. Am. Chem. Soc.* **2010**, *132*, 18273–18280.

[49] T. Santos-Silva, A. Mukhopadhyay, J. D. Seixas, G. J. L. Bernardes, C. C. Romão, M. J. Romão, *J. Am. Chem. Soc.* **2011**, *133*, 1192–1195.

[50] W.-Q. Zhang, A. J. Atkin, R. J. Thatcher, A. C. Whitwood, I. J. S. Fairlamb, J. M. Lynam, *Dalton Trans.* **2009**, 4351–4358.

[51] I. J. S. Fairlamb, J. M. Lynam, B. E. Moulton, I. E. Taylor, A. K. Duhme-Klair, P. Sawle, R. Motterlini, *Dalton Trans.* **2007**, 3603–3605.

[52] S. H. Crook, B. E. Mann, A. J. H. M. Meijer, H. Adams, P. Sawle, D. Scapens, R. Motterlini, *Dalton Trans.* **2011**, *40*, 4230–4235.

[53] F. Zobi, A. Degonda, M. C. Schaub, A. Y. Bogdanova, *Inorg. Chem.* **2010**, *49*, 7313–7322.

[54] F. Zobi, O. Blacque, *Dalton Trans.* **2011**, *40*, 4994–5001.

[55] F. Zobi, O. Blacque, R. A. Jacobs, M. C. Schaub, A. Y. Bogdanova, *Dalton Trans.* **2012**, *41*, 370–378.

[56] L. Hewison, S. H. Crook, T. R. Johnson, B. E. Mann, H. Adams, S. E. Plant, P. Sawle, R. Motterlini, *Dalton Trans.* **2010**, *39*, 8967–8975.

[57] M. A. Gonzalez, N. L. Fry, R. Burt, R. Davda, A. Hobbs, P. K. Mascharak, *Inorg. Chem.* **2011**, *50*, 3127–3134.

[58] L. Hewison, T. R. Johnson, B. E. Mann, A. J. H. M. Meijer, P. Sawle, R. Motterlini, *Dalton Trans.* **2011**, *40*, 8328–8334.

[59] A. J. Atkin, S. Williams, P. Sawle, R. Motterlini, J. M. Lynam, I. J. S. Fairlamb, *Dalton Trans.* **2009**, 3653–3656.

[60] D. E. Bikiel, E. Gonzalez Solveyra, F. Di Salvo, H. M. S. Milagre, M. N. Eberlin, R. S. Correa, J. Ellena, D. A. Estrin, F. Doctorovich, *Inorg. Chem.* **2011**, *50*, 2334–2345.

[61] S. S. Rodrigues, J. D. Seixas, B. Guerreiro, N. M. P. Pereira, C. C. Romão, W. E. Haas, I. M. D. S. Goncalves (Alfama Investigacao e Desenvolvimento de Produtos Farmaceuticos; Lda.; Port.), *patent WO 2009013612,* **2009**.

[62] S. Romanski, B. Kraus, U. Schatzschneider, J.-M. Neudoerfl, S. Amslinger, H.-G. Schmalz, *Angew. Chem. Int. Ed.* **2011**, *50*, 2392–2396.

[63] U. Schatzschneider, *Inorg. Chim. Acta* **2011**, *374*, 19–23.

[64] J. Niesel, A. Pinto, H. W. Peindy N'Dongo, K. Merz, I. Ott, R. Gust, U. Schatzschneider, *Chem. Commun.* **2008**, 1798–1800.

[65] K. Meister, J. Niesel, U. Schatzschneider, N. Metzler-Nolte, D. A. Schmidt, M. Havenith, *Angew. Chem. Int. Ed.* **2010**, *49*, 3310–3312.

[66] H. Pfeiffer, A. Rojas, J. Niesel, U. Schatzschneider, *Dalton Trans.* **2009**, 4292–4298.

[67] G. Dördelmann, H. Pfeiffer, A. Birkner, U. Schatzschneider, *Inorg. Chem.* **2011**, *50*, 4362–4367.

[68] H.-M. Berends, P. Kurz, *Inorg. Chim. Acta* **2012**, *380*, 141–147.

[69] P. C. Kunz, W. Huber, A. Rojas, U. Schatzschneider, B. Spingler, *Eur. J. Inorg. Chem.* **2009**, 5358–5366.

[70] F. Mohr, J. Niesel, U. Schatzschneider, C. W. Lehmann, *Z. Anorg. Allg. Chem.* **2012**, *638*, 543–546.

[71] M. A. Gonzalez, M. A. Yim, S. Cheng, A. Moyes, A. J. Hobbs, P. K. Mascharak, *Inorg. Chem.* **2012**, *51*, 601–608.

[72] R. D. Rimmer, H. Richter, P. C. Ford, *Inorg. Chem.* **2010**, *49*, 1180–1185.

[73] V. P. L. Velasquez, T. M. A. Jazzazi, A. Malassa, H. Goerls, G. Gessner, S. H. Heinemann, M. Westerhausen, *Eur. J. Inorg. Chem.* **2012**, 1072–1078.

[74] R. Kretschmer, G. Gessner, H. Goerls, S. H. Heinemann, M. Westerhausen, *J. Inorg. Biochem.* **2011**, *105*, 6–9.

[75] C. S. Jackson, S. Schmitt, Q. P. Dou, J. J. Kodanko, *Inorg. Chem.* **2012**, *50*, 5336–5338.

[76] M. H. B. Stiddard, *J. Chem. Soc.* **1962**, 4712–4715.

[77] M. H. B. Stiddard, *J. Chem. Soc.* **1963**, 756–757.

[78] A. Vlcek, *Coord. Chem. Rev.* **2002**, *230*, 225–242.

[79] D. M. Manuta, A. J. Lees, *Inorg. Chem.* **1986**, *25*, 1354–1359.

[80] A. Vlcek, *Coord. Chem. Rev.* **1998**, *177*, 219–256.

[81] W.-F. Fu, R. van Eldik, *Inorg. Chem.* **1998**, *37*, 1044–1050.

[82] H. C. Kolb, M. G. Finn, K. B. Sharpless, *Angew. Chem. Int. Ed.* **2001**, *40*, 2004–2021.

[83] C. R. Becer, R. Hoogenboom, U. S. Schubert, *Angew. Chem. Int. Ed.* **2009**, *48*, 4900–4908.

[84] J. C. Jewett, C. R. Bertozzi, *Chem. Soc. Rev.* **2010**, *39*, 1272–1279.

[85] J. E. Moses, A. D. Moorhouse, *Chem. Soc. Rev.* **2007**, *36*, 1249–1262.

[86] J. A. Prescher, C. R. Bertozzi, *Nat. Chem. Biol.* **2005**, *1*, 13–21.

[87] A. Dirksen, T. M. Hackeng, P. E. Dawson, *Angew. Chem. Int. Ed.* **2006**, *45*, 7581–7584.

[88] W. P. Jencks, J. Carriuolo, *J. Am. Chem. Soc.* **1960**, *82*, 675–681.

[89] J. O. Edwards, R. G. Pearson, *J. Am. Chem. Soc.* **1962**, *84*, 16–24.

[90] E. G. Sander, W. P. Jencks, *J. Amer. Chem. Soc.* **1968**, *90*, 6154–6162.

[91] A. Dirksen, P. E. Dawson, *Bioconjugate Chem.* **2008**, *19*, 2543–2548.

[92] R. Huisgen, *Angew. Chem. Int. Ed.* **1963**, *2*, 633–645.

[93] K. V. Gothelf, K. A. Jorgensen, *Chem. Rev.* **1998**, *98*, 863–909.

[94] M. Meldal, C. W. Tornoe, *Chem. Rev.* **2008**, *108*, 2952–3015.

[95] V. D. Bock, H. Hiemstra, J. H. van Maarseveen, *Eur. J. Org. Chem.* **2005**, 51–68.

[96] P. Siemsen, R. C. Livingston, F. Diederich, *Angew. Chem. Int. Ed.* **2000**, *39*, 2632–2657.

[97] C. W. Tornoe, C. Christensen, M. Meldal, *J. Org. Chem.* **2002**, *67*, 3057–3064.

[98] V. V. Rostovtsev, L. G. Green, V. V. Fokin, K. B. Sharpless, *Angew. Chem. Int. Ed.* **2002**, *41*, 2596–2599.

[99] L. M. Gaetke, C. K. Chow, *Toxicology* **2003**, *189*, 147–163.

[100] S. S. van Berkel, A. J. Dirks, M. F. Debets, F. L. van Delft, J. J. L. M. Cornelissen, R. J. M. Nolte, F. P. J. T. Rutjes, *ChemBioChem* **2007**, *8*, 1504–1508.

[101] S. S. van Berkel, A. J. Dirks, S. A. Meeuwissen, D. L. L. Pingen, O. C. Boerman, P. Laverman, F. L. van Delft, J. J. L. M. Cornelissen, F. P. J. T. Rutjes, *Chem BioChem* **2008**, *9*, 1805–1815.

[102] P. Laverman, S. A. Meeuwissen, S. S. van Berkel, W. J. G. Oyen, F. L. van Delft, F. P. J. T. Rutjes, O. C. Boerman, *Nucl. Med. Biol.* **2009**, *36*, 749–757.

[103] W. Hieber, F. Muhlbauer, *Z. Anorg. Allg. Chem.* **1935**, *221*, 337–348.

[104] J. A. Connor, C. Overton, *J. Organomet. Chem.* **1983**, *249*, 165–174.

[105] P. Datta, D. Sardar, A. P. Mukhopadhyay, E. Lopez-Torres, C. J. Pastor, C. Sinha, *J. Organomet. Chem.* **2011**, *696*, 488–495.

[106] M. Ardon, P. D. Hayes, G. Hogarth, *J. Chem. Educ.* **2002**, *79*, 1249–1251.

[107] S. L. VanAtta, B. A. Duclos, D. B. Green, *Organometallics* **2000**, *19*, 2397–2399.

[108] A. C. Coelho, F. A. A. Paz, J. Klinowski, M. Pillinger, I. S. Goncalves, *Molecules* **2006**, *11*, 940–952.

[109] E. M. Sletten, C. R. Bertozzi, *Angew. Chem. Int. Ed.* **2009**, *48*, 6974–6998.

[110] C. Elschenbroich, *Organometallchemie*, 4. Aufl., Teubner, Wiesbaden, **2005**.

[111] P. R. Buckland (Eastman Chemical Co. USA), *patent WO 9518788,* **1995**.

[112] M. Altman, M. Christopher, J. B. Grimm, A. Haidle, K. Konrad, J. Lim, R. N. Maccoss, M. Machacek, E. Osimboni, R. D. Otte, T. Siu, K. Spencer, B. Taoka, P. Tempest, K. Wilson, H. C. Woo, J. Young, A. Zabierek (Merck & Co. Inc.; USA), *patent WO 2008156726,* **2008**.

[113] M. H. Lott, *J. Am. Chem. Soc.* **1948**, *70*, 1972.

[114] U. Hoffmanns, Phd thesis, Universität Heidelberg, **2005**.

[115] S. I. Stupp, J. J. J. M. Donners, G. A. Silva, H. A. Behanna, S. G. Anthony (Northwestern University; USA), *patent WO 2005056039,* **2005**.

[116] D. R. van Staveren, Phd thesis, Ruhr-Universität Bochum, **2001**.

[117] C. G. Hull, M. H. B. Stiddard, *J. Organomet. Chem.* **1967**, *9*, 519–525.

[118] T. H. Dieck, H. Friedel, *J. Organomet. Chem.* **1968**, *14*, 375–385.

[119] S. Trofimenko, *J. Am. Chem. Soc.* **1969**, *91*, 3183–3189.

[120] S. Trofimenko, *J. Am. Chem. Soc.* **1969**, *91*, 588–595.

[121] U. Schatzschneider, J. Niesel, I. Ott, R. Gust, H. Alborzinia, S. Woelfl, *Chem MedChem* **2008**, *3*, 1104–1109.

[122] J. W. Faller, B. C. Whitmore, *Organometallics* **1986**, *5*, 752–755.

[123] J. R. Ascenso, C. G. de Azevedo, M. J. Calhorda, M. A. A. F. d. C. T. Carrondo, P. Costa, A. R. Dias, M. G. B. Drew, V. Felix, A. M. Galvao, C. C. Romão, *J. Organomet. Chem.* **2001**, *632*, 197–208.

[124] D. R. van Staveren, E. Bill, E. Bothe, M. Buhl, T. Weyhermüller, N. Metzler-Nolte, *Chem. Eur. J.* **2002**, *8*, 1649–1662.

[125] P. Leeson, *Nature* **2012**, *481*, 455–456.

[126] P. D. Leeson, B. Springthorpe, *Nat. Rev. Drug Discovery* **2007**, *6*, 881–890.

[127] C. A. Lipinski, F. Lombardo, B. W. Dominy, P. J. Feeney, *Adv. Drug Del. Rev.* **1997**, *23*, 3–25.

[128] A. Leo, C. Hansch, D. Elkins, *Chem. Rev.* **1971**, *71*, 525–616.

[129] S. Schaefer, I. Ott, R. Gust, W. S. Sheldrick, *Eur. J. Inorg. Chem.* **2007**, 3034–3046.

[130] A. Wyllie, V. Donahue, B. Fischer, D. Hill, J. Keesey, S. Manzow, *Apoptosis and Cell Proliferation*, 2. Aufl., Boehringer Mannheim GmbH - Biochemica, Mannheim, **1998**.

[131] A. G. Porter, R. U. Janicke, *Cell Death Differ.* **1999**, *6*, 99–104.

[132] R. U. Jänicke, *Breast Cancer Res. Treat.* **2009**, *117*, 219–221.

[133] R. U. Janicke, M. L. Sprengart, M. R. Wati, A. G. Porter, *J. Biol. Chem.* **1998**, *273*, 9357–9360.

[134] D. Bandarra, M. Lopes, T. Lopes, J. Almeida, M. S. Saraiva, M. Vasconcellos-Dias, C. D. Nunes, V. Felix, P. Brandao, P. D. Vaz, M. Meireles, M. J. Calhorda, *J. Inorg. Biochem.* **2010**, *104*, 1171–1177.

[135] F.-C. Liu, Y.-L. Lin, P.-S. Yang, G.-H. Lee, S.-M. Peng, *Organometallics* **2010**, *29*, 4282–4290.

[136] R. Guilard, N. Jagerovic, A. Tabard, P. Richard, L. Courthaudon, A. Louati, C. Lecomte, K. M. Kadish, *Inorg. Chem.* **1991**, *30*, 16–27.

[137] F. P. J. T. Rutjes, J. L. M. Cornelissen, S. S. Van Berkel, A. J. Dirks (Stichting Katholieke Universiteit Nijmegen), *patent WO 2008075955,* **2008**.

[138] G. R. Fulmer, A. J. M. Miller, N. H. Sherden, H. E. Gottlieb, A. Nudelman, B. M. Stoltz, J. E. Bercaw, K. I. Goldberg, *Organometallics* **2010**, *29*, 2176–2179.

[139] G. M. Sheldrick, *Acta Crystallogr. A* **2008**, *64*, 112–122.

[140] S. I. Kirin, F. Noor, N. Metzler-Nolte, *J. Chem. Educ.* **2007**, *84*, 108–111.

[141] E. Kaiser, R. L. Colescott, C. D. Bossinger, P. I. Cook, *Anal. Biochem.* **1970**, *34*, 595–598.

[142] E. Antonini, M. Brunori, *Hemoglobin and Myoglobin in Their Reactions with Ligands*, Bd. 21 von *Front. Biol.*, North-Holland Pub. Co, Amsterdam, **1971**.

[143] A. J. Atkin, J. M. Lynam, B. E. Moulton, P. Sawle, R. Motterlini, N. M. Boyle, M. T. Pryce, I. J. S. Fairlamb, *Dalton Trans.* **2011**, *40*, 5755–5761.

[144] G. M. Badger, W. H. F. Sasse, *J. Chem. Soc.* **1956**, 616–620.

[145] B. M. Peek, G. T. Ross, S. W. Edwards, G. J. Meyer, T. J. Meyer, B. W. Erickson, *Int. J. Pept. Protein Res.* **1991**, *38*, 114–123.

[146] S.-Y. Lee, A. Hille, I. Kitanovic, P. Jesse, G. Henze, S. Woelfl, R. Gust, A. Prokop, *Leukemia Res.* **2011**, *35*, 387–393.

[147] M. Dobroschke, Y. Geldmacher, I. Ott, M. Harlos, L. Kater, L. Wagner, R. Gust, W. S. Sheldrick, A. Prokop, *ChemMedChem* **2009**, *4*, 177–187.

Appendices

Derivation of the equation for the calculation c(MbCO) in a myoglobin assay

$$A(t) = \epsilon_{540nm}(Mb) \cdot c(Mb) \cdot l + \epsilon_{540nm}(Mb) \cdot c(MbCO) \cdot l \tag{5}$$

$$c(Mb) + c(MbCO) = c_0(Mb) \Leftrightarrow c(Mb) = c_0(Mb) - c(MbCO) \tag{6}$$

$$\begin{aligned} A(t) = & \underbrace{\epsilon_{540nm}(Mb) \cdot c_0(Mb) \cdot l}_{} \\ & - \underbrace{\epsilon_{540nm}(Mb) \cdot c(MbCO) \cdot l + \epsilon_{540nm}(MbCO) \cdot c(MbCO) \cdot l}_{} \end{aligned} \tag{7}$$

$$\frac{A(t)}{l} = [\epsilon_{540nm}(Mb)] \cdot c_0(Mb) + [\epsilon_{540nm}(MbCO) - \epsilon_{540nm}(MbCO)] \cdot c(MbCO) \tag{8}$$

$$\frac{A(t)}{l} = \left[\frac{A(t=0)}{c_0(Mb) \cdot l}\right] \cdot c_0(Mb) + \left[\epsilon_{540nm}(MbCO) - \frac{A(t=0)}{c_0(Mb) \cdot l}\right] \cdot c(MbCO) \tag{9}$$

$$\frac{A(t)}{l} - \frac{A(t=0)}{l} = \left[\epsilon_{540nm}(MbCO) - \frac{A(t=0)}{c_0(Mb) \cdot l}\right] \cdot c(MbCO) \tag{10}$$

$$c(MbCO) = \left[\frac{A(t)}{l} - \frac{A(t=0)}{l}\right] \cdot \frac{1}{\epsilon_{540nm}(MbCO) - \frac{A(t=0)}{c_0(Mb) \cdot l}} \tag{11}$$

Crystallographic data for [Mo(η^3-allyl)(CO)$_2$(bpy)(N$_3$C$_2$(COOCH$_3$)$_2$)] (31)

	31
Empirical formula	$C_{21}H_{19}MoN_5O_6$
Molecular weight [g/mol]	533.35
Temperature [K]	173(2)
Wavelength Mo-$K\alpha$ [Å]	0.71073
Crystal size [mm]	0.34 × 0.11 × 0.06
Crystal system, space group	monoclinic, $P2_1/c$
a [Å]	11.778(2)
b [Å]	9.3237(19)
c [Å]	20.023(4)
α [°]	90
β [°]	103.38(3)
γ [°]	90
Cell volume [Å^3]	2139.1(8)
Z	4
Density $\rho_{calc.}$ [g/cm^3]	1.656
Absorption coefficient μ [mm^{-1}]	0.663
$F(000)$	1080
Θ range for data collection [°]	2.09-26.06
Index ranges ($h/k/l$)	-14/-11/-24
Collected reflections	12344
Unique reflections	3644 [R_{int} = 0.0463
Observed reflections [F_0>4σF_0]	2992
Absorption correction	Semi-Empirical
Goodness-of-fit on F^2 (GOF)	1.063
Final R indices [F_0>4σF_0]	R_1 = 0.0523, wR_2 = 0.1543
R indices (all data)	R_1 = 0.0684, wR_2 = 0.1932
Largest difference peak an hole [e·Å^{-3}]	0.781 and -0.921